St. John's University
St. John's Scholar

Theses and Dissertations

2021

EXPLORING EFFICACY OF AN ANTI-MALARIAL NANOMEDICINE IN NON-SMALL CELL LUNG CANCER TREATMENT

Vineela Parvathaneni

Follow this and additional works at: https://scholar.stjohns.edu/theses_dissertations

 Part of the Pharmacy and Pharmaceutical Sciences Commons

www.manaraa.com

EXPLORING EFFICACY OF AN ANTI-MALARIAL NANOMEDICINE IN NON-SMALL CELL LUNG CA

NCER TREATMENT

A dissertation submitted in partial fulfillment of the

requirements for the degree of

DOCTOR OF PHILOSOPHY

to the faculty of the

DEPARTMENT OF GRADUATE DIVISION

of

COLLEGE OF PHARMACY AND HEALTH SCIENCES

at

ST. JOHN'S UNIVERSITY

New York

by

Vineela Parvathaneni

Date Submitted _____ Date Approved _____

_____ _____

Vineela Parvathaneni Dr. Vivek Gupta

www.manaraa.com

© Copyright by Vineela Parvathaneni 2021

All Rights Reserved

www.manaraa.com

ABSTRACT

EXPLORING EFFICACY OF AN ANTI-MALARIAL NANOMEDICINE IN NON-SMALL CELL LUNG CANCER TREATMENT

Vineela Parvathaneni

New drug and dosage form development faces significant challenges, especially in oncology, due to longer development cycle and associated scale-up complexities. Repurposing of existing drugs with potential anti-cancer activity into new therapeutic regimens provides a feasible alternative. In this project, amodiaquine (AQ), an anti-malarial drug, has been explored for its anti-cancer efficacy through formulating inhalable nanoparticulate systems using high-pressure homogenization (HPH) with scale-up feasibility and high reproducibility. A 3^2 multifactorial design was employed to better understand critical processes and formulation parameters so as to ensure product quality with improved anticancer efficacy in non-small cell lung cancer (NSCLC). Optimized AQ loaded nanoparticles (AQ NP) were evaluated for physicochemical properties, stability profile, *in-vitro* aerosol deposition behavior, cytotoxic potential against NSCLC cells *in-vitro* and in 3D simulated tumor spheroid model while the results confirming the significance of nanoparticle encapsulation for an enhanced anti-cancer efficacy. Furthermore, targeting potential of transferrin ligand conjugated AQ-loaded nanoparticles (Tf-AMQ NPs) was investigated, also evaluated for their physicochemical properties. Tf-AMQ NP (liquid state) exhibited an aerodynamic diameter of 4.4±0.1 µm and fine particle fraction of 83.2±3.0%, indicating drug deposition in the respirable airways. Cytotoxicity studies in NSCLC cell line with overexpressed transferrin receptors revealed significant reduction in IC_{50} values with Tf-decorated AQ-loaded nanoparticles compared to plain

www.manaraa.com

drug or non-targeted NPs, along with significant apoptosis induction (caspase assay) and reduced % colony growth in A549 and H1299 cells with Tf-AMQ NP. Moreover, 3D simulated spheroid studies (~ 7-fold reduction in spheroid volume compared to AMQ NPs) revealed efficacy of conjugated nanoparticles in penetration to tumor core, and growth inhibition. AQ's autophagy inhibition ability significantly increased with nanoparticle encapsulation and transferrin conjugation. Further, another ligand folic acid has been explored for its ability to be conjugated to nanoparticles and to enhance anti-cancer efficacy and were found to exhibit superior anti-cancer efficacy in multiple cancer types such as breast cancer and cervical cancer. To conclude, amodiaquine can be a promising candidate for repurposing to treat NSCLC while delivering inhalable transferrin conjugated nanoparticles developed using a scalable HPH process to the target site, thus reducing the dose, side effects.

Key Words

Drug Repurposing, Targeted Drug Delivery, Inhalation Delivery, 3D-Spheroid Cell Culture

www.manaraa.com

ACKNOWLEDGEMENTS

First and foremost, I would like to thank my husband Mr. Pratheek Tammineni and daughter Ms. Saadhvi Tammineni for their constant support both financially and emotionally. Without them this journey would not have been possible, and I cannot thank them enough. I am greatly indebted to my parents Mr. P. H. Kishore babu and Mrs. P. V. Bharathi for bringing me up to this stage with love and encouragement.

I would like to thank my mentor, my advisor, and my inspiration Dr. Vivek Gupta for his continuous support, push and faith in me. He was always available for me throughout my doctoral studies for all questions I had for him. His immense patience and troubleshooting are something that I wish to learn and achieve in my career as a scientist. I am honored to be part of his lab. His guidance in learning certain scientific techniques was incredible and I would want to learn as much as I can from him in my time here. I also would like to thank my committee members Dr. Lin Mantell, Dr. Abu T Serajuddin, Dr. Sabesan Yoganathan, Dr. Nitesh K Kunda and Dr. Saurabh Agarwal for their constant support and guidance not only towards my project but also to shape me as a disciplined scientist. I was fortunate to have them as a part of my dissertation committee. I would like to express the deepest appreciation to my committee chair, Dr. Sandra Reznik for her precious time. I would also like to thank Dr. Brijesh I Patel, Director of Formulation Development and Analytical Testing at Advanced Bioderma Corporation for his excellent guidance in designing experiments. I would like to thank all faculty members of St. John's university who sharpened my basic knowledge and helped me evolve me as an industrial pharmacist. I would like to extend my gratitude towards Dr. Vijaya L Korlipara, Chair, Department of Pharmaceutical Sciences for her continuous guidance and support while motivating me for

www.manaraa.com

a positive thought process from day 1 at St. John's University. I would also like to thank the PHS department and College of Pharmacy and Health Sciences at St. John's University for supporting me financially through teaching assistantship and doctoral research fellowship. I would like to thank my colleagues in lab, Ms. Snehal Shukla, Nishant S Kulkarni, Ms. Xuechun Wang, Mr. Gautam Chauhan, Ms. Mimansa Goyal, Ms. Sruthi Sarvepalli, Ms. Rasha Elbatanony; and my undergraduate student Mr. Rofadden Lazzare for their support. I would also like to thank our lab alumni Mr. Abdul Althaf Shaik, Mr. Md. Rakib Uddin. I would like to express my deep gratitude to my friend, Mr. Kranthi Venkat Mateti who has always guided on the right path from the day I have started my doctoral degree program.

Finally, I would like to thank all my friends and colleagues at St. John's university for being there for me through my doctoral degree.

www.manaraa.com

TABLE OF CONTENTS

www.manaraa.com

www.manaraa.com

www.manaraa.com

www.manaraa.com

www.manaraa.com

LIST OF TABLES

www.manaraa.com

LIST OF FIGURES

www.manaraa.com

www.manaraa.com

www.manaraa.com

www.manaraa.com

CHAPTER 1

1. Combination of Drug Repurposing and Nanotechnology: Vital in Drug Discovery and Development

1.1. Introduction

For a new chemical entity or molecule to be approved as a drug, traditional *de novo* drug discovery process takes 10-15 years (1,2) which also requires huge investments. A successful drug discovery and development process should identify drugs which are both safe and efficacious to achieve desirable toxicity-to-benefit ratio (3). Majority of the lead candidates identified during traditional *de novo* drug discovery process fails to demonstrate safety and efficacy in the succeeding phases of clinical trials, presenting higher attrition rates during the new drugs' discovery and development. As the probability of success rate is very less; possibility of lead molecules' marketing approval is minimal as well (4). Therefore, pharmaceutical companies investing on the discovery and development of new drugs might not achieve great profits Overall, it delays investigations to address the unmet clinical needs for treating several indications (5). Thus, there raised a great demand to accelerate the drug discovery process. In this context, drug repurposing as an alternative approach offering an expedited drug discovery process.

Drug repurposing (also called drug repositioning or reprofiling) is the identification of new therapeutic indications for known drugs (4). As repurposing builds upon available research efforts, through this strategy FDA review and approvals are speeding up (6). Drugs approved by regulatory agencies such as FDA, European Medicines Agency (EMA),

www.manaraa.com

Medicines and Healthcare Products Regulatory agency (MHRA) are generally used in repurposing (2).

Several approaches that aid in the implementation of organized, systematic, data-driven drug repurposing approaches, majorly through integrating computational assistance (7). Evaluation of a series of compounds in an array of independent models with the aim of identifying a new activity in one or more of the tested models illustrates the vital prerequisites needed for an efficient drug repurposing (8). Proper selection of an optimal repurposing approach is crucial for an effective drug development process. Shortened drug development cycles and availability of preclinical and clinical studies data; avoids large capital investments and also reduces risk of failure rates. Thus, many pharmaceutical companies are currently implementing this method to reprofile FDA approved drugs (2,5). However, in line with the recent developments, repurposed drugs are encountering several challenges such as requirement of rigorous clinical trials and regulatory approval. Other challenges include retention of their efficacy even after formulating into a dosage form. Furthermore, physicochemical properties of repurposed drugs might hinder their new clinical use or new route of administration. Hence, to fulfill the crucial aspects of drug repurposing, encountering challenges need to be overcome. Utilization of an optimal drug delivery system could assist in overcoming these challenges and to achieve a successful drug delivery. In this context, it is necessary to highlight the advantages of nanotechnology in delivering therapeutics.

Nanotechnology-based delivery systems have been widely explored in broad range of fields in medicine ranging from diagnosing applications to diseases treatment. Generally speaking, these delivery systems overcome the drug delivery challenges through carrying

المنارة للاستشارات
www.manaraa.com

enabling higher drug loadings, facilitating site-specific targeting, reducing side effects remarkably. Greater applicability of nanocarriers systems can be attributed to their physicochemical properties, composition and flexibility for surface modifications. Hence, wide variety of drugs could be encapsulated into the nanocarrier systems (9). Due to their site-specific drug delivery, ability to modulate the drug release profiles, pharmacokinetics/*in-vivo* biodistribution of the drugs, nanocarriers have been recognized for their full potential to carry repurposed drugs (10). With recent advancements along with the collected information over the past decades, nanocarrier drug delivery have opened up a new avenue for repurposing drugs and demonstrated promising results in several medical applications (3).

Altogether, combination of drug repurposing and nanocarrier system is of paramount importance to accomplish all the benefits of drug repurposing (10). Significance of drug repurposing, available repurposing strategies along with the challenges encountered by repurposed drugs have been discussed in this review. Importance of nanotechnology in drug repurposing has been discussed with recent research works along with key details against several disorders.

1.2. Discussion on Drug Repurposing

1.2.1. Significance

For a new drug to enter the market, it needs to withstand stringent regulatory guidelines prior to approval. It requires to a larger investments and longer time to obtain a drug meeting all of these regulatory requirements (4,11). Repurposing has gained importance as it can be a less expensive and shorter approach to provide drugs to patients when compared with developing new drugs through traditional discovery and development processes

www.manaraa.com

(4,11). Therefore, repurposing of already approved drugs can cut down on the time and money required to identify a new indication for a medication. Moreover, this approach will help overcome the climate of inflating costs for drug development and ultimately lower the cost for patients (12). Hence, pharmaceutical companies or academic organizations are embracing drug repurposing to quickly and efficiently explore approved drugs for a new therapeutic use (13).

1.2.2. Available Resources

To begin with drug repurposing, drugs to be repurposed can be chosen from any stage of their evolution are shortlisted through *silico* screening. Repurposed drugs could belong to or chosen from one of the following categories:

a. Approved drug identified with a specific side effect (effective in new indication) serendipitously (4).
b. If a drug exhibits a response through a particular mechanism of action which targets more than one disease, they are suitable for drug repurposing. Typically, drugs in clinical development fall under this category for drug repurposing. For example, the clinical development of duloxetine, a nonselective serotonin-reuptake inhibitor was simultaneously carried out for depression and stress urinary incontinence (4,14).
c. Even without any safety concerns, drugs may fail to show efficacy in phase I and phase II trials. They are subsequently rescued and become available to the public where a new target site and corresponding new indication may be identified. This

www.manaraa.com

also includes drugs which have been discontinued for commercial reasons, i.e., budgetary issues, duplicate projects, or change in portfolio strategy (4,14).

d. Drugs that are not launched in large markets (i.e., U.S. and Europe), even though they have been developed and marketed in other emerging markets. This is known as geographic or transnational drug repurposing (14,15).

e. Drugs developed in academic institutions and public sector laboratories can also be sources of drug repurposing. Due to the inadequacy of resources, expertise and collaboration, institutional policy change or a change in a scientist's focus, the drug development research is not taken to a logical conclusion. These candidates can often act as leads for further development (14).

f. Drugs which failed to show efficacy for an approved indication provides a good start for its repurposing. They can then be rediscovered for a new indication and ultimately a patient will find a medication for which a drug is not currently available (14).

1.2.3. Drug Repurposing Strategies

Drug repurposing can be executed serendipitously or can be hypothesis-driven through rational approaches. Experimental and computational strategies constitute hypothesis-driven strategies where experimental approaches include binding assays and phenotypic drug discovery methods. Binding assays can be used to identify binding interactions of ligands to assay components and phenotypic assays assist in identifying lead compounds from large compound libraries. Phenotypic screening approaches have gained importance due to their ability to identify bioactivity in cells or organisms, leading to hit identification. This approach is preferred as it typically is a more accurate portrayal of the underlying

www.manaraa.com

system. Lead compounds identified through *in vitro* screening typically have opportunity higher probability of remaining active when utilized in animal models and ultimately clinical trials (16).

Computational approaches are principally data-driven; involve merging different types of information on drug-diseases relationships and systematic analysis of data of any type (such as gene expression, chemical structure, genotype or proteomic data or electronic health records (EHRs)) (11,17). They exploit known targets, drugs, disease biomarkers or pathways to establish novel methods and further accelerate the process of clinical trials (11). Knowledge based repurposing approach utilizes the data related to drug targets, clinical and biochemical details with a proper experimental design and incorporation of different biological, chemical, and clinical data, results in identification of novel and previously unknown relationships for a particular drug (11,18). Discovery of a drug for a new indication can also be determined through studying its drug-receptor interactions and "off-target" hits, drug centric repurposing approach (18,19). Target-based approaches are utilized to predict the activity against a specific target. The pharmacological effects of these repositioning candidates can be consistently evaluated in molecular, cellular, network backgrounds as well as computational tools such as cheminformatics and bioinformatics (4,11,20). Signature-based approaches emphasize on recognizing gene expression profiles, transcription factors involved in the disease pathogenies (4,11,20). The convenience of signature-based methods is that they reveal underlying molecular mechanisms of disease pathogenesis. Hence, it opens the doors to unravel the unknown mechanisms of the drug and target (4). Signature-based methods utilize mechanistic data at the molecular level, such as an altered gene and subsequent protein expression (21). The efficacy of a drug

www.manaraa.com

depends on individual gene signatures, therefore, a gene signature data base is very helpful in the repurposing of a drug through computational methods (22). Computational tools available to explore the genetic messengers include Connectivity Map (CMap), GWAS, Library of Integrated Network-based Cellular Signatures (LINCS), Sequence Read Archive (SRA), NCBI-GEO (http://www.ncbi.nlm.nih.gov/geo/) and Cancer Cell Line Encyclopedia (CCLE) (2,4).

The ability of a drug to proceed with drug repurposing requires a case by case study while recognizing heterogeneous parameters. In case of rare disorders or diseases for which there is lack of the information about the targets and the disease pathways are unclear, phenotypic assays are paramount for establishing lead molecules (5,23). Repurposing approaches which use different computational tools and technologies have accelerated the research process. Comprehensive review on the significance and practical application of available repurposing strategies have been reviewed earlier by Pushpakom *et al.* (11), Talevi (24), Parvathaneni *et al*. (2) and Xue et al. (17).

Numerous researchers are focusing on finding new uses of old drugs for several indications such as pulmonary hypertension, arthritis, chronic obstructive pulmonary disease etc. Especially, the current pandemic Coronavirus disease (COVID-19) have raised researchers' attention in exploring already approved drugs as there is a high urgency to identify therapeutic treatment (25). A summary of key examples of repurposed drugs is included in **Table 1** (2,26–28).

Table 1. List of various repurposed drugs with details of new indications

S. No.	Drug name	Original indication	New indication
1	Allopurinol	Tumor lysis syndrome	Gout
2	Amphotericin B	Fungal infections	Leishmanaiasis

www.manaraa.com

3	Aspirin	Inflammation and pain	Heart attack and stroke
4	Celebrex	Osteoarthritis	Reduce the risk of additional polyp formation in colon cancer
5	Cymbalta	Antidepressant	Fibromyalgia
6	Doxepin	antidepressant	Antipruritic
7	Finasteride	Benign prostate hyperplasia	Male alopecia
8	Fluoxetin	Antidepressant	Premenstrual dysphoric disorders
9	Gemcitabine	Viral infections	Cancer
10	Glycopyrronium	Gastrointestinal disorder	Chronic obstructive pulmonary disease
11	Hydroxychloroquine	Antiparasitic	Arthritis
12	Ibuprofen	Rheumatoid arthritis	Parkinson's disease
13	Lomitapide	Hypercholesterolemia	Homozygous familial hypercholesterolemia
14	Mifepristone	Pregnancy termination	Cushing's syndrome
15	Minoxidil	Anti-hypertensive	Hair loss
16	Pentostatin	Chemotherapy for specific types of leukemia T-cell-related	B-cell-related, called hairy cell leukemia
17	Raloxifene	Breast cancer	Osteoporosis
18	Rapamycin	Prevents organ transplant rejection	Autoimmune lymphoproliferative syndrome (ALPS)
19	Sildenafil	Angina pectoris	Erectile dysfunction
20	Tamoxifen	Metastatic breast cancer	Bipolar disorder

1.3. Challenges in Utilization of Repurposed drugs

Drug repurposing enables identification of new uses of old drugs while overcoming the limitations of the traditional drug discovery process. Numerous repurposing approaches with recent advancements involve data integration with repurposing approach. Even though, an accelerated drug development is possible, repurposed drugs are encountering major hindrances for their further application. To achieve clinical utility of repurposed drugs, issues related to dosage and delivery capability needs to be resolved. Identified new use of repurposed drugs is required to be within the approved therapeutic window margin of that drug against original indication. Moreover, new indication might demand a different route of administration. In this context of higher dose requirement and change in route of administration, it is prerequisite to conduct safety and efficacy studies to attain marketing approval (29). It is also important to achieve anticipated *in-vivo* drug release profiles to assure the desired pharmacokinetic and biodistribution parameters. If not, release profiles

www.manaraa.com

of repurposed drugs are required to be modulated to establish an effective therapeutic activity. Accordingly, it might require additional efforts to make use of identified repurposed drugs against new indication (10).

Repurposed drugs might also have issues related to solubility, pharmacokinetic, biodistribution behaviors and targeting potential. For an intended new indication, the physicochemical properties such as solubility, release patterns are not suitable. Sometimes, it is necessary to achieve targeted drug accumulation as in case of cancer studies. In certain cases, stability of drug may be another problem which requires to be protected in the biological environment. In addition, repurposed drugs as such are unable to exhibit efficient intestinal permeability, sustained/controlled release profiles, ability to cross blood-brain barrier and cellular penetration as per the respective desired applications towards new indication (10). Hence, following successful drug repurposing, benefits of repurposed drug could be achieved through utilization of suitable drug delivery systems through overcoming challenges. This implies that success in drug repurposing is relying not only on multiple basic and clinical disciplines, but formulation aspects are to be weighed in as well. Novel drug delivery systems such as nanotechnology it is possible to attain desired physicochemical properties (26).

1.4. Potential Advantages of Nanotechnology in Drug Repurposing – Promising Emerging Carriers in Drug Delivery

Due to the challenges encountered in the utilization of repurposed drugs, there raised a great necessity for suitable delivery systems. In this context, nanotechnology has been offering excellent carriers for drug delivery. Nanotechnology is one of the most intensive research areas, applied widely for the prevention, diagnosis as well as in treatment of

www.manaraa.com

diseases. Nanotechnological approach has gained great popularity due to certain properties such as size, structure, flexibility in loading different classes of drugs etc. Nanotechnology comprises of different nanocarrier systems such as lipid-based nanoparticles such as liposomes, solid–lipid particles, micelles and niosomes; polymeric nanoparticles; dendrimers; inorganic nanoparticles such as carbon nanotubes, metal-based nanoparticles, quantum dots and silica nanoparticles (30).

Several types of nanocarriers are extensively used in pharmaceutical applications due to their ability to carry higher amounts of drugs and promote controlled drug release, resulting in reduced dosing frequency. Other advantages of nanocarriers include reduced toxicity and side-effects due to their targeting potential to the specific site of action. Nanocarriers are also known for their capability to improve the stability. Altogether, nanotechnology is contributing for a greater safety, efficacy, patient compliance along with an improved stability profile of drug and ultimately reduced healthcare costs. Different types of nanocarriers exhibit unique physiochemical and biological properties as represented in **Figure 1** (31).

Exploiting nanotechnology for delivering repurposed drugs enable advantages of both drug repurposing and nanotechnology in drug delivery. For instance, these systems present safer therapeutics as the safety profile of drugs is well-known while nanocarriers enable specific drug delivery. Nanocarrier encapsulation would reduce the required drug doses due to their targeting potential. Especially, flexibility in modification of targeting functionalities of nanocarriers establishes applicability across multiple areas of research. While drug repurposing fosters the drug discovery and development process through

www.manaraa.com

skipping initial phases of clinical trials, application of nanotechnology in drug delivery would ultimately yield significant clinical benefits. Overall, with growing knowledge and interest over the past decades, combination of nanotechnology and drug repurposing have opened up a new avenue in drug delivery and demonstrating promising results in broad-range of pharmaceutical applications.

1.5. Applications of Nanotechnology in Drug Repurposing

To accomplish successful drug repurposing, an identified repurposed drug should be made available to the desired site action with more interactions with the new target while

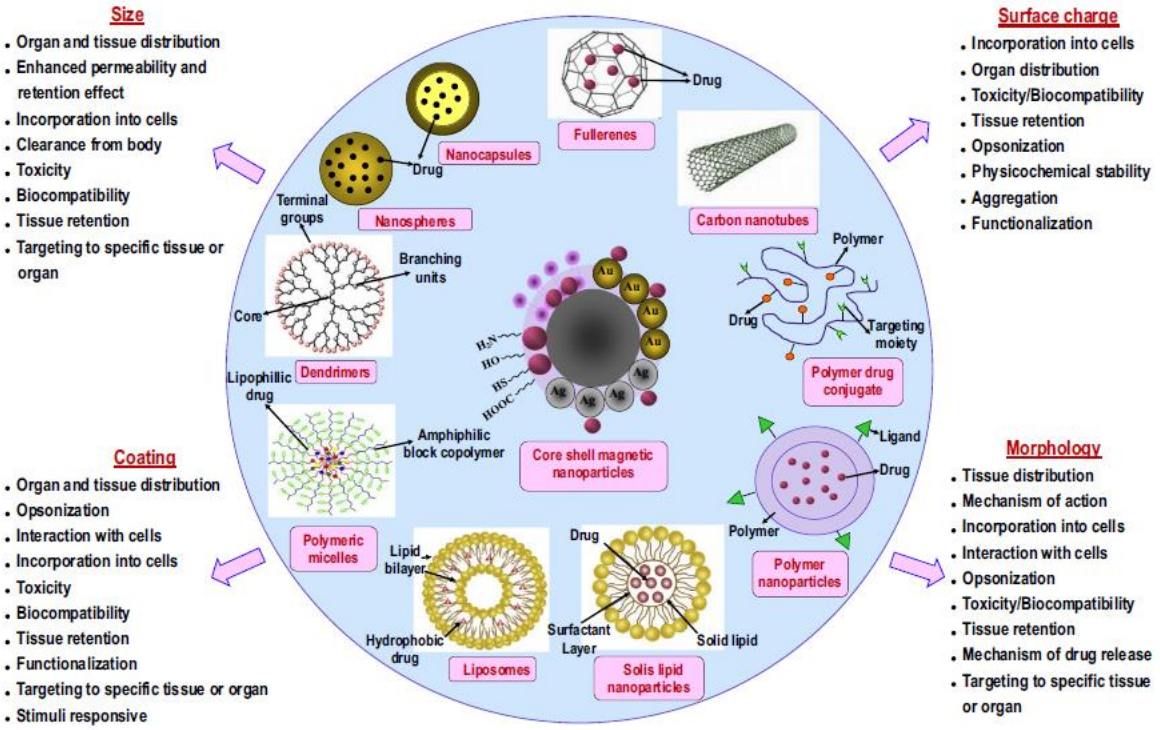

Figure 1. Summary of different nanocarrier systems available for pharmaceutical and biomedical applications

overcoming the challenges encountered in their delivery. Drug delivery refers to the use of a delivery tool or vehicle to carry a therapeutic agent and release it at a specific rate at a particular location. Drug delivery systems have also been used to stabilize components and

www.manaraa.com

increase therapeutic activity. Proper selection of drug delivery systems assists in overcoming the challenges encountered by repurposed drugs.

Nanocarriers enable to adopt a route of administration that is different from the original mode of application of the drug. Modification of the route of administration has been required by several drugs to improve bioavailability or to modify the concentration of drugs at the new site of action, while avoiding the original target effects (32–36). Overall, benefits of changing the route of drug administration, drug targeting, and/or drug modification to ensure proper delivery to the new target are possible through utilization of nanotechnology approach. Nanocarriers can be fabricated according to the desire application due to feasibility of using broad range of materials and to make physical and chemical modifications to obtain unique, adaptable, and/or responsive release profiles (10).

Incorporating repurposed drug into a nanoparticulate system will potentially reduce the required dose to exhibit efficacy. Nanoparticulate drug delivery systems such as polymeric nanoparticle carrier systems can enhance specificity, tolerability and drug efficacy (37). These polymeric nanoparticulate drug delivery systems have been reported for their capability to encapsulate higher amounts of drugs and to provide selective therapeutic activity with less side-effects (38,39). Moreover, biodegradable polymeric nanoparticles have been used regularly due to their versatility and biocompatibility in encapsulation of both hydrophilic and hydrophobic drugs (40). Nanoparticles act as efficient carriers for delivering drug to the tumor while demonstrating higher cellular uptake and tissue penetration; thus exhibiting tumor targeting potential (35,41). In addition, nanoparticles facilitate accumulation of drugs in the desired tissues as in case of tumor treatment, simultaneously reducing the required doses to exert efficacy. For example,

www.manaraa.com

nelfinavir (FDA approved antiretroviral drug) has been reported for its repurposing potential against lung cancer. However, higher dose requirements leading to toxicity are limiting its clinical translation. Parvathaneni *et al* have employed nanotechnology based drug repurposing and reported a potential dose reduction and enhanced anti-cancer efficacy, thus, harnessing the potential clinical use of nelfinavir against non-small cell lung cancer (NSCLC) (42). Polymeric nanoparticles allow introduction of targeting moieties (such as monoclonal antibodies, peptides and proteins) onto the surfaces of delivery systems. These systems can be employed to target the therapeutic agents to certain tissues, which will increase the selectivity of these nanocarriers and accumulation of the encapsulated product at the desired site, which will enhance its efficacy. Capability of nanoparticulate systems in delivering therapeutics through non-invasive pulmonary route of delivery facilitates local drug delivery in case of treating several lung disorders (43).Vaidya *et al*. have used cationic bovine serum albumin nanoparticles to encapsulate quinacrine (anti-malarial drug) and the formulation have demonstrated to have significant anti-cancer efficacy against non-small cell lung cancer with excellent inhalable properties (39). Nanoparticle encapsulated disulfiram, an FDA approved drug to treat alcoholism have reported its repurposing potential in inhibiting tumor growth in ovarian cancer model by He *et al.* Lu *et al.* have developed pH sensitive size shrinkable nanoparticles of metformin in combination with doxorubicin and reported their targeting potential towards tumors. Ebselen (anti-inflammatory) have demonstrated repurposing potential but utility of this drug is hindered by its poor aqueous solubility which requires a nanoparticulate delivery system for topical application for promising, safe and corresponding alternative to the treatment of cutaneous candidiasis (34). Recently, challenges involved in niclosamide

www.manaraa.com

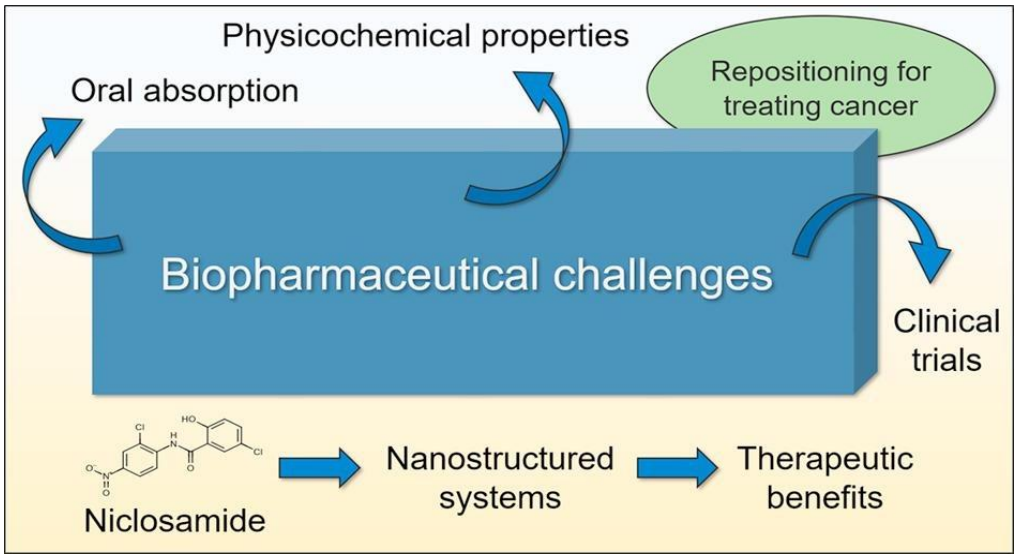

Figure 2. Summary of challenges encountered by niclosamide and importance of nanotechnology in drug repurposing to treating various cancers

(anthelminthic drug) repurposing for cancer diseases has been reviewed by Barbosa *et al*. They have highlighted the therapeutic benefits of encapsulating niclosamide in different nanoparticulate systems (44). **Figure 2** (44) summarizes the challenges encountered by niclosamide and also the benefits of nanotechnology in drug repurposing.

Liposomal drug delivery systems are one of the most promising non-toxic carriers of both lipophilic and hydrophobic drugs (45,46). These systems enhance the therapeutic index of drugs by increasing drug uptake, resulting in increased concentration in tumor cells (47). Parvathaneni *et al*. have formulated liposomal delivery system of pirfenidone (anti-fibrotic drug) to increase its therapeutic activity against non-small cell lung cancer (20). They found that the liposomal encapsulation of metformin has resulted in significant dose reduction compared to plain drug to exert anti-cancer efficacy (33). Shukla *et al*. used liposomal delivery system to increase therapeutic activity of metformin against breast cancer. They found that the liposomal encapsulation of metformin has resulted in significant dose reduction compared to plain drug to exert anti-cancer efficacy (33).

www.manaraa.com

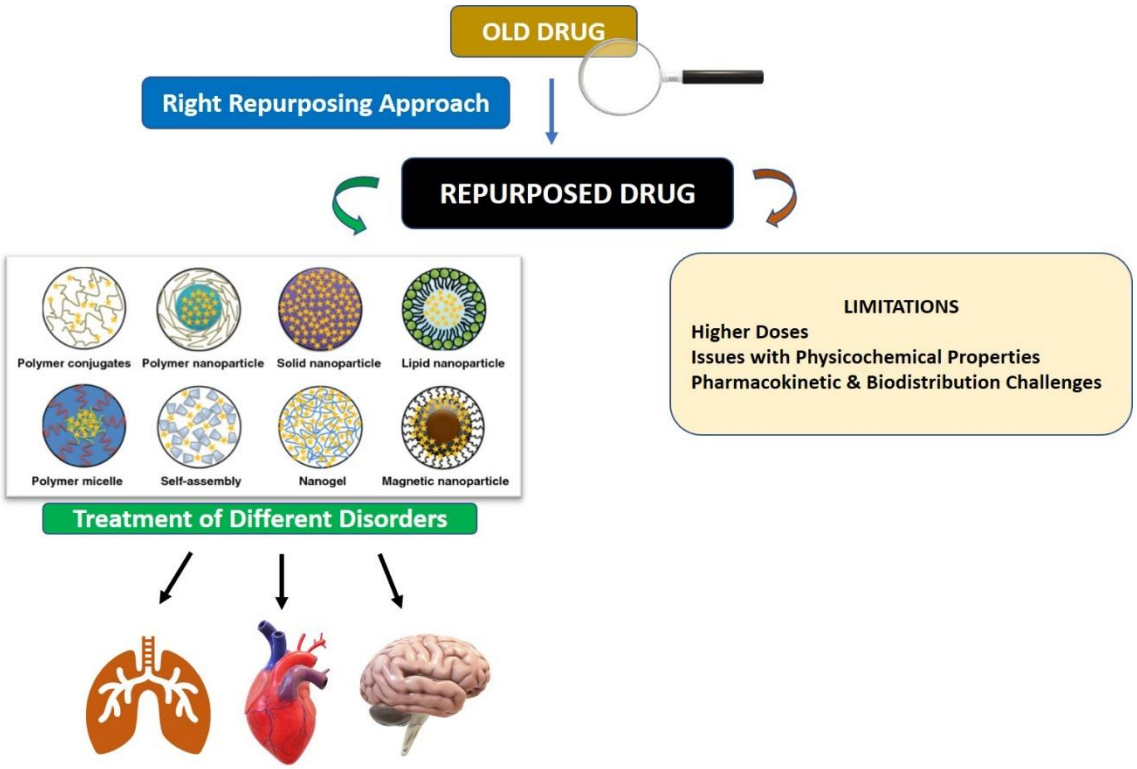

Figure 3. Illustration of significance of combination of drug repurposing and nanotechnology in treating various indications.

Celecoxib (anti-inflammatory drug) entrapped liposomes were prepared to overcome its drawbacks such as low water solubility and rapid plasma clearance and to allow a systemic administration and increase tumor accumulation of drug based on the enhanced permeability and retention mechanism by Matbou Riahi *et al.* (48).

1.6. Exploitation of Nanotechnology in the Treatment of Several Indications

Nanotechnology has been widely exploited in recent years in various applications. Recently, there has been a substantial rise in the use of nanocarriers to deliver therapeutic agents for treating various diseases with many successful outcomes (9). An overview on the significance of nanotechnology in drug repurposing against various disorders has been presented in **Figure 3**. (Image of Nanostructures was adapted from (49)).

The utilization of different nanocarrier systems in delivering repurposed drug is discussed below by disease type. To exemplify the breath of nanoparticle drug delivery

www.manaraa.com

systems and/or drug repurposing, several disorders along with few case studies have been discussed below along with illustration of few examples in **Table 2** (26,27).

Table 2. List of the Application of Nanocarrier Systems in Drug Repurposing to Treat Different Disorders

Drug	Drug delivery system	Original indication/property	New indication	References
Pulmonary diseases				
Simvastatin	Poly(lactic-co-glycolic) acid nanoparticles	Anti-inflammatory and muco-inhibitory	Inflammatory lung diseases	(50)
Niclosamide	Nanocrystals	Anthelmintic	Anti-viral against lung infections in cystic fibrosis	(51)
Etanercept	-	Rheumatoid arthritis	Asthma	(52)
Fasudil	Liposomes	Subarachnoid hemorrhage	pulmonary arterial hypertension	(53)
Cardiovascular diseases				
Methotrexate	Lipid core nanoparticles	Anti-inflammatory	Acute myocardial infarction	(54)
Paclitaxel	Lipid Nanoparticles	Anti-cancer	Coronary allograft vasculopathy	(55)
Lidocaine	-	Local anesthetic	Arrhythmia	(56)
Methotrexate	-	Anti-cancer	Atherosclerosis	(57)
Mesothelioma				
Paclitaxel and Carboplatin	Albumin based nanoparticles	Ovarian, cervical and non-small cell lung cancer.	Malignant pleural mesothelioma	(58)
Metformin	Chitosomes	Anti-diabetic	Malignant pleural mesothelioma	(59)
Quinacrine	-	Anti-malarial	Malignant pleural mesothelioma	(60)
Brain disorders				
Pioglitazone	Nano lipid carriers	Anti-diabetic	Alzheimer's disease	(61)
Melatonin	Polymeric nanoparticles	Insomnia	Glioblastoma	(62)
Clioquinol	Antifungal	PBCA NPs coated with polysorbate	Alzheimer's disease	(63)

www.manaraa.com

1.6.1. Lung diseases

Pulmonary disorders of the airways and lungs include chronic obstructive pulmonary disease, asthma, cystic fibrosis, inflammatory disorders, pulmonary vascular diseases, interstitial lung diseases (pulmonary fibrosis), sarcoidosis and infectious diseases like pneumonia, tuberculosis (64,65). In spite of availability of advanced treatments, still there exists a need to emphasize on delivering therapeutics efficiently to lungs with an application of drug repurposing and nanocarrier drug delivery system. Efficiency of this combination in treating lung disorders has been proved in several studies. Literature comprehends several examples of therapies that have been effectively demonstrated for the treatment of allergic, genetic, and infectious diseases of the respiratory system.

Pulmonary arterial hypertension (PAH) is caused by several pathological changes in the pulmonary vasculature. Majority of the approved PAH medications modulate the endothelin, nitric oxide, and prostacyclin pathways, addressing only the vasoconstrictive phenotype of PAH. Therefore, there is a pressing need to develop novel, effective therapies that target additional molecular pathways that drive the pathogenesis of PAH to enhance current treatment options and accelerate progress in the direction of a PAH treatment (66).

Metformin (antidiabetic drug) have been demonstrated to promote pulmonary vasodilation by increasing endothelial nitric oxide synthase in preclinical models and mitigated pulmonary artery smooth muscle cell proliferation (67). Rosiglitazone (type 2 diabetes) was reported to play a crucial role of peroxisome proliferator-activated receptor *gamma* (PPAR-γ) in PAH pathogenesis and it has been reported to deliberate PASMC proliferation by modulating cell growth and apoptosis. Advantages of rosiglitazone over other PAH treatments include its direct effects on vascular remodeling

www.manaraa.com

in PAH. Thus, presenting rosiglitazone as a potential candidate for repurposing against PAH. In another study, Rashid *et al* have developed PLGA particles of rosiglitazone and evaluated the formulation in Sugen/Hypoxia induced PAH rats. Authors have reported that repurposing potential of rosiglitazone as an anti-PAH drug. In addition, inhaled PLGA particles of rosiglitazone were reported to be more potent compared to than plain intratracheal or oral rosiglitazone, even at much-reduced doses (68).

Niclosamide (anti-helminthic), multiple pathway inhibitor has demonstrated to play a central role in ameliorating *Transforming growth factor beta* 1 (TGF-β1) induced profibrotic effects in fibrotic diseases. Computational biological studies predicted niclosamide to exhibit strong antifibrotic effects in attenuating pulmonary fibrosis (69). Recently, a new formulation of trimetazidine (in Europe and other countries for the treatment of angina pectoris): Livantra has been approved by US FDA for the treatment of pulmonary arterial hypertension (PAH). (70) Fasudil (approved for cerebral vasospasm induced by subarachnoid hemorrhage) have been investigated for its anti-PAH efficacy. It has been found to demonstrate pulmonary vasodilation in both animal model and human PAH. As intravenous fasudil is not selective for the pulmonary circulation and has a short half-life of ~45 minutes, Gupta *et al* have investigated capability of inhalable liposomal systems to deliver fasudil producing prolonged pulmonary selective vasodilation in PAH. Authors have reported the ability of developed fasudil liposomes to produce sustained and selective pulmonary vasodilation while reducing the required doses (36). In another study, inhalable polymeric particles of sildenafil (phosphodiesterase type 5 inhibitor (PDE5), original indication: erectile dysfunction) have been reported to prolong the drug release while producing selective pulmonary vasodilation. Thus, resulting in reduced the systemic

www.manaraa.com

exposure of the drug which highlights the importance of nanotechnology in delivering sildenafil for PAH treatment (71). Tadalafil, PDE5 inhibitor was originally developed for treating erectile dysfunction and later repurposed for PAH. Recently, Teymouri Rad *et al* reported an increased efficacy of tadalafil nanocomposites administered as intratracheal insufflation compared to oral version of tadalafil and concluded that inhalable tadalafil nanocomposites as an alternative strategy for an oral version of tadalafil in PAH treatment (72). Several other repurposed drugs such as pazopanib, imatinib, tofacitinib for treating allergy and asthma have been summarized by Kruse and Vanijcharoenkarn *et al* (73).

In case of treating respiratory infections, emergence of new and resistant strains alarms the researchers about necessity to develop new therapies for combating several viral or bacterial infections. While there are several approved drugs under investigation to repurpose against COVID-19, still there is no approved treatment for that. Many researchers have been exploring nanotechnology to achieve better outcomes of repurposed drugs. Nanomedicine formulations have been investigated for their ability to deliver dexamethasone to inflammation-initiating and -propagating phagocytic cells in the lung, assists controlling cytokine storm. Dexamethasone nanoformulation can increase drug availability and drug activity in the inflamed parts of the lung while exerting anti-fibrotic effects. Thus, dexamethasone nanomedicine have been shown to be useful for preventing fibrosis, key complication in the long-term follow-up management of COVID-19 (74).

1.6.2. Cardiovascular diseases

Cardiovascular and circulatory diseases namely ischemic heart disease, cardiomyopathy, rheumatic disease, endocarditis, peripheral vascular disease etc. are now recognized as the leading causes of death in the world (75). Currently, there is a major current health concern

www.manaraa.com

demanding acceleration of drug development process for cardiovascular disease which have become quiet. In the advent of target deconvolution, reconsideration of previously approved drugs has become significant (76). Recent studies suggest minocycline's (antibacterial drug) protective role in cardiovascular pathology and reported its activity against myocardial ischemia-reperfusion injury (77). In addition, emerging evidence supports the potential repurposing of the disease-modifying antirheumatic drug (DMARD) methotrexate for the management of patients with atherosclerotic cardiovascular disease and residual cardiovascular risks (57). Recent studies have highlighted the beneficial effects of currently marketed anti-inflammatory drugs, such as colchicine and hydroxychloroquine, in reducing cardiovascular events in patients with stable coronary artery disease (78–81). Despite of a large number of therapeutic options being developed for the management of cardiovascular diseases, they are insufficient to stop or significantly reduce the progression of these diseases and may produce unwanted effects. In this context, important advances in the area of nanotechnology and the controlled release of drugs intend to avoid limitations of conventional therapies for the treatment of several CVDs (82). Matoba *et al*. have highlighted the capability of several nanocarrier systems in providing enhanced drug delivery for treating unstable coronary atherosclerosis and their other possible applications against myocardial ischemia-reperfusion injury and pulmonary hypertension. Moreover, it was reported that nanotechnology based drug delivery systems (polymeric nanoparticles) of several drugs have been under clinical trials to investigate their efficacy in critical limb ischemia (83).

www.manaraa.com

1.6.3. Mesothelioma

Malignant mesothelioma (MM), aggressive type of cancer arising from mesothelial cells lining the pleural, peritoneal, and pericardial cavities (84,85). It is characterized by a dismal prognosis and inherent resistance to chemotherapeutics, thus demanding development of therapeutic approaches (85). Despite availability of several standard therapies (cisplatin + pemetrexed), patients' median survival is not improved significantly. Patient survival still needs to be drastically improved with new therapeutic approaches by means of unique mechanisms of action against the MM malignant phenotype (85). Moreover, mesothelioma cells are resistant to traditional chemotherapeutic agents, prompting the need for new drug development (59). As discovery of new molecules with superior therapeutic efficacy is expensive and time-consuming, several researchers have been exploring repurposing potential of old drugs for a better MM prognosis. Recently, anti-tumor activity of pyrvinium pamoate (anti-helminthic) drug has been demonstrated in MM. Moreover, pyrvinium pamoate significantly impaired MM cell proliferation, colony formation, migration, and tumor spheroid formation (86). Szymiczek *et al* immunosuppressant FTY720, approved for multiple sclerosis treatment, has been investigated for its anti-cancer efficacy in MM. However, to alleviate the side effects of repurposing drugs (Eg. FTY720), development of optimal nanoparticle drug delivery system is essential (85). In a recent study, our research group have reported the research findings demonstrating the efficacy of quinacrine (FDA approved anti-malarial) (60). Besides highlighting the importance of drug repurposing, researchers have realized the necessity of delivery systems towards better performance. They have evaluated the effects of quinacrine on cell viability of normal cells (human embryonic kidney cells, HEK-293). Quinacrine was reported to

www.manaraa.com

exhibit toxicity on normal cells along with cancer cells in this study. Thus, it is highlighting the importance of a delivery system to reduce exposure to normal tissues. There are several studies reporting the repurposing potential of metformin against MPM (87,88). However, metformin upon intrapleural administration suffers from rapid elimination thus requiring higher doses with frequent dosing. In another study, Shukla *et al* have demonstrated the improved cytotoxic efficacy of metformin loaded into chitosomes which prolonged retention and drug release of metformin (59).

1.6.4. Brain disorders

Most commonly occurring brain disorders are brain seizure (89), multiple sclerosis (90); neurodegenerative diseases like parkinson's disease (PD), alzheimer's disease (AD) (91), glioblastoma and dementia (92,93); infectious diseases like meningitis and encephalitis (94), vascular diseases like stroke, aneurysm, and hematoma (95,96). Major factors contributing to the limitations of brain delivery are the blood-brain barrier (BBB) and the blood-cerebrospinal fluid barrier (BCSFB) (97,98). Disulfiram (inhibitor of acetaldehyde dehydrogenase) used to treat chronic alcoholism has been investigated for its efficacy against glioblastoma (99). Recently, nanoparticles have withdrawn great attention due to their ability to carry drugs across the BBB. Furthermore, these systems offer controlled drug release, which potentially allow for a decrease in the frequency of administrations. Moreover, nanoparticles are expected to improve the drug physicochemical stability and increase the biological availability (62). Da Silveira *et al*. investigated and reported the antitumoral effect of ketoprofen-loaded nanocapsules in treating glioblastoma (100). Zhou *et al.* have developed brain penetrating PLGA nanoparticles loaded with agents identified (library screening approach) as active against brain cancer stem cells. They have reported

www.manaraa.com

the significance of a combination of drug repurposing and nanoparticle-based drug delivery in treating glioblastoma (101). In another study, epilepsy have benefitted from repurposing drugs with the use of liposomal systems loaded with curcumin (anti-inflammatory) in treating seizures (102).

1.6.5. Cancer

Cancer is one of major health issues worldwide, even though there are several current therapies available. Limited success with new drug developments which have required huge investments is alarming the researchers to choose an alternative strategy. Moreover, for approved oncology drugs, prices have raised steeply in recent years; increasing the economic burden on the public. Hence, there is a growing interest for drug repurposing, i.e. using already approved drugs for treating new indications (cancer) to improve success rates, shorten time frames for drug development while reducing the overall costs.

Several recent studies have reported the repurposing potential of FDA approved drugs against cancer both in its prevention and therapy. In addition, advantages of different types of nanocarrier systems in overcoming the challenges encountered by repurposed drugs have been discussed here along with respective examples. Generally speaking, two major prerequisites for an optimal cancer drug delivery therapy include avoiding pre-release of drug and resulting in desirable drug release profile at site of action (3). Thus, several researchers are utilizing different types of nanocarriers to fulfill the crucial aspects in drug repurposing and delivery. Major aspects include drug efficacy enhancement through modified bio-distribution profile, minimizing side effects; prolonging the drug release; resolving the solubility, bioavailability issues and facilitating a targeted or localized tumor therapy (10).

www.manaraa.com

El-Moslemany *et al*. have investigated the repurposing potential of miltefosine, an alkylphosphocholine initially developed as an anticancer drug, to use leishmaniasis treatment as a antischistosomal agent. They have reported the capability of respective nanocarrier system (lipid nanocapsules) in dose reduction from the *in-vivo* studies (103). In another study, Alhakamy *et al*. have reported the efficacy of Itraconazole, a broad-spectrum antifungal drug in NSCLC treatment. They have loaded the drug into chitosan-coated polymeric nanoparticles to overcome issue of poor water solubility the drug which hinders its use as a therapeutic agent. (104). Recently, our research group have reported repurposing potential of various classes of drugs such as anti-fibrotic and an anti-viral category. While these drugs have demonstrated anti-cancer efficacy, to enhance the efficacy further and to achieve a safe delivery of the therapeutics, different types of delivery systems have been investigated. Anti-malarial drug, amodiaquine have also been under investigation to explore its anti-cancer efficacy in melanoma and its repurposing potential has been reported by Salentin et al (105). There are several reports stating the presence of redox imbalance in cancer environment. Amodiaquine is a mannich base 4-aminoquinoline. Cationic complexes of amodiaquine base with Rhodium have been reported for their anti-tumor activity (106). In addition, several other properties of amodiaquine such as ability to inhibit ribosome function, autophagy inhibition were also reported. Furthermore, loading amodiaquine into a polymeric nanoparticulate system could enhance the anti-cancer efficacy of drug against non-small cell lung cancer (NSCLC). Utilization of targeting approach facilitates targeted drug delivery to the specific cancer cells. Overexpression of transferrin receptors in several NSCLC cells has been reported, thus targeting them directs therapeutics towards cancer cells with overexpression of

www.manaraa.com

transferrin receptors (107). TFR1 and TFR2 are two subtypes of TFRs those bind with iron-transferrin complex to facilitate iron into cells. TFR1 is ubiquitously expressed on the surfaces of generic cells, whereas TFR2 is specially expressed in liver cells. Recently reports showed that TFR1 is abnormally expressed in various cancers. Hence, targeting TFR1 through respective drugs or drug delivery systems demonstrated strong anti-tumor effects, herein TFR1 probably became a potential molecular target for treatment for cancers (108).

Parvathaneni et al have successfully encapsulate pirfenidone (anti-fibrotic) into liposomes and reported their superior anti-cancer efficacy against NSCLC. Other example includes zoledronate–calcium NPs (zoledronate: approved for osteoporosis) has been loaded into PLGA NPs which were further functionalized with octadecanoic acid-hydrazine-polyethylene glycol by Li et al. This delivery system has minimized the burst release of zoledronate and enhanced toxicity in cancer cells as well as macrophages. Moreover, results from in-vivo experiments have revealed that developed nanoparticulate formulation has reduced drug accumulation in bone and demonstrate better extra skeletal tumor-targeting efficacy compared to plain drug (109). Curcumin has demonstrated anti-cancer activities through several different signaling pathways (110), yet it requires a delivery system to overcome the challenges pertaining to its poor water solubility and low bioavailability. Laha *et al.* have developed folic acid-conjugated curcumin-loaded metal-organic nanoparticles for treating triple-negative breast cancer which exerted an effective tumor growth inhibition in mice (111). Repurposing of anti-inflammatory drugs such as ibuprofen, ketoprofen, and celecoxib as anti-cancer agents against gastric, brain, breast, and colon cancers is relied on utilization of nanoparticulate systems to ensure tumor-

www.manaraa.com

targeted delivery (10). To elaborate, even though celecoxib demonstrated anticancer activity against many cancer types, serious side effects of it are hindering its successful repurposing. Thus, Venkatesan *et al* have developed chitosan modified hydroxyapatite nanocarriers-mediated celecoxib to resolve these issues (112).

1.7. Conclusion

Even though discovering a new drug is better, time, cost and success rate in the discovery are making researchers to look towards alternative strategies. Thus, drug repurposing is becoming an attractive avenue in drug discovery and development. Hence, existing drugs could be explored for their new use with lower investments and higher success rates in shorter timeframes. However, utilization of repurposed drugs is encountering several challenges such as higher dose requirement compared to that for original indication etc. Hence, considering delivery of repurposed drugs using nanotechnology could be an interesting opportunity to achieve the whole benefits of drug repurposing. Several nanocarriers have been proven to deliver repurposed drugs to exert desired therapeutic effect while overcoming the respective challenges confronted by majority of repurposed drugs.

1.8. Expert Opinion

Due to the advent of drug repurposing approach, drug discovery and development process has been accelerated to combat the shortage of drugs. Exploration of new uses of old drugs cuts down the time and costs invested in lengthy, expensive *de novo* drug discovery. Multiple resources of approved drug library or of other categories are available for drug repurposing. Known approved drugs or clinically failed drugs could be repurposed against

www.manaraa.com

new diseases of interest. Several repurposing strategies are available ranging from phenotypical screening to complex computational methods with data integration to employ drug repurposing. Through phenotypic screening approaches, lead molecules can be identified based on their bioactivity in cells or organisms. Target-based approaches are utilized to predict the activity against a specific target. Moreover, pharmacological effects of repositioning candidates can be consistently evaluated in molecular, cellular, network backgrounds as well as computational tools such as cheminformatics and bioinformatics can be applied. The ability of a drug to proceed with drug repurposing requires a case by case study while recognizing heterogeneous parameters. However, even after identification a repurposed drug, there are certain hurdles hindering their successful utilization. Challenges encountered by repurposed drugs generally include requirement of higher doses (than approved doses for original indication) of these drugs to exert activity against new indication, possibility to administer via different route and feasibility of their physicochemical properties. Hence, there arises a need of drug delivery system to deliver these repurposed drugs. Moreover, nanotechnology (nanocarriers systems) has now been an attractive strategy to deliver therapeutics to desired site with optimal release profiles. These systems are becoming critical tools in addressing the limitations of repurposed drugs. Majority of research studies have investigated several FDA approved drugs for their repurposing potential and evaluated their efficacy through their encapsulation in various nanocarriers. Thus, a combination of drug repurposing and nanotechnology could open a new avenue for successful drug discovery and development to treat variety of indications.

www.manaraa.com

CHAPTER 2

2. Hypothesis & Study Objectives

2.1. Hypothesis

We hypothesize that scalable, targeted nanoparticulate delivery systems of amodiaquine are capable of delivering drug into the deep lungs, thus reducing the dose and off-target effects.

2.2. Objectives

2.2.1. Development of Pharmaceutically Scalable Inhaled Anti-cancer Nanotherapy – Repurposing Amodiaquine for Non-Small Cell Lung Cancer (NSCLC)

2.2.1.1. Exploration of Anti-cancer efficacy of amodiaquine against NSCLC

Amodiaquine is an anti-malarial drug and no studies were reported on its anti-cancer efficacy in non-small cell lung cancer. Hence, our objective is to screen different NSCLC cell lines to study cytotoxicity effect of AQ.

2.2.1.2. Formulation and Characterization of AQ-loaded Nanoparticles

A scalable approach, high-pressure homogenization has been chosen for the formulation of NPs in the current study. However, for obtaining an optimal product, variables pertaining to process and formulation composition needs to be considered. A systematic experimental design assists in identifying the critical process and product parameters. Assessment of physicochemical properties of the developed AQ NPs would provide details on the characteristic features of NPs.

www.manaraa.com

2.2.1.3. Determination of Anti-cancer Efficacy of AQ and AQ-loaded NPs

Developed formulations are required to be evaluated for their anti-cancer efficacy and to compare with that of plain AQ, if nanoparticulate encapsulation have enhanced the therapeutic efficacy of AQ or not. In brief, several *in-vitro* cell culture studies such as cytotoxicity studies, scratch assay, clonogenic assay and *ex-vivo* studies (3D spheroid studies) help in assessing the efficacy of NPs.

2.2.2. Development and Characterization of Transferrin Functionalized Amodiaquine Loaded Nanoparticles-Efficacy in Non-Small Cell Lung Cancer (NSCLC) Treatment

2.2.2.1. Conjugation of PLGA polymer with Transferrin and its Characterization

Conjugation of Trasferrin onto PLGA polymer will be carried out using EDC/NHS chemistry.

2.2.2.2. Formulation and Characterization of Tf-AQ-loaded Nanoparticles

To impart targeting potential to the NPs, non-conjugated and ligand (transferrin) conjugated polymer has been chosen to use at ratio of 5:1.

2.2.2.3. Determination of Inhalable properties of NPs

In-vitro lung deposition test using Next Generation Impactor (NGI) determines the respirability of the developed NPs (both non-targeted and targeted).

www.manaraa.com

2.2.2.4. Comparing efficacy of non-targeted and transferrin receptor Targeted AQ-loaded Nanoparticles

To determine the superior anti-cancer efficacy of targeted AMQ NPs compared to both plain AQ and non-targeted AMQ NPs, several cell culture studies will be carried out which include both two-dimensional and three-dimensional models. These studies include different NSCLC cell lines with varied expression levels of transferrin receptors.

2.2.3. Development and Characterization of Folic acid Conjugated Amodiaquine Loaded Nanoparticles-Efficacy in Cancer Treatment

2.2.3.1. Conjugation of PLGA polymer with Folic acid

PLGA needs to be conjugated with folic acid (FA) via set of reactions utilizing EDC/NHS chemistry and PEG-bis-amine for the formation of PLGA-PEG-FA conjugate.

2.2.3.2. Formulation and Characterization of FA decorated AQ-loaded Nanoparticles

To impart targeting potential to the NPs, non-conjugated and ligand (folic acid) conjugated polymer has been chosen to use at ratio of 5:1.

2.2.3.3. Comparing the efficacy of non-targeted and transferrin receptor Targeted AQ-loaded Nanoparticles

To determine the superior anti-cancer efficacy of targeted AMQ NPs compared to both plain AQ and non-targeted AMQ NPs, several cell culture studies will be carried out which include both two-dimensional and three-dimensional models. These studies utilize multiple cancer types with variable folic acid receptor expression levels.

www.manaraa.com

CHAPTER 3

Lung cancer is the leading cause of cancer deaths worldwide in both men and women with non-small cell lung cancer (NSCLC) accounting for approximately 85% of lung cancer cases (113). Even though there are major advancements in the field of discovery and development of novel drugs and delivery systems, it still remains a challenging task to treat NSCLC. Moreover, there is growing evidence that cancer cells develop resistance to chemotherapeutic agents upon chronic use, which makes it imperative to identify newer drugs with exceptional anticancer activity. As it takes 12-15 years for developing a new drug in the traditional drug discovery process, drug repositioning (repurposing) has been drawing significant attention because of its ability to identify new use of already FDA approved molecules and hence accelerate the development process at lower costs (114). Altogether, to harness the potential clinical use of different class of drug as an anticancer agent, a suitable drug delivery system facilitating enhanced efficacy and dose reduction is required. Especially, nanoparticulate drug delivery systems have been reported for their capability to encapsulate higher amounts of drugs and to provide selective therapeutic activity with less side-effects (38,39).

3. Development of Pharmaceutically Scalable Inhaled Anti-cancer Nanotherapy – Repurposing Amodiaquine for Non-Small Cell Lung Cancer (NSCLC)

3.1. Introduction

Nanoparticles (NPs) have attained considerable attention in delivering therapeutics due to their unique characteristics related to size, surface, payload capacity and flexibility in surface modifications to exert targeting potential (115). Available marketed products of

www.manaraa.com

NP systems include Cimzia®, Eligard®, Pegasys®, Renagel® etc. (116). NPs have demonstrated reproducible results on small laboratory scale production batches, however, a major hindrance exists in the translation from laboratory scale to commercial production due to manufacturability challenges (117,118). Manufacturing challenges such as feasibility of scale-up, product quality and process repeatability are to be considered during the development of NPs (119). Moreover, lack of sufficient information and knowledge on the scale-up technologies makes it difficult to introduce NPs into the market at the same pace of their development (115,119). Further, scale-up is known to affect the characteristics of NPs and necessitates further optimizations at industrial scale. A better strategy would be to develop NPs using commercially scalable approaches at the laboratory scale, and researchers should pay more attention to formulation scale-up in addition to the development of complex delivery systems (119). Among several existing methods of NPs production, high pressure homogenization (HPH) has gained much importance due to its scale-up feasibility and efficiency in providing reproducible results (120). HPH allows for seamless translation from academic/small scale research labs to commercial scale production in cGMP facilities, and facilitates manufacturing of various formulations such as emulsions, suspensions and NPs in larger quantities (118,120,121). During the HPH process, formulations are subjected to both mechanical forces such as cavitation, impact, shear, turbulence and high pressure (122) which aid in accomplishing NPs with optimal characteristics such as minimal particle size and maximum drug loadings as reported by Hoyer *et al* (120). Shi *et al* have reported that optimal homogenization pressure and number of homogenization cycles have resulted in small sized NPs with uniform size distribution

www.manaraa.com

(123). In another study, high HPH was used to achieve NPs of minimal particle size and good stability (124).

While effective, there are multiple variable parameters in HPH process, which need to be optimized and fine-tuned to reproducibly develop a stable and effective delivery system. Due to the involvement of several critical processes and formulation parameters, it is imperative to utilize statistical design of experiment (DoE) approach to assist in optimizing formulation while improving the knowledge of several parameters (118). For instance, *Petersen and Steckel* have investigated various parameters such as homogenization pressure, pre-emulsion quality and formulation variables using DoE to identify the critical parameters and developed an optimized emulsion (125). The importance of DoE can be understood from several recent works where application of systematic DoE approach has assisted in developing solid lipid nanoparticles of Efavirenz, poorly soluble drug (118) and inhalable microparticles of highly lipophilic drug (126).

One therapeutic area where particle characteristics play a vital role in particle accumulation and performance, is localized delivery to the lungs for respiratory diseases. Accumulation into the deep lungs is imperative for treatment of majority of respiratory diseases including pulmonary hypertension, pulmonary fibrosis, and non-small cell lung cancer (NSCLC) (127,128). Accumulation of drug-loaded nanocarriers in the lungs after pulmonary delivery has been studied by several researchers, and improved efficacy of inhalable carriers in NSCLC has been reported earlier (129). For instance, gemcitabine-loaded gelatin nanocarriers (130), paclitaxel-loaded nanocomposite microparticles (131), quinacrine-loaded bovine serum albumin modified cationic nanoparticles (129), pirfenidone-loaded liposomes (20) and lactoferrin/chondroitin-functionalized monoolein

www.manaraa.com

nanocomposites (132) etc. have been reported for their capability as inhaled nanocarriers in providing localized drug delivery in NSCLC treatment. In addition, Abdelaziz *et al* (127), Mangal *et al* (133), Ahmed *et al* (134) and Anderson *et al* (135) have also highlighted the significance of nanocarriers in pulmonary delivery along with details of further investigations being carried out. Particle size, surface morphology and mass median aerodynamic diameter (MMAD) of inhaled therapeutics determines their fate and the site of deposition in deep lungs (136). MMAD within the range of 2-5μm is essential for deep lung accumulation of particulate therapeutics, which is otherwise difficult to maintain due to inherent differences in particles' physicochemical properties. Variability in physicochemical properties brings immense variability in therapeutic performance, thus making scalability a major challenge (137,138).

In this study, we aim to investigate the utility of DoE based nanoparticle development using HPH and test the efficacy of optimized formulations in a relevant respiratory disease model. Here, we chose amodiaquine, 4-[(7-chloroquinolin-4-yl) amino]-2- [(diethylamino) methyl] phenol (AQ), an FDA approved anti-malarial compound (Basoquin), to formulate biodegradable polymer (PLGA)-based NPs using HPH and to evaluate their efficacy against NSCLC. While AQ has been approved as an anti-malarial therapeutic, it is also a potent autophagy inhibitor with an ability to induce apoptosis *in-vitro* (139,140). Qiao *et al* for the first time reported AQ's ability to cause autophagic-lysosomal and proliferative blockade in melanoma cells (139). Another recent report has also highlighted AQ for its drug repurposing efficiency through a structure-based screening approach (105). Non-small cell lung cancer (NSCLC) is also characterized by autophagy induction and deficits in apoptotic mechanisms for its pathogenesis (141), hence

www.manaraa.com

targeting these processes using AQ is of considerable interest. AQ makes an interesting model drug as (i) its long-term safety is well documented being a FDA approved molecule; (ii) there is no AQ nanoparticulate delivery system developed so far thus making it feasible to understand the effects of its physicochemical properties on formulation development and characterization. As discussed earlier, NSCLC is a disease of the deep lungs, and inhalation therapy is gaining importance in recent years due to successful local delivery of therapeutics to cancer cells in treating NSCLC, where NPs act as potential carriers (127). Combination of drug repurposing and nanotechnology have been reported for its efficacy in treating NSCLC by several researchers recently (32,42).

In this project, a 3^2 multifactorial design has been applied for better understanding of critical processes and formulation factors to ensure product quality with accepted Quality Target Product Profile (QTPP) for improved anticancer efficacy. The objective of this project is to formulate scalable, inhalable AQ-loaded PLGA NPs using HPH approach and to explore their efficacy in NSCLC.

3.2. Materials and Methods

3.2.1. Materials

Poly (lactic-*co*-glycolic) (PLGA 50:50, 25–35 kDa, acid terminated), polyethyleneimine (PEI), poly vinyl alcohol (PVA), and amodiaquine (AQ) were purchased from Sigma-Aldrich (St. Louis, MO, USA). A549, H4006, H358, H2122, H460 and H157 NSCLC cell lines were obtained from ATCC and maintained in RPMI medium (Corning) supplemented with 10% FBS (Atlanta Biologicals), sodium pyruvate, penicillin-streptomycin (Corning) at 5% CO_2/37°C. Human embryonic kidney cell line (HEK-293)

www.manaraa.com

was obtained from ATCC and maintained in DMEM medium (Corning) supplemented with 10% FBS (Atlanta Biologicals) and penicillin-streptomycin (Corning, NY, USA) at 5% CO_2/37°C. 3-(4,5-dimethylthiazol-2-yl)-2,5-diphenyltetrazolium bromide (MTT), dichloromethane (DCM), dimethyl sulfoxide, coumarin-6, crystal violet dye, 16% paraformaldehyde (PFA) solution, HPLC grade methanol, acetonitrile (ACN) and water were purchased from Fisher Scientific (Hampton, NH, USA). Molecular biology kits, supplies, and antibodies were purchased from other commercial vendors which are listed at appropriate places throughout the manuscript.

3.2.2. UPLC Method Development for Amodiaquine (AQ)

A reverse-phase liquid chromatography method was developed for quantifying AQ using Waters series Acquity UPLC (Waters, USA). The column used was Xselect™ HSS T3 (3.0 × 100 mm; 2.5 µm particles). The mobile phase consisted of aqueous phase of 0.1% orthophosphoric acid in water, and organic phase of ACN at 50:50 at a flow rate of 0.5 mL/min at 343 nm wavelength. Retention time was found to be 0.731 min with total run time of 1.5 min. Data were collected and analyzed using the Empower 3.0 software.

3.2.3. Optimization of Process and Formulation variables using Design of Experiment (DoE)

In this study, design of experiment (DoE) was used to develop nanoparticle formulations through which all potential factors were evaluated simultaneously, systematically, and quickly; using MINITAB statistical software (Minitab release 17, State College, PA, USA). Critical parameters such as probe homogenization speed and formulation variables involved in the formulation of nanoparticles were identified and were studied for their effect on drug loading which has been identified as a critical attribute while screening

www.manaraa.com

through DoE approach. The aim was to establish Quality Target Product Profile (QTPP) for drug-loaded nanoparticles with optimal characteristics of (i) the highest drug loading (>3%), (ii) lower particle size (<250 nm), along with (iii) uniform size distribution (polydispersity index of <0.1). These specifications were established according to the intended route of administration i.e., inhalation route to ensure product safety and efficacy. A 3^2 randomized full factorial design, in which two factors (PEI concentration and homogenization speed) were studied at three levels (i) PEI concentrations – 0, 0.5 and 1% (w/v) (ii) homogenization speed– 6,000, 12,500 and 25,000 rpm. A design-space was estimated from these two factors (probe homogenization speed and PEI concentration), with a risk of failure limit of ±30 mV zeta potential and 600nm particle size. The levels were chosen based on the preliminary studies performed to formulate nanoparticles using high pressure homogenization. Homogenization pressure of 30,000psi, reverse flow pattern, and number of cycles of 7 to circulate the formulation was kept constant throughout the study. Reverse flow pattern refers to the configuration where inlet and outlet fluids flow in opposite direction resulting in maximum shear, cavitation and impact. This results in products of desired quality due to the efficient emulsification during each pass through the emulsifying cell (142). Experimental trials (n=3) were performed at all nine possible combinations; coded as A1-A9. From this set of experiments, an optimized formulation with the highest % drug loading (>3%) and lower particle size (<250nm) will be identified to establish the optimal parameters for further studies. Experimental trials of factorial design containing different combinations are shown in **Table 1**. The effect of different variables on three different responses [i.e. particle size (PS), zeta potential (ZP) and drug loading (%DL)] was investigated.

www.manaraa.com

Optimized formulation, A6, with respect to predetermined particle size, zeta potential and entrapment efficiency, was subjected to further investigation to establish the optimal drug quantity to achieve QTPP as described earlier. Effect of different drug quantities (1, 2.5, 5 and 10 mg) on particle size, PDI, % entrapment efficiency (%EE) and % drug loading (%DL) is shown in **Table 2**. Formulations were coded as C1-C4. Other variables (including; formulation and operation parameters) were kept constant throughout the study. The association between dependent variables and responses was interpreted using response surface plots.

In brief, AQ NPs were formulated through high-pressure homogenization by modifying a method reported by Dong and Feng (143) with slight modifications. Briefly, coarse emulsion was prepared by homogenization of aqueous solution of AQ at 5mg/mL (Set I) or varying concentrations such as 2,5,10 and 20mg/mL (C1-C4) respectively and organic solution of PLGA RG-502H (20mg/ml of DCM) in aqueous 1% w/v PVA solution in 1X phosphate buffered saline (PBS; pH 7.4) with or without PEI at respective concentrations. Coarse emulsion was then processed through high-pressure homogenizer (Nano DeBee; BEE International, South Easton, MA, USA) at a pressure of 30,000psi for 7 cycles. The obtained emulsion was subjected for overnight stirring to remove organic solvent. Next day, nanoparticles were washed twice using 1X PBS by centrifugation at 21,000 RCF for 15 min, to remove excess PVA and unprocessed drug/polymer.

www.manaraa.com

3.2.4. Characterization of AQ NPs

3.2.4.1. Particle size, Poly Dispersity Index (PDI) and Zeta potential

Particle size, PDI and zeta potential were measured by dynamic light scattering (DLS) using Zeta Sizer (Malvern Instruments, Malvern, UK). Formulations were diluted 100-fold with milli-Q water to obtain samples for measurement of size and zeta potential. The respective samples were loaded into the zeta cells (DTS 1070) and analyzed.

3.2.4.2. Drug Content

To determine encapsulated drug amount in nanoparticle formulation, a direct vesicle lysis approach was carried out. To 20µL of formulation, 1,980µL of ACN:Water:DCM – 98:1.5:0.5 was added followed by centrifugation for 45 min at 4°C at 21,000 RCF to lyse nanoparticles. Clear supernatant was collected, analyzed for the drug content using UPLC as described earlier and % EE/%DL was calculated.

$$\%\ Entrapment\ efficiency\ (\%EE) = \left[\frac{Drug\ entrapped\ in\ nanoparticles}{Total\ drug\ added\ initially}\right] \times 100$$

$$\%\ Drug\ loading\ (\%DL) = \left[\frac{Drug\ entrapped\ in\ nanoparticles}{Total\ polymer + drug\ added}\right] \times 100$$

3.2.4.3. *In-vitro* Release Studies

In-vitro release studies were performed for determining the drug release pattern from optimized AQ NPs using dialysis method as reported previously (53). Briefly, 10,000 MWCO dialysis cassettes (Slide-A-Lyzer, 10,000 MWCO, 0.1–0.5 mL were preconditioned in PBS buffer (pH 7.4) for 10 min to allow them to get hydrated. Then, using syringe with 19G$1_{1/2}$ TW BD filter needle, 500µL of formulation was loaded into the

www.manaraa.com

cassettes membrane though one of the ports. The cassettes were immersed in a beaker with 150 mL of PBS buffer with 1% polysorbate 80 (pH 7.4; 37ºC) using a floater while stirring at a speed of 200 rpm. At regular time points of 0.5, 1, 2, 4, 8, 12 and 24 hours, samples were withdrawn with replenishing the dissolution medium with fresh PBS with 1% polysorbate 80. The amount of drug released was estimated using UPLC as discussed above.

3.2.4.4. Morphological Analysis using Scanning Transmission Electron Microscopy (STEM):

Morphology of nanoparticles was studied by Scanning Transmission Electron Microscope (STEM) using FEI Talos F200x Transmission/Scanning Transmission Electron Microscope (S/TEM) equipped with A-Twin objective lens operating in STEM mode. The samples were prepared by placing 10µL of the sample solution carefully on a lacey carbon-coated copper grids (300 mesh, Ted Pella Inc., Redding, CA, USA). The sample was allowed to adhere to the grid by subjecting it to air drying. The grids were then imaged using Smartcam digital search and view camera.

3.2.4.5. Solid State Characterization Studies:

Powder X-ray Diffraction (PXRD) Studies: X-ray diffraction spectroscopy was carried out using XRD-6000 (Shimadzu, Kyoto, Japan). The diffractometry was performed by using a graphite monochromator consisting of copper-Kα1 radiation of wavelength 1.5418 Å operating at 40 kV, 30 mA. The samples were spread uniformly on a glass micro sample holder and were analyzed in the range of 5 to 60° at the scanning speed of 2° (2θ)/minute.

www.manaraa.com

Differential Scanning Calorimetry (DSC) Studies: The thermograms for AQ, AQ NP, blank NP and physical mixture of AQ and blank NP were generated using a DSC 6000 (PerkinElmer, Inc; CT, USA) equipped with an intra-cooler accessory. An accurately weighed sample (1-5 mg) was sealed in an aluminum pan and analyzed over a temperature range of 30°C to 210°C and compared to a sealed empty aluminum pan maintained as reference. The heating rate was maintained at 10°C/min under a nitrogen purge having flow rate of 50 mL/min.

3.2.4.6. *In-vitro* Aerosol Performance Lung Deposition Test:

In-vitro lung deposition behavior of AQ NPs was evaluated using a M170 Next Generation Impactor™ (NGI: MSP Corporation Shoreview, MN, USA) in accordance with earlier published studies (144). The NGI was equipped with a stainless-steel induction port (USP throat adaptor) attachment and specialized stainless steel NGI™ gravimetric insert cups (NGI Model 170, MSP Corporation, Shoreview, MN, USA). AQ NP formulation (2 mL) was placed into a PARI LC PLUS® nebulizer cup of Pari FAST-NEB compressor system. (Boehringer Ingelheim Pharmaceuticals, Inc. Ridgefield, CT, USA), which was attached to a customized rubber mouth piece connected to the NGI™. A Copley HCP5 vacuum pump (Copley Scientific, UK) was used to produce a flow rate of 15 L/min. Using a Copley DFM 2000 flow meter (Copley Scientific, UK), flow rate was adjusted before each experiment. In brief, 2 mL of formulation was nebulized with PARI LC PLUS® nebulizer which passed through induction port into the NGI using pump at a flow rate of 15 L/min for 4 min. Prior to running the NGI, the plates were refrigerated at 4°C for 90 minutes to cool the NGI plates. Samples were collected from each stage i.e. Stages 1-8 including throat and induction port as well which is important in determining emitted dose through rinsing

www.manaraa.com

with ACN:water (75:25) and analyzed with established UPLC method for drug content and effective deposition at each stage. All experiments were performed in triplicate (n=3). Fine particle fraction (FPF, %) was determined as the fraction of emitted dose deposited in the NGI with d_{ae}< 5.39µm. Mass median aerodynamic diameter (MMAD, d_{ae}< 5.00µm) and geometric standard deviation (GSD) are the critical parameters for inhalation testing, and were calculated by quantifying the nanoparticle deposition at each stage in the NGI using log probability analysis (n=3) (144,145).

3.2.5. Stability Studies

Stability of the optimized AQ NP (C3) was evaluated while storing the samples at temperatures of 4ºC, 25ºC and 37ºC for four weeks as reported previously (53). Samples were withdrawn after week 1, 2, 3 and 4; diluted with water (100-fold) and analyzed for particle size, PDI and zeta potential using Malvern Zeta Sizer. Entrapment efficiency was determined by lysing the samples as described above using UPLC. All experiments were performed in triplicate.

3.2.6. Cellular Uptake Studies

Cellular uptake studies were performed using a protocol reported earlier (146). NPs for cellular uptake were formulated by replacing AQ with coumarin-6, a fluorescent dye, for easier tracking. In brief, A549 cells were plated in tissue culture treated cell imaging 8 chambered cover glass (Eppendorf, Hauppauge, NY, USA) at a seeding density of 10,000 cells/chamber followed by overnight incubation. Next day, cells were incubated with coumarin-6, coumarin-6 loaded nanoparticles at 1µg/mL concentration for 1 and 3 hours. After each interval, cells were washed with ice cold PBS twice and fixed with 4% PFA for

www.manaraa.com

10 min. Fixed cells were washed again with ice cold PBS twice. Then, the chamber was removed and 20µL of vectashield hardset mount with DAPI nuclear stain (H1500, Vector laboratories, Burlingame, CA, UAS) was placed on a glass slide dropwise followed by placing a cover glass. After hardening of mounting medium through overnight at 4°C, slide was imaged using EVOS-FL microscope (Thermo Scientific, Waltham, MA, USA).

3.2.7. Cytotoxicity Studies

AQ NPs along with plain AQ were evaluated for their cytotoxicity in six different non-small cell lung cancer (NSCLC) cell lines: A549, H157, H358, H2122, H460 and H4006 as reported earlier with slight modifications (146,147). Briefly, cells were grown in FBS supplemented RPMI-1640 media as described in *Materials* section, and were seeded in TC treated 96-well plates (Eppendorf, Hauppauge, NY, USA) at a seeding density of 2,500 cells/well (7,500 cells/cm^2), incubated overnight for adherence at 37ºC/5% CO_2, and treatments were added next day at different AQ concentrations ranging from 0.39-100µM. Corresponding volumes of AQ NPs were calculated based on the drug entrapment efficiency. Blank culture media was added as control. After 72 hours of incubation, % cell viability was determined by performing MTT assay as described earlier (147), by reading the absorbance of dissolved formazan crystals at 570nm (Tecan Spark 10M; Tecan, Männedorf, Switzerland). AQ and AQ NP were also tested for their cytotoxicity efficacy against A549 cells with different incubation periods of 6 and 12 hours. The safety of AQ NP formulations was determined by evaluating the cytotoxicity of Blank-NPs on human embryonic kidney (HEK-293) cell line. Briefly, cells were seeded into 96-well plates as described earlier and were incubated overnight followed by treatment with equivalent

www.manaraa.com

amounts of Blank-NP corresponding to 10µM of AQ NP for 72 hours. % cell viabilities were determined through MTT assay as described earlier.

3.2.8. Scratch Assay

In-vitro scratch assay was used to study the cell migration. Briefly, scratches were created on a confluent cell monolayer. The cells on the edge of the scratch will migrate toward the center to close the scratch, thus establishing new cell-cell contacts. The assay was performed as previously reported (148). Briefly, A549 or H460 cells were plated in 24 well cell culture plates at a seeding density of 1 x 10^5 cells/well followed by overnight incubation. Next morning, scratches were made along the center of all wells with the help of a sterile p200 (200µL) pipette tip. All the wells were washed with PBS twice and reference markings were drawn near the scratch area from the bottom side of the plate with a fine tip marker. Then scratch images were captured within the marked area using inverted microscope (Laxco, Inc., Mill Creek, WA, USA) with 10X magnification. Later treatments of control, AQ, AQ NP (10µM) were added to the respective wells and incubated followed by imaging after 24 and 48 hours (A549); 24 and 120 hours (H460). The images captured were analyzed quantitatively to assess the inhibitory effect of nanoparticles on cell migration. Scratch width was measured from all wells using ImageJ software and % scratch closure was calculated further.

3.2.9. Clonogenic Assay

Clonogenic assay is an *in-vitro* cell survival assay which is based on the single cell's capability to grow into a colony. Using this assay, the effectiveness of the AQ and AQ NPs toward colony inhibition was determined. The protocol reported previously (146,149) was

www.manaraa.com

briefly modified and followed in this study. A549 or H4006 cells were seeded into 6-well cell culture plates at seeding density of 500 cells per well for each cell line. Plates were kept for overnight incubation to allow time for cells to adhere. Next day, media was replaced, and cells were treated with AQ or AQ NPs (10μM), or control for 48 hours after which media was replaced with fresh culture medium on alternative days for 7 days. On 7^{th} day, the colonies were stained with crystal violet. Briefly, the contents of the well were removed and washed with ice-cold PBS buffer twice followed by fixation with 4% PFA solution (in ice-cold PBS) for 10 min. Fixed cells were again washed with ice-cold PBS twice followed by staining with 0.01% (w/v) crystal violet solution with 1-hour incubation. After staining cells were washed with distilled water and images were captured using digital camera. Cell colonies were counted by colony counter software Open CFU (150).

3.2.10. 3D Spheroid Study

An effective NSCLC therapy is not only determined by enhanced cellular uptake or cytotoxic potential, but also improved penetrability of nanoparticles into solid tumors. 3D spheroid cell culture studies are capable of mimicking the *in-vivo* features of tumors as reported in our previous studies (147). Briefly, 2,000 cells per well were seeded in Nunclon Sphera 96-well U bottom plates, and were allowed to grow into solid tumor mass due to the shape of these ultra-low attachment cell culture plates. This *in-vitro* spheroid study was conducted through two kinds of models i.e. prophylactic and therapeutic models, differing in tumor growth and treatment strategies.

In prophylactic study, 2,000 cells (A549) were seeded into each well of Nunclon Sphera 96 well ultra-low attachment treated spheroid microplates (Thermo Fisher

www.manaraa.com

Scientific, Waltham, MA, USA) and incubated overnight under standard conditions of 37°C/5% CO_2. Next day, media was replaced with either fresh media (control) or respective treatment solutions of AQ or AQ NP to achieve 10 and 25 µM in the wells. On day 1, all the wells were observed for spheroid formation with a rigid margin. Images were captured using inverted microscope (Laxco, Mill Creek, WA, USA) on day 3, 5, 7 10 and 12. NIH ImageJ software was used to measure diameter of all the spheroids. Spheroids were treated on respective days by replacing half of the medium (100µL) from every well with respective treatments in a gentle manner to avoid the bubble formation and the aspiration of spheroid itself.

In therapeutic 3D model, A549 cells were seeded into Nunclon Sphera plate at density of 500 cells/well and were incubated at 37°C/5% CO_2. Then, all wells were observed for spheroid growth and images were captured on day 1, 3, 5 and 7. On day 7, spheroids were subjected to two kinds of dosing treatments i.e. a single dose and a multiple dose treatment. Briefly, both single and multiple dosing spheroids were treated with 20µM and 50µM concentrations of AQ and AQ NP (to maintain original concentrations of 10 and 25µM employed in the beginning), and images were captured. For single dosing, 100µL of media was replaced with fresh media on further days of imaging. For multiple dosing, wells were replenished with 10 and 25µM concentrations of AQ, AQ NP or fresh media (control). Images were captured on day 3, 7 and 10 and 15 days following treatment.

3.2.11. Live-Dead cell assay

Live-dead cell assay was performed on spheroids on day 15 of single and multiple dosing in therapeutic model according to manufacturer's protocol. Briefly, 100 µL of 2µM calcein AM/4µM Ethidium homodimer III (EthD-III) staining solution was added to spheroids

www.manaraa.com

after complete removal of media from the respective wells. The plate was incubated for 45 min at room temperature. This provides green/red fluorescent staining of viable and dead cells, respectively. Images were captured using (EVOS-FL, Thermo Fisher Scientific) and mean green fluorescence intensity/mm^2 of spheroid was quantified using ImageJ software which signifies the presence of live cells in spheroid mass.

3.3. Mechanism of Action

3.3.1. Autophagy Inhibition Microplate Assay

Autophagy enables cancer cells to survive under micro-environmental stress conditions and promotes tumorigenesis (151). While AQ is a known autophagy inhibitor, it is crucial to determine the capability of AQ NPs to inhibit autophagy. Autophagy inhibition microplate assay was performed using CYTO-ID® Autophagy Detection Kit (Enzo Life Sciences, Farmingdale, NY, USA). In brief, A549 cells were plated at density of 2.5 x 10^4 cells/well in 96 well plate (Fisher scientific, Hampton, NH, USA), and starved for 24 hours in serum free media, and were later incubated with AQ 10µM, AQ NP 10µM or drug-free control for 18 hours. Treatments were replaced with 100µL of 1X assay buffer followed by addition of 100µL of dual color detection reagent (CYTO-ID® Green Detection Reagent + Hoechst 33342 nuclear stain in cell culture medium without phenol red indicator supplemented with 5% FBS). Plates were protected from light and incubated for 30 min at 37°C. Later, cells were washed with 200 µL of 1X assay buffer to remove excess dye. Then 100µL of 1X assay buffer was added to each well, and plates were read with a FITC filter (Ex ~480nm, Em ~530; green detection reagent), and with a DAPI filter set (Ex ~340nm, Em ~480nm; Hoechst 33342 Nuclear Stain). Here, CYTO-ID® Green

www.manaraa.com

Detection Reagent serves as a bright fluorescent probe in vesicles produced during autophagy (152).

3.3.2. Apoptosis: Caspase 3/7 Assay

Apoptosis, or programmed cell death, plays a critical role in assessing the potency of drug delivery systems. Caspase-3 is one of the major markers of apoptotic cell death, which can be activated in apoptotic cells both by extrinsic and intrinsic pathways (153). AQ and AQ NP were tested for their cytotoxicity efficacy against A549 cells with different incubation periods as well. Representative graph related to their cytotoxicity after 6 and 12 hours can be found in **Figure 17A.** After 6 hours of incubation, no significant difference was observed between AQ and AQ NP in their cytotoxicity potential. Hence, incubation period of 6 hour and treatment concentration of 10µM were chosen in performing the present assay. Caspase-3 activity was measured using EnzChek™ Caspase-3 Assay Kit (Molecular Probes, Eugene, OR, USA) and assay was performed as per manufacturer's specifications. Briefly, A549 cells were seeded at a density of $1x10^6$ cells per tissue culture dish (100 mm diameter) (Thermo Scientific, Rochester, NY, USA) and treated with AQ, AQ NP (10µM) or control for 6 hours followed by harvesting and washing of cell pellets. Cell lysis was carried out using 1X cell lysis buffer while subjecting to freeze-thaw cycle, followed by centrifugation at 3,000 RCF for 5 minutes. Supernatants obtained were transferred to 96 well plate to which 50µL of 2X substrate working solution (10mM Z-DEVD-AMC substrate + 2X reaction buffer) was added and incubated for 20 min. Fluorescence was measured at excitation/emission 342/441nm (154).

www.manaraa.com

3.3.3. *In-vitro* Angiogenesis study

Angiogenesis or formation of new blood vessels from preexisting vasculature is a key process in some physiological conditions including cancer pathogenesis. Angiogenesis have a pivotal role in pathogenesis of NSCLC among other cancer kinds in the form of over-proliferation of blood vessels (155). To understand AQ loaded nanoparticles' anti-angiogenic ability, angiogenesis assay was performed as per manufacturer's instructions (3470–096-K; R&D Systems, Minneapolis, MN, USA). Briefly, human umbilical vein endothelial cells (HUVEC: LONZA, Basel, Switzerland) cells were seeded into a T-25 flask prior to performing angiogenesis assay. Next day, 50 µL of Cultrex® RGF BME was aliquoted into each well of a 96 well plate and incubated at 37 °C for 60 minutes to allow the BME to gel. HUVEC cells were then labeled with 2µM calcein AM; seeded at 1.3x 10^4 cells/well on BME coated 96-well plates after preparing dilutions of AQ and AQ NP (10µM). Cells were incubated for 6 hours at 5% CO_2/37 °C. Images were taken using fluorescence microscope (EVOS-FL, Thermo Fisher Scientific, Waltham , MA, USA) and tube formation was evaluated and quantified using NIH ImageJ software with the angiogenesis analyzer plug-in (156).

Statistical Analysis:

All data were addressed as mean ± SD or SEM, with n=3 unless otherwise mentions. Three trials of cytotoxicity studies were performed for each control or treatment with n=6 for each trial. data Unpaired student's t-test was used to compare two groups and one-way ANOVA followed by Tukey's multiple comparisons test was used to compare more than two groups using GraphPad Prism software (Version 7.04 for Windows, GraphPad Software, San Diego, California USA). A p value of <0.05 was considered statistically

www.manaraa.com

significant and was presented in data figures as a single asterisk (*). However, some studies have demonstrated a smaller *p*-value of 0.01 or less, which is included at respectively places.

3.4. Results

3.4.1. UPLC Method Development for Amodiaquine

A rapid, UPLC method was developed for determination of AQ. Retention time was found to be 0.731 min with run time of 1.5 min. Peak was eluted with good resolution. A representative chromatogram is presented in **Figure 4A**. The method provided excellent linearity between 0.05 to 6 µg/ml.

Optimization of Process and Formulation Variables using Design of Experiments (DoE):

As presented in **Table 3**, adopted Minitab® 18 software provided a numerical optimization technique to produce set of formulations with anticipated responses such as lower particle size, positive zeta potential with highest % drug loading. The developed model of experimental runs for three quality attributes supported the proposed design space. Accordingly, the acceptable region that fulfills those targeted features is achieved when 1% or <1% (w/v) PEI is used in nanoparticle preparation. Results revealed that PEI concentration had great impact on particle size, zeta potential and % DL; each studied at three levels. As for particle size, it was found that particle size increased with increasing PEI concentration, at same homogenization speed, while positive zeta potential was observed only at PEI concentration of ≥0.5% w/v. % DL was found to be higher in case of 0.5% and 1% w/v

www.manaraa.com

PEI. Positive charge density of PEI enhances encapsulation of weakly basic drug molecules such as AQ (157).

Table 3: Composition and Characteristics of Amodiaquine Loaded Nanoparticles in a 3^2 Full Factorial Design

Formulation	Coded Value		Particle Size (nm)	PDI	Zeta Potential (mV)	% Entrapment Efficiency	% Drug Loading
	X1	X2					
A1	-1	-1	211.57±37.5	0.33±0.2	-18.7±5.1	22.0± 7.8	0.9±0.3
A2	-1	0	202±3.6	0.23±0.1	-13.0±1.8	24.8±10.9	1.0±0.4
A3	-1	+1	195±5.5	0.22±0.0	-13.5±6.4	31.8±1.5	1.3±0.1
A4	0	-1	382±60.1	0.30±0.2	10.2±5.9	41.5±2.6	1.7±0.1
A5	0	0	453.73±88.9	0.38±0.1	7.3±3.3	77.2±28.4	3.1±1.1
A6	0	+1	214.66±2.9	0.31±0.0	11.8±3.4	70.8±11.3	2.8±0.5
A7	+1	-1	235.5±45.0	0.23±0.1	15.2±5.3	61.5±20.7	2.5±0.8
A8	+1	0	544.2±70.6	0.41±0.1	14.2±12.2	51.1±12.9	2.0±0.5
A9	+1	+1	645.76±92.0	0.35±0.1	17.9±5.7	78.5±3.5	3.1±0.1

Coded Values	Actual Values	
	X1	X2
-1	0	6000
0	0.5	12500
+1	1	25000

Drug Quantity: 2.5mg
Polymer: PLGA 502H
EAP: PVA 1% (w/v)
Probe Homogenization Time: 10min
X1- Polyethyleneimine concentration (%w/v) in EAP, X2-Probe Homogenization speed (RPM), EAP-External Aqueous Phase, PDI-Poly Dispersity Index

Results showed that coarse homogenization speed could only affect particle size; while having negligible effect on zeta potential and drug entrapment. Coarse homogenization at 6,000 rpm resulted in smaller particle size compared to 12,500 and 25,000 rpm; at all PEI concentrations. Largest particle size (645.8±92.0nm) was observed in formula (A9); containing 1% PEI and homogenized at 25,000 rpm. At 0.5% PEI concentration, increase in speed from 6,000 to 25,000 rpm rendered a concomitant increase in the breaking energy, resulting in smaller emulsion droplets (158). For future investigations on effect of initial drug amount on PS, ZP, %EE and %DL, an optimized formula was selected through relating constraints between independent variables and dependent responses. The criteria for optimized formulation was set to be demonstrating the highest % drug loading (>3%)

www.manaraa.com

and lower particle size (<250nm). According to obtained results, formulation A6 (0.5% PEI, 25,000 rpm) was selected for further optimization. Even though, A7 had the highest entrapment and lower particle size, it was not chosen considering the presence of highest concentration of PEI, a cationic polymer, with potential of intracellular toxicity. While both A5 and A6 exhibited significantly higher % drug loading (>3%), only A6 resulted in optimal particle size (214.7±2.9nm). Hence, parameters pertaining to A6 were chosen for further experimental trials to optimize drug quantity.

Results describing effect of varying initially loaded drug amount on particle size, zeta potential and entrapment efficiency are demonstrated in **Table 4**. From results, it can be observed that increasing initial drug loading led to subsequent increase in %EE and

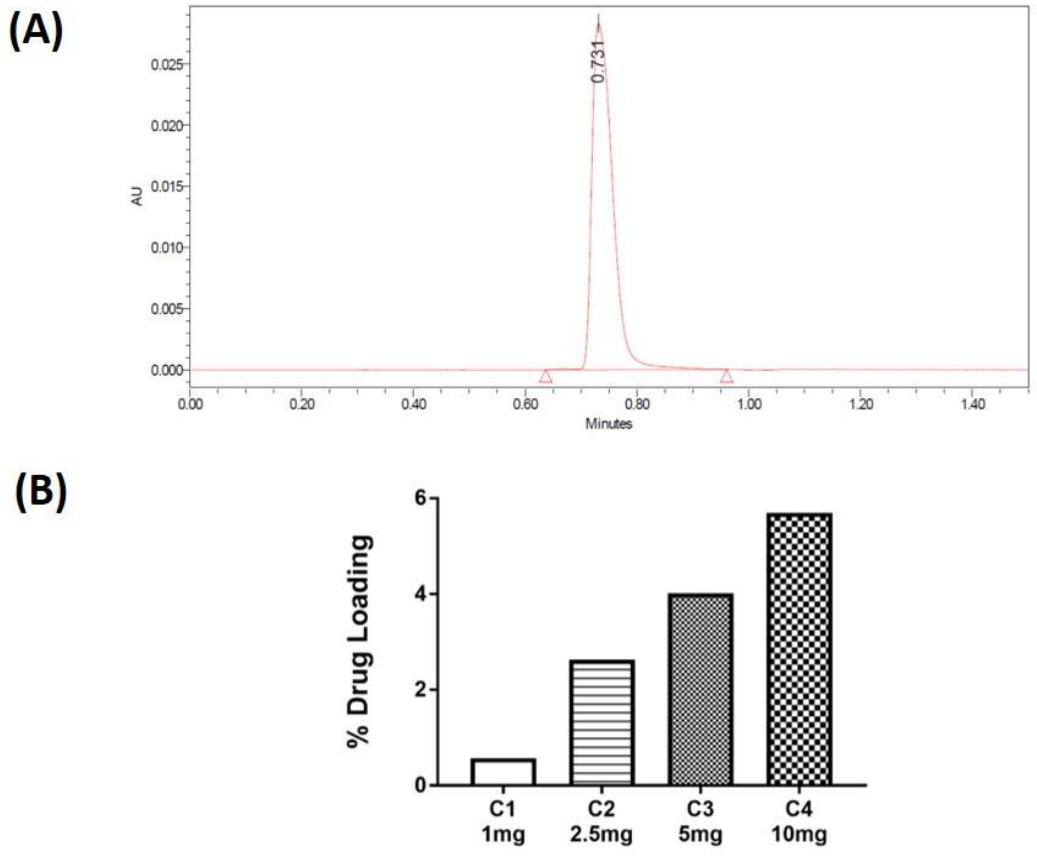

Figure. 4. A. UPLC chromatogram of amodiaquine. **B.** Effect of drug quantity on % drug loadings of AQ NP of amodiaquine

www.manaraa.com

%DL. The highest %DL was observed in formula C3 and C4, loaded with (5 and 10 mg) amodiaquine; 4.0% for C3 and 5.7% for C4 respectively **(Figure 4B)**. Formula (C3; further denoted as AQ NP) containing 5 mg amodiaquine was chosen to be the best achieved formulation, as it showed higher %EE (52.3%) compared to C4 (39.8%), thus indicating significantly less wastage of starting raw material, as seen in **Table 4**.

Moreover, C3 was found to exhibit a particle size of 229.4nm with a PDI of 0.058 i.e. an almost monodispersed nanoparticle formulation. These studies revealed that C3 (AQ-NP) was able to meet the specification set as per QTPP. Hence, further *in-vitro* studies were performed using C3 formulation which is denoted as AQ NP.

Table 4: Characterization of different formulations with different drug quantities

Formulation	Drug Quantity (mg)	Particle Size (nm)	PDI	Zeta Potential (mV)	% Entrapment Efficiency	% Drug Loading
C1	1	222.9	0.2	11.3	35.3	0.6
C2	2.5	211.5	0.1	10.1	65.7	2.6
C3	5	229.4	0.1	17.8	52.3	4.0
C4	10	229.9	0.2	14.3	39.8	5.7

3.4.2. Characterization of AQ NPs

3.4.2.1. Particle Size, Polydispersity Index (PDI), Zeta Potential

Nanoparticle formulation (C3) was found to have a particle size, PDI and zeta potential of 250.3±43.0nm, 0.18±0.1 and 16.96±1.0mV respectively. Formulations were found to have a positive zeta potential due to the presence of PEI. A histogram representing particle size distribution of C3 can be found in **Figure 5A** representing uniform particle size distribution with single peak.

www.manaraa.com

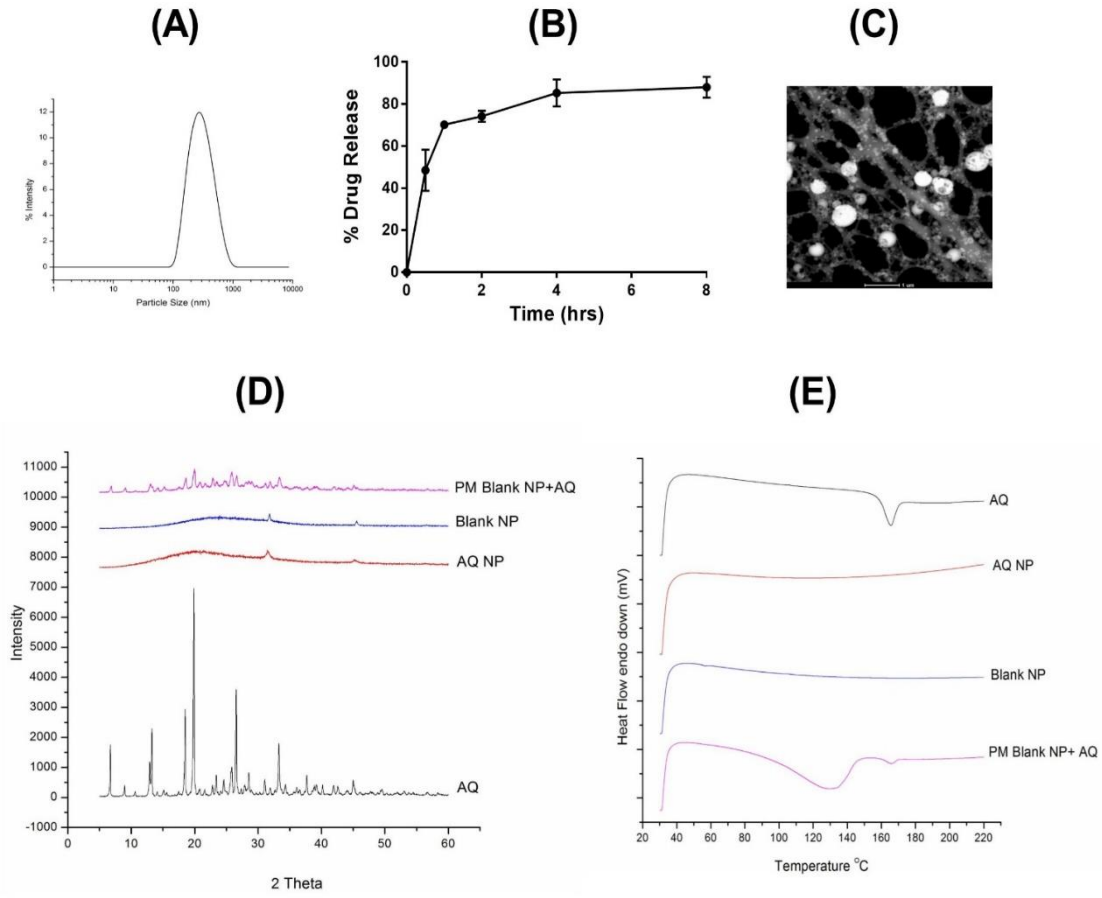

Figure 5. Physicochemical characterization of nanoparticles.

3.4.2.2. Drug Content:

As shown in **Table 3**, A6 was found to be an optimized formulation among A1-9 with lower particle size and highest % DL. It was found that C3 had the highest % EE of 52.3% along with high % DL (4.0 %) as seen in **Table 4** and **Figure 5D**. C3 was chosen for further studies and denoted as AQ NP.

3.4.2.3. *In-vitro* release studies:

In-vitro release studies were performed to determine the drug release pattern from AQ NP (C3) in phosphate buffered saline (PBS; pH 7.4, 37°C) to mimic physiological fluid

www.manaraa.com

environment. The AQ NP (C3) was found to exhibit a controlled release pattern with about 80% (85.3±6.4%) drug being released after 4 hours as shown in **Figure 5B**. This reveals the ability of nanoparticles to release drug completely in 4-8 hours after reaching physiological environment.

3.4.2.4. STEM studies:

A representative STEM image presented in **Figure 5C** indicated that the nanoparticles had uniform spherical shape with a smooth surface. As anticipated based on zeta potential measurement, no aggregation of nanoparticles was observed during STEM analysis. This reveals the uniform dispersion of nanoparticles in the formulation. These results agree with DLS measurements.

3.4.2.5. Solid State Characterization:

Powder X-ray Diffraction (PXRD): Due to its crystalline nature, AQ showed distinct peaks at 2θ values of 19.88 and 25.88 in XRD spectra whereas there were no AQ peaks present in AQ NP indicating encapsulation of drug inside the nanoparticles as shown in **Figure 5D**. Results were found to be consistent with earlier studies of artesunate-amodiaquine microparticles (159). Physical mixture of Blank NP and AQ also exhibited peaks inferring the crystalline nature of drug.

Differential Scanning Calorimetry (DSC): The DSC studies were performed to understand melting and crystallization behavior of AQ when present in different forms such as NP encapsulated AQ, physical mixture with blank NPs, as compared to control. As can be seen in **Figure 5E**, thermogram of AQ showed a sharp endothermic peak at 166.8°C due to its melting transition. The absence of a sharp peak in AQ NP indicated complete

www.manaraa.com

drug encapsulation in the nanoparticle formulation core and suggested a consistent result with that of XRD as discussed above. Results found to be consistent with earlier studies (160).

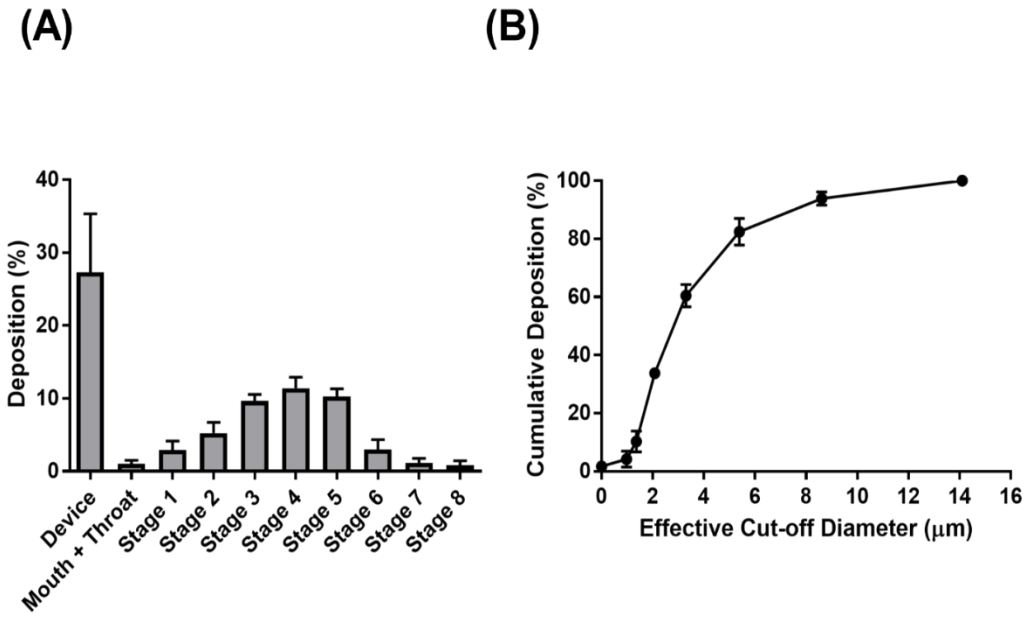

Figure 6. *In-vitro* deposition profile of AQ NPs. **A.** Aerosol dispersion performance as % deposited on each stage of the NGI™. **B.** Cumulative % deposition plot representing cumulative % of particles deposited at each stage.

3.4.2.6. *In-vitro* Aerosol Performance and Lung Deposition:

Once nebulized, aerodynamic properties of particles govern their deposition profile in the airways and alveolar deep lung regions. Using a next generation cascade impactor (NGI), crucial parameters to determine respirability of the nanoparticles were determined. Mass median aerodynamic diameter (MMAD), which describes the aerodynamic particle size distribution of an aerosol by mass, and geometric standard deviation (GSD), which describes the spread of the aerodynamic particle distribution, were determined. The MMAD of AQ NP was 4.7±0.1μm suggests that majority of the emitted dose will be

www.manaraa.com

delivered to respirable region of the lungs, while the GSD was 2.0±0.4µm. The % fine particle fraction (FPF), also called the respirable fraction, was 81.0±9.1% as shown in **Table 5** which suggests good aerosolization performance. Aerosol dispersion profile at each stage of NGI, and a graph representing % cumulative deposition respective to each stage can be seen from **Figures 6A & 6B** respectively. Particle size distribution is one of the most important parameters in inhalational delivery which determines efficiency of the delivery system to deliver the particles deep enough to the alveolar region (161). These data suggest that the prepared formulations possess all the characteristics to render them inhalable with deep lung deposition.

Table 5: *In vitro* Aerosol Deposition Profile of Amodiaquine Nanoparticles.

Formulation	MMAD (µm)	Recovery (%)	FPF (%)	GSD (µm)
C3	**4.7±0.1**	**72.8±25.1**	**81.0±9.1**	**2.0±0.4**

3.4.3. Stability Studies

Stability is a major concern while dealing with nanosized drug delivery systems due to emulsion instability and particle aggregation (53). As shown in **Figure 7**, stability analysis data reveal that AQ NP formulation was stable at 4º and 25ºC, with no significant changes in particle size or zeta potential **(Figures 7A & 7B)**. Here, the positive zeta potential of the AQ NP prevents the particles from coalescing and aggregating. There was no detrimental effect of temperature and storage time on entrapment efficiency either. Hence, the formulations were found to retain their physicochemical properties during their storage at different temperatures of 4°C and 25°C over a period of 4 weeks. Formulations stored at

www.manaraa.com

37°C to expose them for temperature excursions (162) and were found to exhibit increased particle size which could be due to coalescence. However, regular labeled storage conditions do not include 37°C.

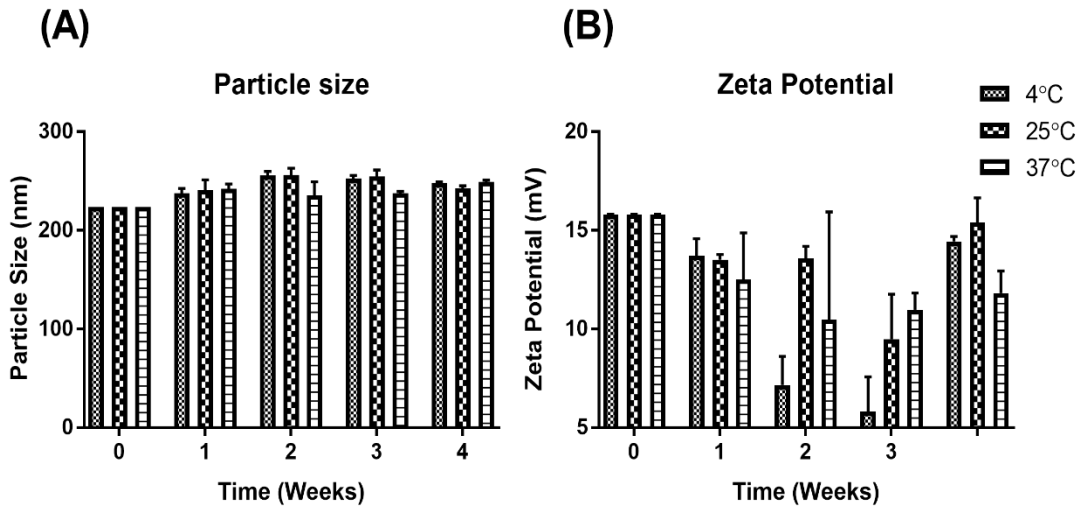

Figure 7. Influence of storage temperature and length of storage on **(A)** particle size and **(B)** zeta potential of amodiaquine nanoparticles.

3.4.4. Cellular Uptake Studies

Figure 8 represents intracellular uptake of nanoparticle formulations using A549 NSCLC cells. In this experiment, AQ was replaced with fluorescent coumarin to make it possible to visualize the uptake and accumulation. Fluorescent images taken following 1- and 3-hour incubation with coumarin loaded nanoparticles clearly demonstrated significant internalization compared to plain coumarin in A549 cancer cells even after 1-hour incubation period. It can also be observed that there was higher accumulation of the Coumarin-NP around the nucleus (DAPI stained), the most evident location for nanoparticle disruption and drug release inside the cells (163). Presence of positive charge

www.manaraa.com

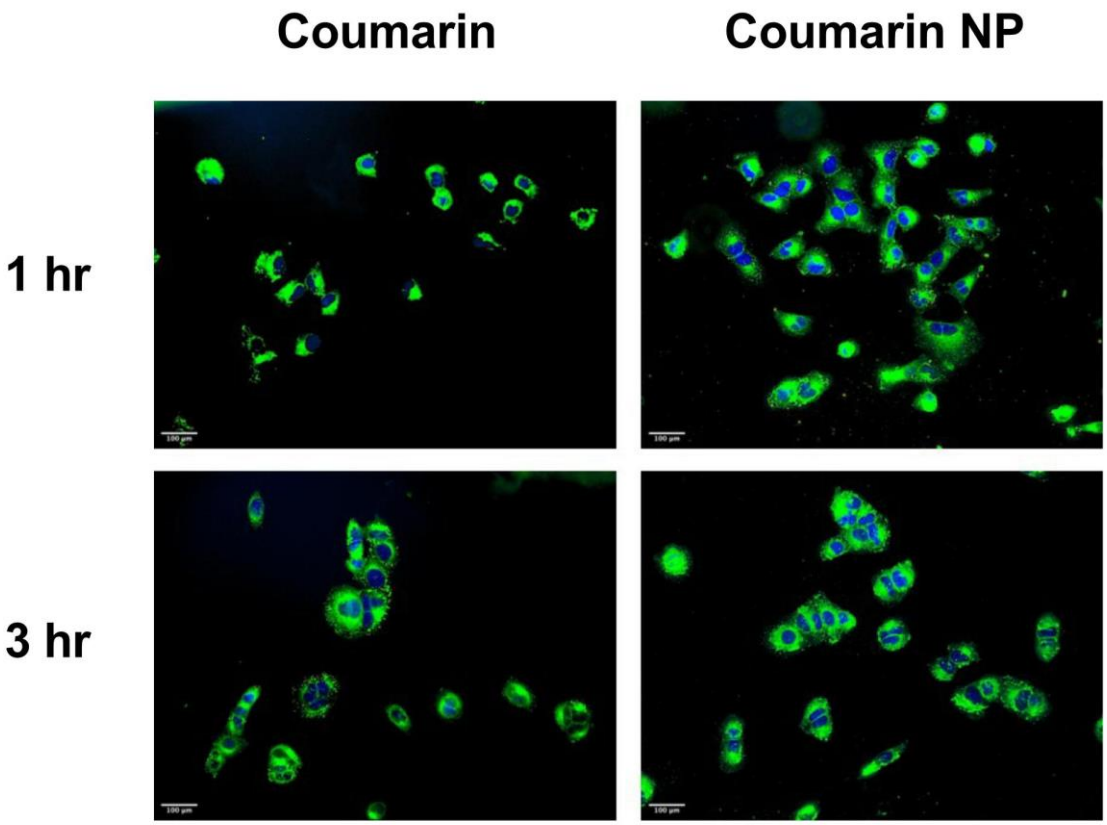

Figure 8. Representative *in-vitro* cellular uptake of coumarin-6 loaded nanoparticles by A549 cells at two different time points; 1 h and 3 h. Scale b*ar* 100µm.

on the Coumarin-NP enables interaction of nanoparticles with cell surfaces (negatively charged), thus further resulting in efficient cellular internalization.

3.4.5. Cytotoxicity Studies

Cell viability studies were performed using MTT assay to evaluate the cytotoxic potential of AQ-loaded NPs versus plain drug. From this study, it was revealed that AQ cytotoxicity against NSCLC cell lines was significantly enhanced by nanoparticle encapsulation. Similar trend was found in all six NSCLC cell lines: A549, H4006, H157, H358, H2122 and H460. **Figure 9** illustrates the cytotoxic effects of AQ and AQ NP in all six NSCLC cell lines. The IC_{50} values for plain AQ and AQ NP were found to be 21.8±8.3µM, and

www.manaraa.com

9.4±2.1µM in A549 cell line; 14.4±1.6µM, and 1.9±0.5µM in H2122 cell line; 22.5±2.3µM, and 16.3±2.8µM in H157 cell line; 28.8±17.7µM, and 10.3±10.2µM in H460 cell line; 28.8±9.7µM, and 13.5±5.3µM in H4006 cell line; 35.7±9.7µM, and 13.6±8.0µM in H358 cell line respectively **(Table 6).**

Smaller and consistent particle size and positive surface charge of AQ NP facilitates efficient internalization of nanoparticles resulting in more accumulation of nanoparticles

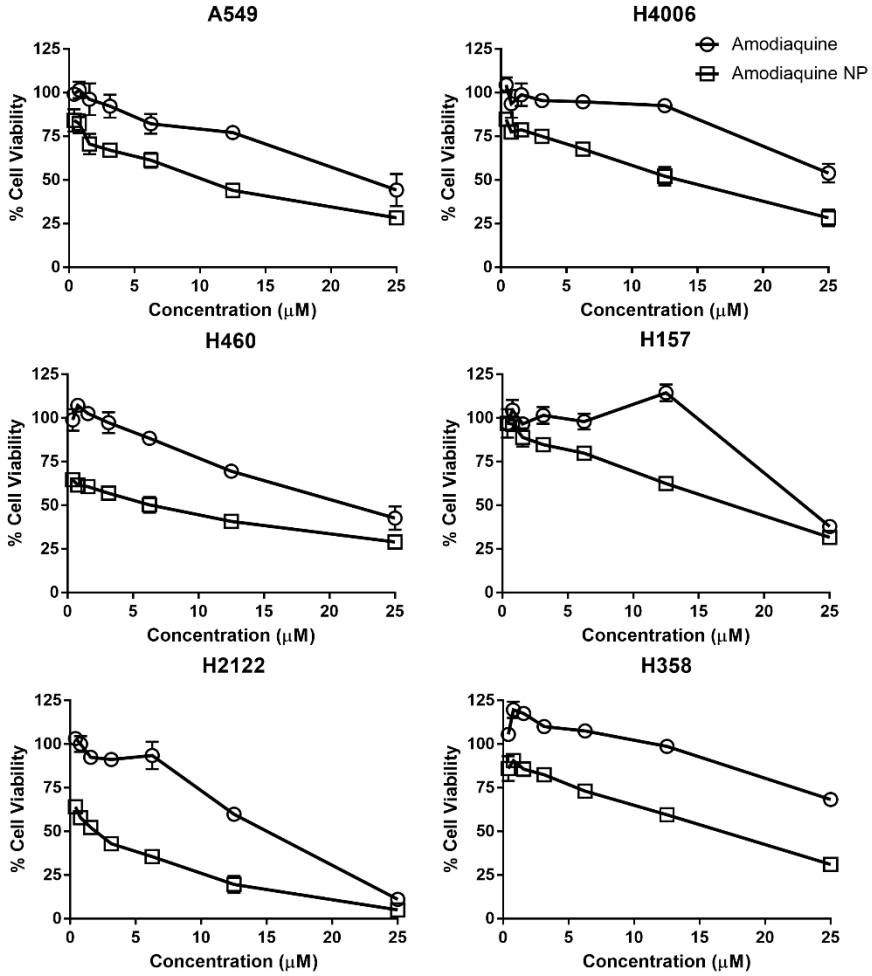

Figure 9. Inhibitory effects on different NSCLC cells after treatments with amodiaquine (AQ), and amodiaquine nanoparticle (AQ NP).

inside the cells, thus leading to higher cytotoxic potential at the same dose. From 6 and 12 hours cytotoxicity study, it was observed that toxicity towards A459 was found at *In-vitro*

www.manaraa.com

studies to establish safety of optimized nanoformulation were performed on HEK-293 human embryonic kidney cell line. When HEK cell line was treated with blank drug-free AQ-NP equivalent nanoformulation equivalent to 10µM AQ for 72 hours, cell viability of >80% (81.7±12.4%) suggested that optimized AQ-NP was not toxic to HEK cells, in absence of the drug. The tested concentration of 10µM was chosen based on the observed IC_{50} values from cytotoxicity studies in NSCLC cell lines. These observations were expected since polymer used to prepare nanoparticles have long been known to produce little or no cytotoxicity. The safety profile of nanoparticles has been presented in **Figure 17B.**

Table 6: Comparison of IC_{50} for AQ and AQ NP in Different NSCLC cell lines. Data represent mean±SD (n=6) for 3 independent trials.

Cell Line	**IC_{50} (µM)**	
	AQ	**AQ NP**
A549	21.8±8.3	9.4±2.1[a]
H2122	14.4±1.6	1.9±0.5[b]
H157	22.5±2.3	16.3±2.8[c]
H460	28.8±17.7	10.3±10.2[d]
H4006	28.8±9.7	13.5±5.3[e]
H358	35.7±9.7	13.6±8.0[f]

a, b, c, e, f: ****; d: ****
***p (α < 0.001), ****p (α < 0.0001)

3.4.6. Scratch Assay

Scratch assay is a well-established method to access cell-cell interaction, and cellular migration (148). For these experiments, a scratch was made as described earlier, cells were treated with AQ or AQ NP or fresh media (control), and images of scratched area were taken at respective time points.

www.manaraa.com

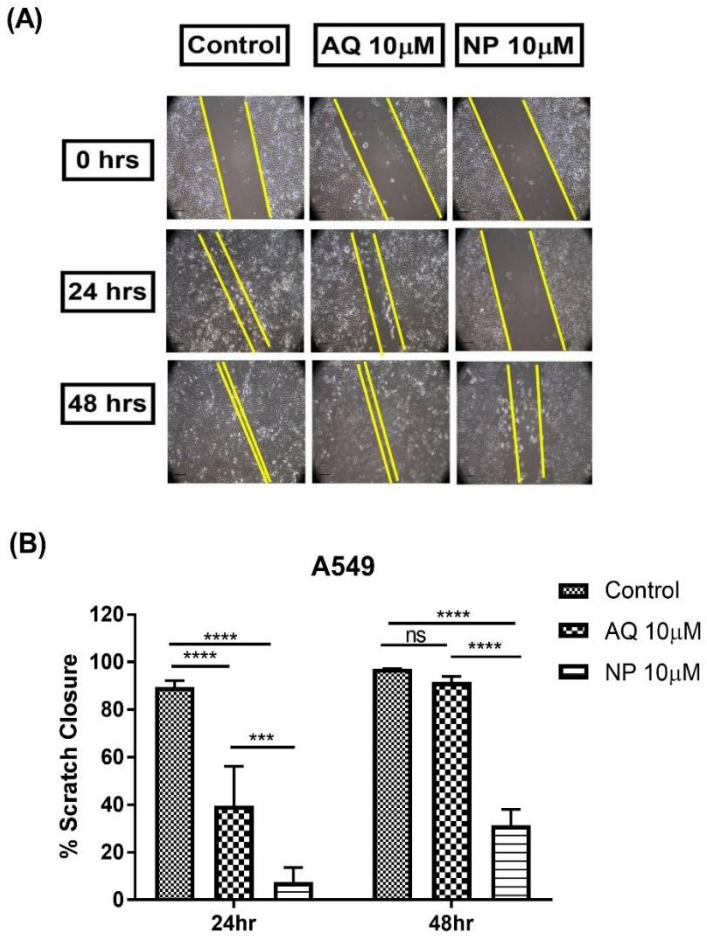

Figure 10. *In-vitro* scratch wound healing assay with A549 cells treated with AQ and AQ NP with no treatment as a control. **A.** Shows representative images for indicated treatments. **B.** The graph shows % area closure of scratch after 24 and 48hrs. Scale Bar 500μm. Images were taken at 10X magnification.

Figure 10A represents images at 0, 24 and 48 hours following treatment in A549 cells. After 48 hours, % scratch closure was found to be 97.2±0.1, 91.7 % ± 2.3 and 31.4% ± 6.8 for control, AQ 10μM and NP 10μM respectively in case of A549 (AQ 10μM vs NP 10μM; $p<0.0001$). From **Figure 10A & 10B**, it can be understood that scratches treated with control and AQ show migration of cells and those treated with AQ NP didn't exhibit any significant cell migration or scratch closure. Similarly, AQ NP also inhibited scratch closure in case of H460 cell line as well, imaged at 0, 24 and 120hrs (not shown); respective

www.manaraa.com

graph can be found in **Fig 11**. This indicates the efficacy of AQ NP with enhanced anti-migratory effects, thus reducing the tumor metastasis probability.

3.4.7. Clonogenic Assay

Clonogenic assay is an *in-vitro* cell survival assay used to determine the colony formation capability of single cancer cells (164). AQ and AQ NP were evaluated for their long-term efficacy using clonogenic assay in two different NSCLC cell lines, A549 and H4006. From **Figure 12A**, it can be illustrated that colony growth was significantly inhibited by AQ NP compared to AQ, in both A549 and H4006 cell lines. After 48-hour treatment period and 7-day incubation, % of colonies survived after treatment with 10µM AQ or AQ NP were 94.5±15.5%, 27±3.0% (A549; **Figure 12B,** $p<0.001$); and 49.3±6.2%, 13.7±3.0% (H4006; **Figure 12C,** $p<0.0001$) respectively, considering number of colonies to be 100% in drug free treatment control wells **(Figure 12B & C)**. The data suggest an approximately 4-fold higher efficacy against cancer colony formation with AQ-loaded NPs as compared to plain AQ. This data may be considered a representative of AQ NP's efficacy in

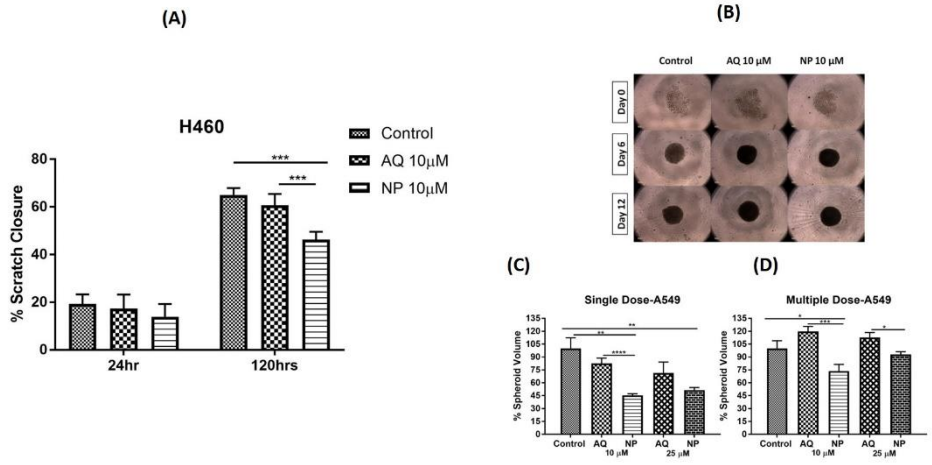

Figure 11. A. *In-vitro* scratch wound healing assay with H460 cells treated with AQ and AQ NP with no treatment as a control. **B.** Prophylactic single dose spheroid study images. **C** (Single Dose), **D** (multiple Dose). Therapeutic spheroid study on 15th day of Post treatment

www.manaraa.com

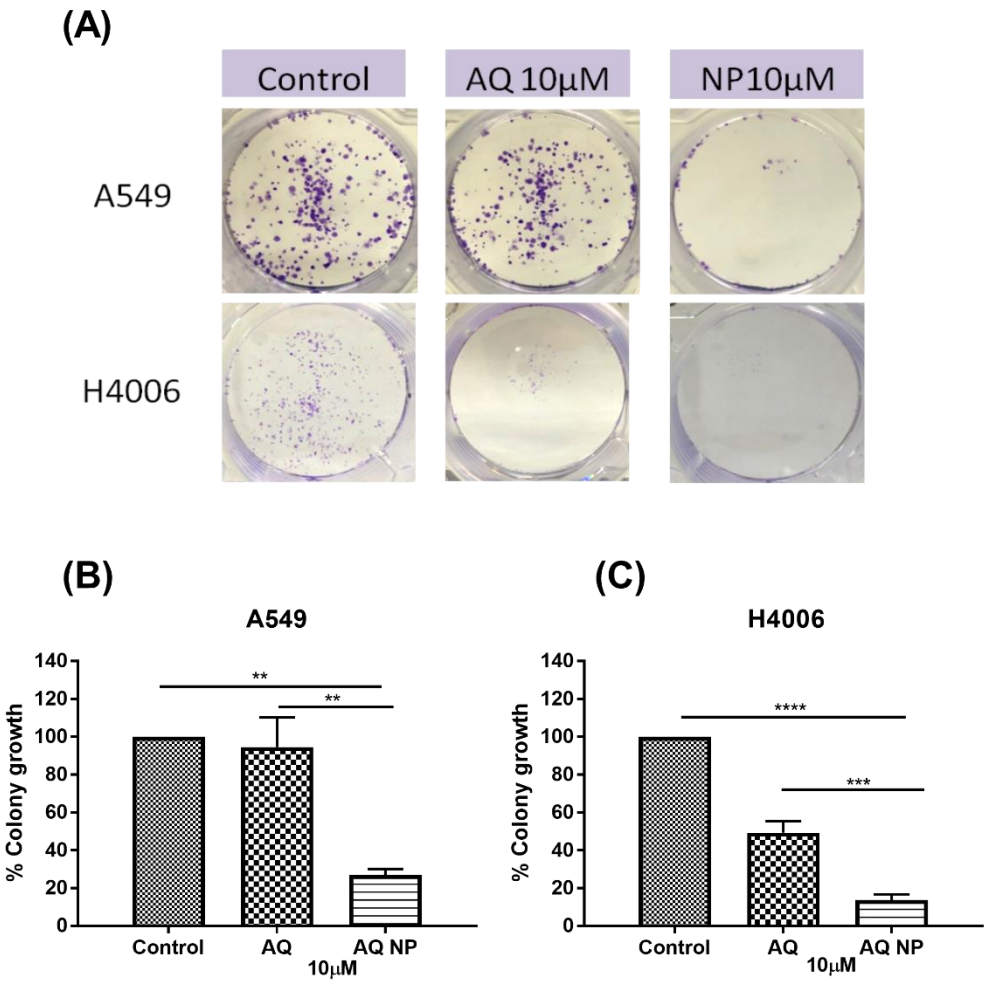

Figure. 12. A. Clonogenic assay images of A549 and H4006 cells **B, C**. Quantitative representation of clonogenic assay as % colony growth with AQ or AQ NP treatment as compared to control **(B:** A549, **C.** H4006**)**.

eliminating the possibility of tumor relapse, from single cancer cells left behind following chemotherapy and surgical intervention; and can well be linked to enhanced intracellular (and intratumoral) drug accumulation with nanoparticles formulation.

3.4.8. 3D Spheroid Cell Culture Study

A549 cell line was able to form spheroid masses from day 1 during culture, which indicated strong cell-cell communications. While preventive or prophylactic treatment assists in determining the treatment's potential in inhibiting tumor growth, and may mimic therapy

www.manaraa.com

following early diagnosis; therapeutic model represents traditional cancer therapy focused on reducing an already established tumor mass.

Preventive (prophylactic) model involves plating of cells followed by overnight incubation and treatment on next day as soon as the cells accumulate to take shape of a conglomerated mass. Representative images for A549 cell line can be seen in **Figure 11B (Day 0)**, where cells are seen to be loosely associated in the form of a mass. % Spheroid volumes 12 days after a single treatment with AQ & AQ NP (10 or 25µM) are shown in **Figure 13A**. As can be seen, on day 12 spheroid volumes for AQ NP treated groups were

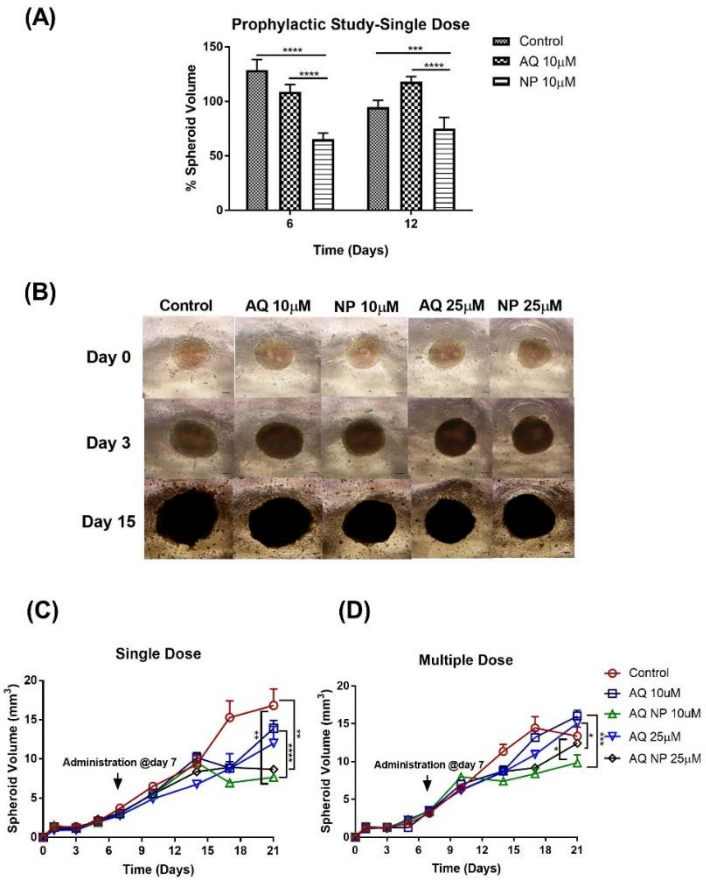

Figure. 13. A. 3D Prophylactic spheroid study on A549 cell line. **B.** Therapeutic Study Spheroid images of A549. **C, D.** Spheroid volume vs time (days) plot for single **(C)** and multiple dose **(D)** study. Scale bar for the images represents 400µM.

www.manaraa.com

found to be significantly smaller than control volumes. Spheroid diameters (μm) and volumes (mm^3) on day 12 after respective treatments were as follows respectively: Control: 1,850.0±77.9μm, 3.3±0.4 mm^3; AQ 10μM: 1,818.8±58.9μm, 3.2±0.3mm^3; AQ NP 10μM: 1,704.5±226.2μm, 2.7±0.9mm^3. With time, spheroid volumes increased significantly in control groups. However, AQ-loaded NP inhibited spheroid growth significantly compared to plain AQ ($p<0.001$). Results revealed that nanoparticle formulation was able to inhibit the spheroid growth in NSCLC cell line (A549).

In therapeutic spheroid model, cells were allowed to form tight cellular masses for a period of 7 days, as would be the case with late diagnosis of a well-established tumor. After tumor formation, spheroids were treated by either a single dose (one dose in the beginning) or a multiple dose (dosing every 3rd day, mimicking chemotherapy treatments).

As can be seen **Figure 13B**, spheroids were found to achieve a diameter and spheroid volume of 1,835.4±97.4μm and 3.3±0.5mm^3 on an average after 7 days of culture i.e. day 0 for the treatments. After 15 days of treatment, A549 spheroids of single dose study had spheroid volumes of 16.8±5.1mm^3 (Control), 13.9±2.5mm^3 (AQ 10μM), 7.7±0.67 mm^3 (AQ NP 10μM), 11.9±5.2mm^3 (AQ 25μM), and 8.7±1.2 mm^3 (AQ NP 25μM), thus demonstrating significant growth inhibition as compared to both drug free treatment and plain AQ (Control vs AQ NP 10μM: $p<0.01$; AQ 10μM vs AQ NP 10μM: $p<0.01$; Control vs AQ NP 25μM: $p<0.01$) **(Figure 13C; Single dose)**. Multiple dosing (every 3rd day treatment) also resulted in significant spheroid growth inhibition after AQ NP treatment compared to AQ (10μM: $p<0.001$; 25μM: $p<0.05$) **(Figure 13D; Multiple dose)**. Interestingly, no significant reduction in tumor volume was observed with plain AQ treatment compared to AQ NP treatment groups for both single and multiple dose studies.

www.manaraa.com

Line graphs representing spheroid volume comparison after single and multiple dosing can be found in **Figure 13C&D** respectively. Bar graphs representing spheroid volume (normalized to control) comparison can be seen in **Figures 11C & 11D** confirming superior tumor growth inhibition by AQ NP compared to control and plain AQ treatments.

From the observed efficacy in both spheroid models, it was confirmed that AQ NP could inhibit tumor growth in earlier as well as later stages.

3.4.9. Live-Dead Cell Assay

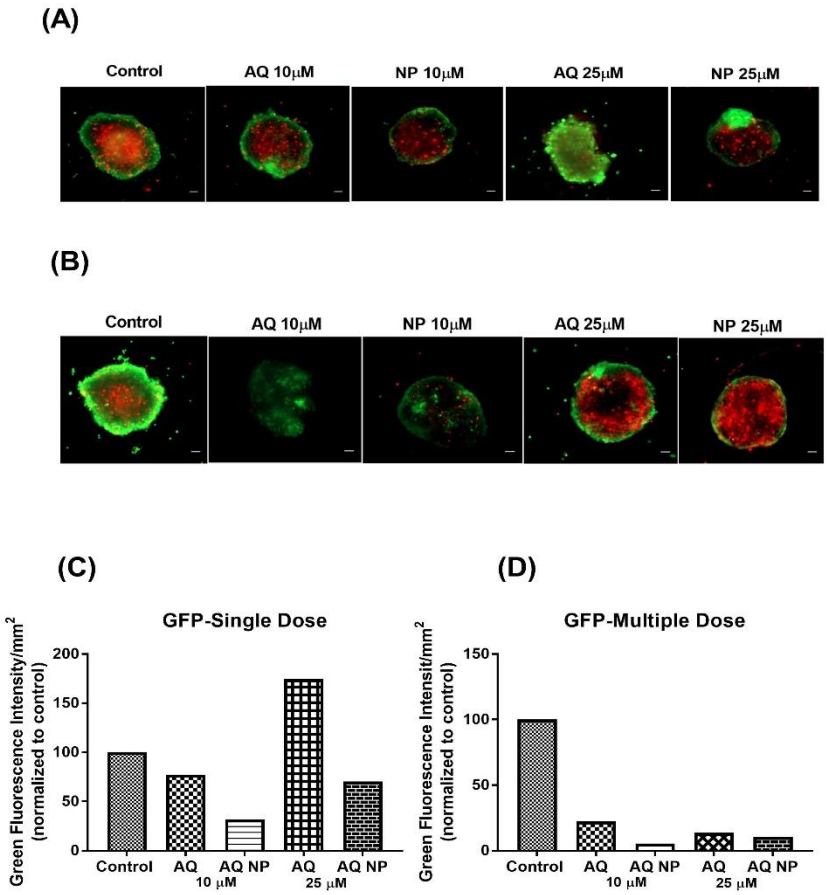

Figure. 14. A, B. Live dead cell assay Images of A549 spheroids of therapeutic model (Single and multiple dosing respectively). **C, D.** The graph represents comparison of green fluorescence intensity/mm^2 (live cells) of A549 spheroids.

www.manaraa.com

This study assists in determining viable and dead cells within a solid spheroid mass. One of the main objectives of developing a drug-loaded nanocarriers is to facilitate drug's entry into the deep core of the tumor, otherwise inaccessible to the plain drug. However, a 2D tumor diameter or volume measurement may not reveal a nanoformulation's efficacy in killing tumor cells within the tumor core, as the spheroid masses may consist of a dead cell core surrounded by a well-established structural periphery of live cells. 3D spheroid masses were reported to comprise of different regions where cells undergo proliferation, quiescence and necrosis (165).

Therefore, it is necessary to quantify live-dead cell portions out of a spheroid mass. **Figure 14A** (single dose) & **14B** (multiple dose) are representing terminal spheroid images on day 15^{th} after treatment.

Like regular xenograft tumor in mice, 3D spheroids are also grown over an extended period, with intratumoral core regions going through lack of O_2, and nutrients, resulting in presence of necrotic and quiescent cells in the core regions (165). Due to this, even control spheroids are likely to exhibit red fluorescence due to the presence of necrotic cells. While AQ-NP treatments demonstrated significant reduction in tumor volume and cellular viability, a reduced red fluorescence (dead cells) were seen with all AQ/AQ-NP treatments in **Figure 14A &14B.** This observation can be explained on the basis of loss of tumor integrity with AQ/AQ-NP treatment, resulting in removal of dead cells during media changes. However, green fluorescence (live cells)/mm^2 of tumor surface area has been quantified, which represented distinct reduction in presence of live cells with AQ-NP treatment at both doses, in both single- and multiple-dose treatment **(Figure 14C & 14D)**. Green fluorescence intensity comparison on day 15^{th} day of single dose (AQ NP) post

www.manaraa.com

treatment period revealed presence of live cells, 1.4-3.2 folds lower as compared to control and also there observed a clear reduction in live cell population compared to plain AQ treated groups (**Figure 14C)**.

For multiple dose study, AQ NP of 10μM and 25μM were found to exhibit 4.5-9-fold reduction in live cell population compared to control group. In addition, live cell population observed for AQ NP treated groups was found to be less compared to that of plain AQ groups (**Figure 14D)**. For both single and multiple dose studies, live cell proportion was found to be lowered in case of nanoparticle group compared to plain AQ or control treated groups, indicating ability of AQ NP in inhibiting tumor cell proliferation.

3.5. Mechanism of Action

3.5.1. Autophagy Inhibition Microplate Assay

AQ NP (10μM) treated cells exhibit accumulation of green fluorescent vesicles with higher intensity compared to cells treated with plain amodiaquine or starved media, as seen in **Figure 15A** (blue fluorescence represents Hoechst 33342 nuclear stain)**.** Following normalization of data to control as 100%, relative fluorescence intensities, representing co-localization of LC3 protein and thus accumulation of autophagosomes, were found to be 126.2±1.4% (AQ), and 173.9±28% (AQ NP) after treating A549 cells for 18 hours (**Figure 15B).** Increased green signal indicated accumulation of autophagic vesicles further confirming autophagy inhibition which leads to tumor growth due to blockade of this crucial pathway required for the survival and proliferation of cancer cells (166).

www.manaraa.com

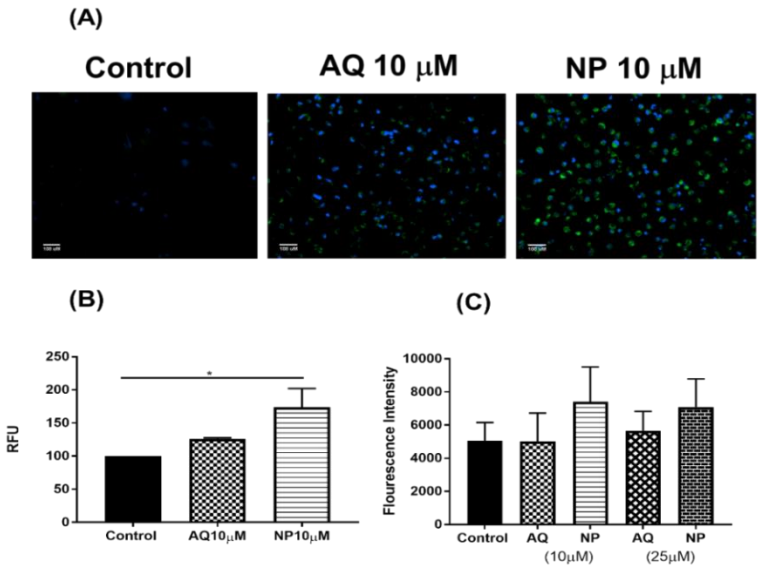

Figure. 15. A. Autophagy Inhibition Microplate Assay on A549 cells. **B.** Graph represents the comparison of relative fluorescence units (RFU) after incubating with respective treatments. **C.** Detection of caspase-3 levels in A549 cells using the EnzChek® Caspase-3 Assay.

3.5.2. Caspase 3 Assay

To evaluate induced active caspase-3 enzyme, cleavage product of a fluorogenic caspase substrate, DEVD-AMC was measured. The EnzChek® Caspase-3 Assay Kit allows the detection of apoptosis by assaying for increases in caspase-3 and other DEVD-specific protease activities (e.g., caspase-7). As seen in **Figure 15C**, increased caspase-3 activity was observed in A549 cells with nanoparticle treatment compared to plain drug and control (fluorescence intensity measurements – Control: 5063.3±1093.8, AQ 10μM: 5018.0±1715.1; AQ NP 10μM: 7408.7±2095.9; AQ 25μM: 5664.7±1161.6; AQ NP 25μM: 7096.7±1694.0) as seen in **Figure 15C.** However, the results were not found to be statistically significant ($p>0.05$). This experiment may signal toward presence of an alternate apoptotic pathway responsible for AQ's tumor inhibiting properties.

www.manaraa.com

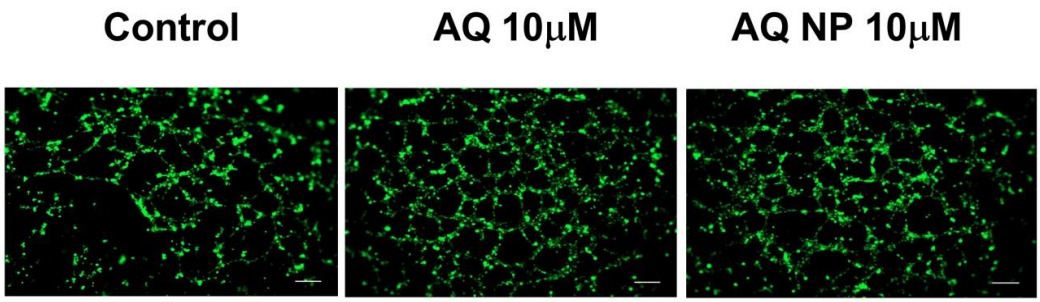

Figure 16. *In-vitro* angiogenesis assay: Fluorescence microscopy imaging of capillary tube formation by HUVEC cells after treating with AQ, AQ NP or control. Scale Bar 100 μm.

3.5.3. *In-vitro* Angiogenesis Study

Angiogenesis i.e. formation of new blood vessels is a paramount mechanism for tumor growth, with its inhibition being a major anti-tumor mechanism. Endothelial tube formation and inhibition can easily be determined and quantified by analyzing microscopy

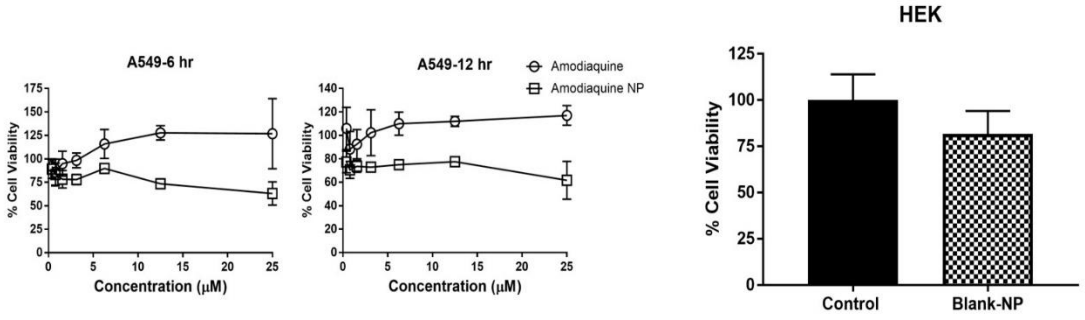

Figure 17. Inhibitory effects on A549 cells after treatments with amodiaquine (AQ), amodiaquine nanoparticle (AQ NP). **B.** Safety studies: Cytotoxicity studies on HEK cell line after treatment with Blank-NP.

images. While significant tube formation was observed in HUVEC endothelial cells mediated tube formation assay with drug free treatment (negative control), neither plain AQ nor AQ NP appeared to inhibit the tube formation *in-vitro* **(Figure 16)**. It was found that there was no potential angiogenesis inhibition activity suggesting the requirement of altered doses to exert their anti-angiogenesis activity or further investigation.

www.manaraa.com

3.6. Discussion

Nanoparticle drug delivery systems are promising carriers for both hydrophilic and hydrophobic anticancer drugs. Tseng *et al* developed gelatin nanoparticles with biotinylated epidermal growth factor conjugation for targeting lung cancer (167). Through standard manufacturing approaches such as ultra-probe sonication, there exists a difficulty in scaling up to a large commercial scale. Moreover, payload capacities for hydrophilic drugs are low in those cases. Hence, there is great need to explore scalable approaches to develop nanoparticles at a laboratory scale. High pressure homogenization (HPH) has been utilized to formulate nanoparticles due to its scale-up feasibility and reproducible product quality (120). HPH has been widely used in industries for large scale production of nanoemulsions and solid lipid nanoparticles (120). However, formulation of nanoparticles using HPH involves multiple complex parameters to consider while obtaining an optimized system. Both process and formulation parameters can be studied to develop an optimized system. Application of design of experiments (DoE) assists in identifying the critical parameters and their respective levels (118). Critical formulation parameter such as PEI concentration in external aqueous medium and critical process parameter such as probe homogenization speed were studied in the present study. For this, we have utilized multifactorial design to identify optimal levels related to pre-emulsion quality and cationic polymer concentration in the formulation while keeping all other optimized variables constant. Cationic polymer such as PEI is capable of imparting positive surface charge to the nanoparticle formulations. As drug repurposing provides an excellent opportunity to find novel anti-cancer uses for previously FDA approved drugs, a vital approach to explore them where toxicity and safety data is already available in the public domain (2,105), AQ

www.manaraa.com

(FDA approved anti-malarial) has been chosen to formulate NPs using scalable HPH approach. Qiao *et al* have reported the anti-cancer efficacy of AQ in melanoma. But, till now there were no studies reporting the efficacy of AQ or AQ nanoparticles in NSCLC. Moreover, development of efficacious NPs against NSCLC using a scalable approach is of significant translational value. Optimized nanoparticle formulation was identified through DoE and used further to assess the efficacy in treating NSCLC. As shown in **Table 3**, effect of PEI concentration on NP particle size prepared at lower homogenization speeds of 6,000rpm, formulations A1, A4, and A7 is not distinctive. Increasing trend of particle size/polydispersity was observed at medium homogenization speed of 12,500rpm with an increase in PEI concentration. Preparation of pre-emulsion at high speed of 25,000rpm resulted in the reduction of coarse emulsion globule size and allowed formation of smaller uniform sized nanoparticles. Increase in encapsulation efficiency at higher speed of homogenization was found to be significant at 0.5% of PEI concentration. This may be due to the fact that a unidirectional and less turbulent flow in case of lower speed may have resulted in loss of drug from the organic phase as reported earlier by Sharma *et al* (168). No significant effect of the drug quantity was observed on the particles size. However, the PDI, % entrapment efficiency (%EE) and overall drug loading was greatly affected by the drug quantities. With an increase of drug quantity from 1 to 10 mg, %EE declined drastically from 47.5% to 22.6%. It seems that at higher drug quantity, %EE was less, resulting in lower actual:theoretical drug loading ratio. A possible explanation is that the higher drug loading resulted in increased drug concentration gradient between the polymer matrix and outer aqueous phase, which in turn led to more drug loss in the fabrication process. The polymer itself may have a limited capacity to encapsulate the specific drug.

www.manaraa.com

Beyond its maximum capacity, more drug may be wasted during fabrication process and the EE thus decreased correspondingly (169). Moreover, C3 formulation was found to exhibit particle size of <250nm, and PDI of <0.1 along with highest % drug loading of 4.02. Hence, C3 formulation was identified as the monodispersed nanoparticulate system with optimal characteristics with and used for further studies.

STEM images represented in **Figure 5C** revealed that the nanoparticles were of spherical shape with smooth surface with little or no aggregations indicating that the vesicles were uniformly dispersed. XRD and DSC studies as seen in **Figure 5D&E** were found to be consistent with earlier reports (159,160), and also revealed AQ encapsulation inside nanoparticles while being amorphous.

Presence of positive charge on AQ NP surface refers to the stability of nanoparticles through inhibiting aggregation. STEM studies revealed that the nanoparticles were spherical in shape. Cationic surface charge of nanoparticles associates with higher cellular uptake and greater cytotoxicity in cancer cells (170). Intracellular uptake shown in **Figure 8** reveals the same where coumarin nanoparticles were internalized by A549 cells efficiently within an hour compared to plain coumarin solution. Due to smaller particle size, there is a possibility of NP aggregation. Hence, stability studies were performed to determine stability of AQ nanoparticles at different temperatures. Results revealed that there was no significant difference in particle size (**Figure 7A)**, zeta potential (**Figure 7B)** and drug entrapment over 4 weeks indicating formulation integrity.

Pulmonary route of administration is well known for its ability to deliver therapeutics locally to site of action but is challenged by major obstacles like poor control over deposition rates and site of inhaled molecules for efficacious delivery at the same

www.manaraa.com

time. NPs exhibiting optimal *in-vitro* aerosol lung deposition can be administered via inhalation, facilitating local delivery to the deep lungs, thus resulting in reduced exposure to other organs and reduced adverse events. Nebulizers can deliver the formulations as small droplets which will be deposited in the lung airways based on their MMAD (137). PLGA polymer was chosen to formulate NPs due to its ability to produce small size systems, excellent stability, high cytocompatibility and rapid cellular uptake (171). Moreover, it has been well documented about the distribution of PLGA NPs within alveolar cells (172). In current study, MMAD value was found to be 4.7±0.1µm with 72.8±25.1% FPF, confirming the respirability of formulated AQ nanoparticles and efficient lung deposition. Developed amodiaquine nanoparticles are capable of providing a promising strategy to overcome the physiological barriers involved in respiratory tract, and ensuring their capability to reach the respirable regions of the lung (137).

Extensive *in-vitro* cell culture studies were carried out to investigate the efficacy of AQ NP against different NSCLC cell lines. Even though each of the NSCLC cell line used in cytotoxicity study has its own characteristics, it was found that a significant reduction in IC_{50} values was observed for AQ after encapsulating into nanoparticles in all 6 NSCLC cell lines as seen in **Table 6** and **Figure 9.** This reveals the significant anti-cancer efficacy of AQ NPs among wide range of NSCLC types. This could be a result of efficient cellular internalization of nanoparticles. Generally, cell migration is an important characteristic of any cancer which involves the movement of cells from one location to another, associated with cancer metastasis (173). In this study, results from scratch assays seen in **Figure 10B** and **Figure 11A** revealed that amodiaquine nanoparticles had greater ability to inhibit cell migration significantly compared to amodiaquine in NSCLC cell lines. Clonogenic assay

www.manaraa.com

study revealed that AQ NPs can inhibit the ability of single cells to form colonies. Hence, it ensures the effectiveness of AQ NP on long term basis while preventing tumor recurrence. Altogether, AQ NP could be further evaluated for their establishment in NSCLC treatment explicitly.

Development of 3D *in-vitro* models is of utmost necessity today to mimic *in-vivo* solid tumor conditions which could be achieved by using specific low attachment spheroid plates as reported by Vaidya *et al* (146). From results seen in **Figure 13A-D**, it can be understood that nanoparticles were able to deliver the drug to spheroids' core efficiently in both prophylactic and therapeutic model ensuring their clinical use. Drug-loaded nanoparticles facilitated the entry of drug into deep tumor core, which would otherwise be inaccessible for plain drug. Thus, the physicochemical properties of nanoparticles such as small particle size, charge or surface modifications are crucial in imparting good penetration behavior to them (174). It has also been reported in the literature that smaller the nanoparticle size, more efficient will be their transport within the tumor (175). In addition, live dead cell assay results confirmed ability of AQ NP to inhibit tumor cell proliferation in solid mass of spheroids leading to the diminished live cell proportion. In accordance with earlier report by Qiao *et al* (139), AQ exhibited autophagy inhibition with AQ NP demonstrating significantly higher efficacy in autophagy inhibition, potentially due to higher cellular internalization of the treatment (105). Here, distinct accumulation of autophagosmes was found indicating the inhibition of autophagy process. AQ causes an increase in lysosomal pH, which inhibits lysosome function and blocks fusion of autophagosomes with the lysosomes (139), thus conserving LC-3 protein and producing a positive signal in the CYTO-ID® Autophagy detection assay as seen in **Figure 15A&B**.

www.manaraa.com

Apoptosis is referred to a programmed cell death. Caspases are cysteine proteases, which play a key role in apoptosis. They will be activated in presence of death inducing stimuli (141). From the results, it was observed that AQ NP treatment induced caspase-3 levels, demonstrating their ability to induce cell death through apoptosis as well. However, the results weren't significant indicating toward presence of an alternate cell death pathway. The tube formation assay is a fast, reproducible method for *in-vitro* measurement of angiogenesis, a major event in tumorigenesis (176). No significant difference was observed between AQ and AQ NP in their ability to inhibit tube formation compared to control indicating toward an alternate mechanism.

As the major challenge being scale-up issue with development of nanoparticulate systems, exploring a scalable approach of HPH is of special interest for successful translation of nanomedicines. Moreover, optimal respirable properties of the developed NPs enable a local delivery into the lungs. Repurposing of anti-malarial drugs for cancer treatment could be a promising approach to target predominant processes such as autophagy and proliferation involved in NSCLC progress. By utilizing the advantage of drug repurposing, AQ was found to be an efficacious molecule against NSCLC with enhanced efficacy in an optimized NP identified by DoE. Taken together, results from the current study including *in-vitro* cell culture studies as well as 3D spheroid models illustrating their pronounced efficiency in NSCLC treatment. Within this study, the potential of scalable HPH approach in formulating amodiaquine nanoparticles and the repurposing feasibility of an anti-malarial drug to treat NSCLC has been evaluated through a systematic approach, and optimal *in vitro* cell culture studies. Altogether, no research work has been reported until today, which accomplishes a comprehensive task of bridging

www.manaraa.com

the gap between laboratory scale and industrial scale manufacturing of nanoparticles while reducing development costs due to repurposing feasibility of amodiaquine, achieved in the present project.

3.7. Conclusion

With the present investigations, it can be concluded that inhalable nanoparticles of amodiaquine were successfully formulated and optimized using systematic approach of design of experiments by a scalable high-pressure homogenization (HPH) approach. As HPH approach is feasible for scale-up while providing reproducible results, developed nanoparticles can be easily scaled-up with ensured product quality. Despite involvement of multiple factors, by using a 3^2-factorial design, it was possible to develop an optimized formulation with ease. In addition to cellular uptake studies, cytotoxicity studies and 3D spheroid studies, assays exhibiting the autophagy inhibition or apoptosis inhibition capability of amodiaquine nanoparticles are promising them as a potential treatment strategy for NSCLC. While the preliminary results are promising, large animal preclinical studies should be carried out to emphasize the drug repurposing of amodiaquine to treat NSCLC.

www.manaraa.com

CHAPTER 4

4. Development and Characterization of Transferrin Functionalized Amodiaquine Loaded Nanoparticles-Efficacy in Non-small Cell Lung Cancer (NSCLC) Treatment

Non-small cell lung cancer (NSCLC) is a malignant tumor type leading to very high mortality. Transferrin receptors are overexpressed in many NSCLC, playing a crucial role in cellular proliferation. Targeting these receptors through specific targeting ligands (Transferrin: Tf) is advocated to achieve superior anti-cancer efficacy. Thus, simpler conjugation of Tf enables specific targeting of overexpressed transferrin receptors on NSCLC cells, further facilitating targeted delivery of therapeutics. As per the previous studies as reported in ***Chapter 1***, AQ was found to exhibit anti-cancer efficacy which is improved after nanoparticulate encapsulation, we aim to develop inhalable and scalable transferrin conjugated AQ-loaded nanoparticles for targeted and efficient NSCLC treatment regimen, using an efficient scalable process of HPH.

4.1. Introduction

Nanoparticulate drug delivery systems are contributing greatly to the design and development of various therapeutics to overcome various limitations of plain drug administration without any carrier system while improving the therapeutic efficacy (177). Recently, there has been a prominent escalation in nanomedicine approval encouraging further nanotechnology based research (178). Reports from several recent research studies have been signifying the capability of nano-based systems to deliver higher payload

www.manaraa.com

amounts of therapeutics to the target site and enhance therapeutic benefits while reducing the toxicity related to free drugs (179). As a result, noted growing attention towards nano-based pharmaceutical products is considered to be appropriate (178). Especially, these delivery systems are evolving rapidly with great emphasis on understanding the complexities involved in certain lung disorders such as cystic fibrosis, idiopathic pulmonary fibrosis (IPF) and lung cancer (127,180,181). Due to their nanoscale size, nanoparticles (NPs) have demonstrated their ability to deliver drugs efficiently to the tumor site in lungs while outperforming their free drug counterparts (179,182). Lung cancer is the leading cause of all cancer -related deaths and is responsible for approximately 1.38 million annual mortalities worldwide number of deaths (183). Being a highly prevalent indication and representing approximately 85% diagnosed lung cancer cases, exploring further advancements in treatments for non-small cell lung cancer (NSCLC) is of highest attention to the researchers (184).

Properties of NPs, such as nanoscale size, favorable drug release profiles and high flexibility are allowing modification of properties such as shape, size, and surface charge (185). In addition, surface of the NPs can be modified through conjugating with targeting ligands of specificity towards cancer cells. These ligands can include, peptides, nucleic aptamers, vitamins, proteins, small molecules and monoclonal antibodies (186). Cancer cells necessitate more iron for their uncontrolled growth and proliferation, resulting in overexpression of transferrin-receptors (TFR) in several malignant tumors including breast, brain, prostate cancers including NSCLC (187). Cellular iron uptake takes place through interaction of transferrin (Tf) with TFR which can be used as a targeting site for cancer-specific drug delivery to enhance therapeutic efficacy against various cancer cells

www.manaraa.com

that overexpress transferrin receptors (188,189). Utilizing targeted NPs in drug delivery establishes a platform for an efficient, tumor-specific interactions by interacting with receptors on the surface of cancer cells (190). Altogether, NPs are presenting potential candidates for therapeutic applications because of their ability to specifically target cancer cells while minimizing side-effects. However, systemic administration of these systems has its own drawbacks demanding an alternative delivery route for an efficient local drug delivery to the lungs (127).

In recent times, inhalation therapy has gained importance as it facilitates efficient delivery of therapeutics to target tissues in the lungs (191). Local pulmonary inhalational delivery of anti-cancer drug loaded nanoparticulate system offers substantial benefits in lung cancer treatment as the most current systemic treatments are not very effective or cause associated side-effects (191,192). Delivering nanocarriers to the lung through an inhalation therapy is potential enough to result in enhanced local drug accumulation, prolonged pulmonary residence time, improved cellular internalization while minimizing exposure of healthy cells to the drugs (193,194). Furthermore, inhalable therapy may also enhance drug penetration into the tumoral mass due to sustaining significantly higher drug concentration at the lung tumor site compared to other non-target sites (133). Several studies have evaluated the accumulation of drug-loaded nanocarriers in the lungs after pulmonary delivery and have reported improved efficacy of inhalable carriers in NSCLC (21). Other therapeutic applications of inhalational therapy include treatment and management of chronic obstructive pulmonary disease (COPD), pulmonary fibrosis, inflammation and cystic fibrosis (195,196). Hence, inhalational therapy remains the mainstay of clinical treatment in the care of pulmonary diseases; and sought after for lung

www.manaraa.com

cancer therapeutics. The efficacy of inhalation therapy depends on suitable drug and carrier system while considering the physicochemical properties of drug, formulation characteristics and the inhalation device (133).

In the current study, amodiaquine, 4-[(7-chloroquinolin-4-yl) amino]-2-[(diethylamino) methyl] phenol (AQ) has been chosen to formulate PLGA-based transferrin-conjugated NPs using a scalable, reproducible high-pressure homogenization approach and to evaluate their anti-cancer efficacy. Drug repurposing facilitates identification of novel anti-cancer uses for old drugs for which toxicity and safety data is already available in the public domain (2,105).While AQ have been explored for its repurposing potential against NSCLC by our research group where superior efficacy of AQ through nanoparticle encapsulation was reported. In another study repurposing potential of AQ was highlighted through a structure-based screening approach (105).

In the present study, the anticancer activity of Tf conjugated amodiaquine loaded nanoparticles (Tf-AMQ NP) against Tf-receptors expressing human non-small cell lung cancer cells has been evaluated. Targeting ligand transferrin was chosen in this study as the overexpression of transferrin receptors in non-small cell lung cancer is evident from the patient data meta-analysis (197). Process of functionalization/conjugation refers to the chemical addition of targeting ligand transferrin to enhance the target nanoparticles to the lung tumor tissue. Targeted nanoparticles were evaluated to verify the hypothesis that transferrin decorated NPs are capable of demonstrating superior efficacy in NSCLC treatment while exhibiting excellent respirability.

www.manaraa.com

4.2. Materials and Methods

4.2.1. Materials

Poly (lactic-*co*-glycolic) (PLGA 50:50, 7-17 kDa, acid terminated), poly vinyl alcohol (PVA), and amodiaquine (AQ) were purchased from Sigma-Aldrich (St. Louis, MO, USA). A549 and H1299 NSCLC cell lines were obtained from ATCC (Manassas, VA, USA) and maintained in RPMI-1640 medium (Corning) supplemented with 10% FBS (Atlanta Biologicals, R&D Systems, Minneapolis, MN, USA), sodium pyruvate, penicillin-streptomycin (Corning, NY, USA) at 5% CO_2/37°C. Human embryonic kidney cell line (HEK-293) was obtained from ATCC and maintained in DMEM medium (Corning) supplemented with 10% FBS (Atlanta Biologicals) and penicillin- streptomycin (Corning, NY, USA) at 5% CO2/37 °C. 3-(4,5-dimethylthiazol-2-yl)-2,5-diphenyltetrazolium bromide (MTT), dichloromethane (DCM), dimethyl sulfoxide (DMSO), coumarin-6, crystal violet dye, 16% paraformaldehyde (PFA) solution, Triton X100, HPLC grade methanol, acetonitrile (ACN) and water were purchased from Fisher Scientific (Hampton, NH, USA). Molecular biology kits, supplies, and antibodies were purchased from other commercial vendors which are listed at appropriate places throughout the manuscript. All other solvents including UPLC grade chemicals and solvents, unless it is otherwise specified, were purchased from Fisher Scientific (Hampton, NH, USA).

4.2.2. Development of UPLC method for Determination of Amodiaquine (AQ)

A reverse-phase liquid chromatography method was developed for quantifying AQ using Waters series Acquity UPLC (Waters, USA). Detailed description of method was reported in our recent publication (198).

www.manaraa.com

4.2.3. Calibration curve for Texas Red-Transferrin

Standard solutions of 0.4, 0.8, 1.6, 3.1, 6.3, 12.5, 25, 50 and 100 µg/ml were prepared by diluting with DMSO: water (1:2.5). Fluorescence intensity was measured at excitation/emission 590/635nm using SPARK Tecan plate reader (Tecan Spark 10M; Tecan, Männedorf, Switzerland). The calibration curve was constructed between concentration of Texas-Red Transferrin (Tf) and fluorescence intensity values.

4.2.4. Synthesis of Transferrin conjugated PLGA

Target-specific drug delivery coupling of Tf ligand to nanoparticle has been carried out by employing a surface-activation method as reported earlier with slight modifications (199). In brief, PLGA polymer (PLGA Resomer 502H; 10mg) Tf was activated by EDC-NHS chemistry (0.25 mL of EDC and NHS solutions in DMSO at 1mg/mL concentration) through stirring at room temperature for 4 hours. Activated PLGA will be recovered by addition of 4mL of water and centrifugation at 10,000 rpm for 10min. For Tf conjugation, activated PLGA was dissolved in DMSO followed by dropwise addition of 100 µl of Texas Red-Transferrin (Tf) (1 mg/ml), agitation for 2 hours, and then incubated overnight at 4°C. Excess of Tf will be removed the next day by centrifugation. Collected conjugated PLGA after centrifugation at 10,000 rpm for 30min was utilized in the formulation of nanoparticles. The supernatant obtained was analyzed for unconjugated Tf using the standard curve obtained.

4.2.5. Formulation of Tf Conjugated AQ NPs (Tf-AMQ NPs)

Non-targeted and transferrin conjugated amodiaquine nanoparticles were formulated through HPH process. In brief, nanoparticles were formulated through high pressure

www.manaraa.com

homogenization using an established, recently published method from our research group (198) with slight modifications. Briefly, AQ-loaded nanoparticles were prepared by using organic solution of polymer PLGA 502H (20mg/1ml of DCM, aqueous solution of AQ (2.5mg/0.5ml), a stabilizer (20ml of 1% w/v polyvinyl alcohol solution in PBS). Tf-conjugated NPs were formulated using both non-conjugated and Tf-conjugated PLGA at (5:1) ratio while other formulation components are the same as for non-targeted AQ-loaded NPs. A stable pre-emulsion was formed by use of a probe homogenizer at 25,000 RPM for 10 minutes. Then, pre-emulsion was processed through high-pressure homogenizer (Nano DeBee®) at homogenization pressure of 30,000 psi and seven number of cycles to recirculate the formulation with reverse flow pattern. These process parameters have been chosen based on our previous investigations as reported in our recent publication (198). Later, formulations were subjected for overnight stirring for organic solvent removal followed by washing of nanoparticles for removal of excess PVA.

4.2.6. Characterization of Tf-PLGA using Fourier Transform Infrared Spectroscopy (FT-IR)

FT-IR spectrum of PLGA, Tf and Tf-PLGA were obtained using FT-IR (Perkin Elmer, Inc., Branford, CT, USA). Organic solvent, DMSO (PLGA, Tf-PLGA) or milliQ water (for Tf) were used for background correction and 10 µL of samples were used for detection. Different peaks in plotted IR spectrum were then interpreted to detect the presence of distinct Tf group.

www.manaraa.com

4.2.7. Determination of Conjugation Efficiency

Supernatants were analyzed for the florescence intensity measured at excitation/emission 590/635nm using Tecan plate reader (Tecan Spark 10M; Tecan, Männedorf, Switzerland). Texas red Transferrin was conjugated to PLGA by formation of an amide bond between an amine and a hydroxyl group. The bond cleavage was carried out by using esterase enzymes from porcine liver (Esterase from porcine liver: E3019-20KU, Sigma Aldrich,) to analyze Texas red Transferrin present in the nanoparticles. Esterase of 40 U/ mL in PBS (pH 7.4) was used in this experiment using a previously reported method with slight modifications. Briefly, esterase enzyme (0.5ml) and Tf-AMQ NP formulation (diluted 10-fold) were added to a tube in the ratio of and samples were shaken at 37°C for 72 hours. A control tube was maintained with AMQ NP formulation and enzyme at the same ratio in the same conditions. After 72 hours, samples were centrifuged (3000 x g, 5 min) using MWCO centrifugal filters and the collected supernatant was analyzed at Ex/Em 590/635nm using Tecan plate reader (Tecan Spark 10M; Tecan, Männedorf, Switzerland).

4.2.8. Physicochemical characterization: Particle size, PDI and Zeta potential

Physicochemical properties such as size, polydispersity, and surface charge of AMQ NP and Tf-AMQ NPs were measured using Malvern® zeta-sizer. Drug loading efficiency was measured using Waters UPLC by quantifying AQ.

4.2.9. Drug Content

Encapsulated drug amount in nanoparticle formulation was determined using a direct vesicle lysis approach. To 20µL of formulation, 1,980 µL of ACN:water:DCM – 98:1.5:0.5 was added followed by centrifugation for 45 min at 4°C at 21,000 x g to lyse nanoparticles

www.manaraa.com

and to acquire loaded drug into the analyzing solution. Obtained supernatant was analyzed for the drug content using UPLC and % EE/%DL was calculated.

$$\%\ Entrapment\ efficiency\ (\%EE) = \left[\frac{Drug\ entrapped\ in\ nanoparticles}{Total\ drug\ added\ initially}\right] \times 100 \qquad \textbf{(Eq. 1)}$$

$$\%\ Drug\ loading\ (\%DL) = \left[\frac{Drug\ entrapped\ in\ nanoparticles}{Total\ polymer+drug\ added}\right] \times 100 \qquad \textbf{(Eq. 2)}$$

4.2.10. *In-vitro* Release Studies

In-vitro release studies were performed for determining the drug release pattern from optimized AQ-loaded NPs using dialysis method as reported previously (53). Briefly, 10,000 MWCO dialysis cassettes (Slide-A-Lyzer, 10,000 MWCO, 0.1–0.5 mL, Thermo-Scientific, Waltham, MA) were preconditioned in PBS buffer (pH 7.4) for 10 min to allow them to get hydrated. Then, using syringe with $19G1_{1/2}$ TW BD filter needle, 200µL of formulation was loaded into the cassettes' membrane though one of the ports. The cassettes were immersed in a beaker with 100 mL of pH 5.5 buffer with 1% polysorbate 80 (37ºC) using a floater while stirring at a speed of 200 rpm. At regular time points of 0.5, 1, 2, 4, 6, 8, 24 and 48 hours, samples were withdrawn with replenishing the dissolution medium with fresh pH 5.5 buffer with 1% polysorbate 80. The amount of drug released was estimated using UPLC.

4.2.11. Morphological Analysis

Imaging of unconjugated and conjugated amodiaquine nanoparticles was performed using transmission electron microscopy (TEM) for assessing nanoparticles' morphology. The Formvar® carbon-coated copper grids 400-mesh (Electron Microscopy Sciences, PA, USA) were made hydrophilic using glow discharge plasma treatment for 60s. About 5µL

www.manaraa.com

of diluted nanoparticles sample was added to the grid and allowed to adhere for 1 minute. The samples were negatively stained by adding 5 µL of uranyl acetate (1%) and excess was removed by using Whatman filter paper after 30s. This process was repeated twice and the sample was finally allowed to air dry. The grids were then imaged using Tecnai Spirit TWIN TEM operated at 120 kV voltage.

4.2.12. Solid-state Characterization Studies

Powder X-ray Diffraction (PXRD) Studies: The samples were first lyophilized into dry powders using Labconco FreeZone® freeze dryer system. X-ray diffraction spectroscopy was carried out using XRD-6000 (Shimadzu, Kyoto, Japan). The diffractometry was performed by using a graphite monochromator consisting of copper-Kα1 radiation of wavelength 1.5418 Å operating at 40 kV, 30 mA. The samples were spread uniformly on a glass micro sample holder and were analyzed in the range of 5 to 60° at the scanning speed of 2° (2θ)/minute.

Differential Scanning Calorimetry (DSC) Studies: The thermograms for AQ, AMQ NP and Tf-AMQ NP were generated by closed pan technique using a DSC 6000 (PerkinElmer, Inc; CT, USA) equipped with an intra-cooler accessory. An accurately weighed sample (2mg) was sealed in an aluminum pan and analyzed against a sealed empty aluminum pan maintained as reference. Study was performed over a temperature range of 30°-210°C The heating rate was maintained at 10°C/min.

4.2.13. Stability Studies

Stability of Tf-AMQ NPs was evaluated while storing the triplicate samples at temperatures of 4ºC (storage temperature) and 25ºC (room temperature) for 4-week period

www.manaraa.com

as reported previously (53). Aliquot of each sample was withdrawn at the end of week 1, 2, 3 and 4; diluted with water (100-fold) and analyzed in terms of particle size, PDI and zeta potential using Malvern Zeta Sizer as described earlier. % entrapment efficiency was determined by lysing the samples using UPLC.

4.2.14. *In vitro* Aerosol Performance Lung deposition test

In-vitro aerosol lung deposition was assessed using Next Generation Impactor™ (M170 NGI: MSP Corporation, Shoreview, MN, USA) according to previously published studies (198). NGI can categorize particles based on their size which is useful in predicting *in-vivo* deposition of particles (200). Briefly, prior to operation, NGI plates were placed in refrigerator (4°C; 90 min) for pre-conditioning NGI to minimize solvent evaporation during the process. 2 ml AMQ NP or Tf-AMQ NP formulation was then loaded into a PARI LC PLUS® nebulizer cup attached to a customized rubber mouth-piece connected to the NGI™. A Copley HCP5 vacuum pump (Copley Scientific, Nottingham, UK) was used to produce a flow rate (15 L/min; 4 min). After the run, samples were collected from every stage (1-8) as well as from throat and induction port by using ACN: water (75:25) for rinsing. Samples were centrifuged for 45 min at 21,000 x g, and lysed supernatant was then analyzed using previously established UPLC method.

4.2.15. Determination of Targeting Capability

4.2.15.1. Cellular Uptake Studies

Cellular uptake studies were performed in order to determine the effect of NP loading and transferrin targeting on intracellular uptake of the drug encapsulated using a protocol reported earlier (201). NPs for cellular uptake were formulated by replacing AQ with

www.manaraa.com

coumarin-6 (1mg), a fluorescent dye since it offers simple and sensitive detection for easier tracking while it has been frequently used in cellular uptake studies of PLGA nanoparticles. In brief, A549 or H1299 cells were plated in 8 chambered tissue culture (TC) treated cell imaging cover glass (Eppendorf, Hauppauge, NY, USA) at a seeding density of 10,000 cells/chamber followed by overnight incubation. Next day, cells were incubated with coumarin-6, coumarin-6 loaded unconjugated and Tf conjugated nanoparticles at 1 µg/mL concentration in fresh culture medium for 3 and 24 hours. At each time point (3- and 24-hours), cells were washed with ice cold PBS twice and fixed with 4% paraformaldehyde (PFA) for 10 min. Fixed cells were washed again with ice cold PBS twice. Then, the chamber was removed and 20µL of vectashield hardset mount with DAPI nuclear stain (H1500, Vector laboratories, Burlingame, CA, UAS) was placed on a glass slide dropwise followed by placing a cover glass. After hardening of mounting medium overnight at 4°C, slides were imaged using EVOS-FL microscope at 20X magnification (Thermo Scientific, Waltham, MA, USA).

4.2.15.2. Quantification of Cellular uptake by Determining Fluorescence Intensity:

A549 or H1299 cells were seeded into 24-well assay plates at 1 x 10^5 cells/well. Once, the cells reach confluency, incubated them with 1ml at 1µg/ml concentration of coumarin, coumarin-loaded NPs and transferrin conjugated coumarin nanoparticles at 5% CO_2/37°C for 3 or 24 hr. At each time interval (3- and 24 hour), media was removed from the wells and washed three times with ice-cold PBS. Cells were harvested using trypsin and to the obtained cell pellets, 100 µl of 0.5% Triton X-100 was added for cell lysis. These samples were kept for sonication for one hour at 4°C. The fluorescence intensity of supernatants

www.manaraa.com

from each sample was measured for coumarin quantification at Ex/Em 420/465nm (Tecan Spark 10M; Tecan, Männedorf, Switzerland).

4.2.16. Cytotoxicity Studies

AMQ NP, Tf-AMQ NPs along with plain AQ were evaluated for their cytotoxicity in two non-small cell lung cancer (NSCLC) cell lines: A549 and H1299 as reported earlier with slight modifications (59,202). Both of these immortalized NSCLC cell lines were reported to exhibit overexpression of transferrin receptors (107). In brief, cells were grown in FBS supplemented RPMI-1640 media as described in *Materials* section, and were seeded in TC treated 96-well plates (Eppendorf, Hauppauge, NY, USA) at a seeding density of 2,500 cells/well (7,500 cells/cm^2), incubated overnight for adherence at 37°C/5% CO_2, and treatments were added next day at different AQ concentrations ranging from 0.39-50 µM. Corresponding volumes of AMQ NP and Tf-AMQ NPs were calculated based on the drug entrapment efficiency. Untreated cells were used as a control. After 72 hours of incubation, % cell viability was determined by performing MTT assay as described earlier (20), by reading the absorbance of dissolved formazan crystals at 570 nm (Tecan Spark 10M; Tecan, Männedorf, Switzerland). Further cytotoxicity studies were performed following same protocol to evaluate the safety of drug-free nanoparticles (A549 and HEK) using equivalent amounts of Blank NP at concentrations of 0.39, 0.78, 1.56, 3.13, 6.25, 12.5, 25 and 50µM and AQ-loaded NPs along with plain drug (HEK) with 72 hours of incubation period.

www.manaraa.com

4.2.17. Clonogenic Assay

Clonogenic assay is an *in-vitro* cell survival assay which is based on the single cell's capability to grow into a colony. Using this assay, the effectiveness of the AQ, AMQ NP and Tf-AMQ NP toward colony inhibition was determined. The protocol reported previously (20,149) was briefly modified and followed in this study. A549 or H1299 cells were seeded into 6-well cell culture plates at seeding density of 5 x 10^2 cells per well for each cell line and incubated overnight at 37°C (5% CO_2) Then, media was replaced, and cells were treated with AQ, AMQ NP and Tf-AMQ NP (10µM), or control for 48 hours followed by its replacement with fresh culture medium on alternative days for 7 days. On 7^{th} day, the colonies were stained with crystal violet as reported earlier (20). After staining cells were washed with distilled water. Colonies were photographed using digital camera and were counted by colony counter software Open CFU (150).

4.3. Mechanism of Action

4.3.1. Autophagy Inhibition Assay

Autophagy enables cancer cells to survive under micro-environmental stress conditions and promotes tumorigenesis (151). While AQ is a known autophagy inhibitor, it is crucial to determine the capability of AMQ NP and Tf-AMQ NPs to inhibit autophagy. Autophagy inhibition microplate assay was performed using CYTO-ID® Autophagy Detection Kit (Enzo Life Sciences, Farmingdale, NY, USA) as reported earlier (60). In brief, A549 cells were plated at density of 1.0 x 10^4 cells/well in 96 well plate (Fisher scientific, Hampton, NH, USA) and starved for 24 hours in serum free media, and were later incubated with 25µM of AQ, AMQ NP and Tf-AMQ NP or drug-free control for 18 hours. Treatments were replaced with 100µL of 1X assay buffer followed by addition of 100µL of dual color

www.manaraa.com

detection reagent (CYTO-ID® Green Detection Reagent + Hoechst 33342 nuclear stain in 1X assay buffer). Plates were protected from light and incubated for 30 min at 37°C. Later, cells were washed with 200 µL of 1X assay buffer to remove excess dye. Then 100 µL of 1X assay buffer was added to each well, and plates were read with a FITC filter (Ex ~480 nm, Em ~530; green detection reagent), and with a DAPI filter set (Ex ~340 nm, Em ~480 nm; Hoechst 33342 Nuclear Stain). Here, CYTO-ID® Green Detection Reagent serves as a bright fluorescent probe in vesicles produced during autophagy (152).

4.3.2. Apoptotic Assay

Apoptosis, or programmed cell death, plays a critical role in assessing the potency of drug delivery systems. Caspase-3 is one of the major markers of apoptotic cell death, which can be activated in apoptotic cells both by extrinsic and intrinsic pathways (153). Caspase-3 enzymatic activity was measured using EnzChek™ Caspase-3 Assay Kit (Molecular Probes, Eugene, OR, USA) as reported earlier (203). Briefly, A549 or H1299 cells were seeded at a density of $1x10^6$ cells per tissue culture dish (100 mm diameter) (Thermo Scientific, Rochester, NY, USA) followed by treatment with AQ, AMQ NP, Tf-AMQ NP (25µM) or control for 6 hours. Then, cells were harvested and cell pellets were washed with ice-cold PBS followed by cell lysis using 1X cell lysis buffer. Lysed pellets were centrifuged and supernatants obtained were transferred to 96 well plate to which 50 µL of 2X substrate working solution (10mM Z-DEVD-AMC substrate + 2X reaction buffer) was added and incubated for 20 min. Fluorescence was measured at excitation/emission 360/460nm (154). Control without enzyme was used to estimate the background florescence of substrate in each assay.

www.manaraa.com

4.4. 3D Spheroid Cell Culture Studies

Tumor microenvironment plays an important role in its progression and development. This can be explored by developing 3D spheroids, which would simulate the microenvironmental tumor conditions and thus serve as a important tool for improving relevance to *in vitro* results. An effective NSCLC therapy is not only determined by enhanced cellular uptake or cytotoxic potential, but also improved penetrability of nanoparticles into solid tumors. 3D spheroid cell culture studies are capable of mimicking the *in-vivo* features of tumors as reported in our previous studies (20,42,147). Briefly, cells were seeded in in Corning® ultralow attachment spheroid 96-well plate (Corning, NY, USA) at a seeding density of 2 x 10^3 cells: A549, 2.5 x 10^3 cells: H1299 per well and were incubated overnight at 37°C/5% CO_2. For later 3 days, spheroids were allowed to grow into solid tumor mass due to the shape of these ultra-low attachment cell culture plates as published in our studies (204). On day 3, all the wells were observed for spheroid formation with a rigid margin. In case of A549, images were captured using inverted microscope (Laxco, Mill Creek, WA, USA). Next day, media was replaced with either fresh media (control) or respective treatments of AQ, AMQ NP or Tf-AMQ NP. Briefly, spheroids were treated with 20 µM concentration of AQ, AMQ NP and Tf-AMQ NP (to maintain original concentrations of 10 µM employed in the beginning), and images were captured. Only half the volume of media (100µL) was replenished to avoid any chance of tumor aspiration of media was replaced with fresh media in a gentle manner to avoid the bubble formation and the aspiration of spheroid itself. on further days of imaging. Images were captured on day 1, 3, 6 and 9 and 12 days following treatment. NIH ImageJ software (Version 1.44) was

www.manaraa.com

used to measure diameter of all the spheroids and spheroid volumes were calculated. H1299 spheroids were imaged using live-dead cell staining on Day 15.

4.4.1. CellTiter-Glo Luminescent Cell Viability Assay

CellTiter-Glo cell viability assay was performed using a commercially available kit (CellTiter-Glo®, Promega, Madison, WI, USA) to determine viable cells in spheroids of day 12 as per the manufacturer's protocol. On day 12, 100µL of medium was removed and replaced with 100µL of CellTiter-Glo® 3D reagent in each well (n=3 for each treatment group). The contents were mixed for 2 min, followed by incubation at room temperature for 30 min. The luminescence was measured using Spark 10 M plate reader (Tecan, Männedorf, Switzerland).

4.4.2. Live-Dead Cell Assay

Live-dead cell assay was performed on H1299 spheroids on day 15 according to manufacturer's protocol. Briefly, 100 µL of 2µM calcein AM/4µM Ethidium homodimer III (EthD-III) staining solution was added to spheroids after complete removal of media from the respective wells. The plate was incubated for 45 min at room temperature. Green fluorescent staining represents viable cells. Images were captured using (EVOS-FL, Thermo Fisher Scientific).

Data Analysis and Statistical Evaluation

All data were addressed as mean ± SD or SEM, with n=3 unless otherwise mentions. Three trials of cytotoxicity studies were performed for each control or treatment with n=6 for each trial data. Unpaired student's t-test was used to compare two groups and one-way ANOVA followed by *Tukey's* multiple comparisons test was used to compare more than

www.manaraa.com

two groups using GraphPad Prism software (Version 7.04 for Windows, GraphPad Software, San Diego, California USA). A *p* value of<0.05 was considered statistically significant and was presented in data figures as a single asterisk (*). However, some studies have demonstrated a smaller *p*-value of 0.01 or less, which is included at respective places.

4.5. Results

4.5.1. Development of UPLC method for Determination of Amodiaquine (AQ)

A rapid, UPLC method was developed for determination of AQ. Retention time was found to be 0.731 min with run time of 1.5 min. Peak was eluted with good resolution. The method provided excellent linearity between 0.05 to 6 µg/mL. Further details of this developed method have been reported in a recent publication from our group (198).

4.5.2. Calibration curve for Texas Red-Transferrin

Calibration curve for Texas Red-Transferrin has been plotted between fluorescence intensity and concentration of Tf. The linear regression data for the calibration curve showed good linear relationship over the concentration range 0.4-100 µg/ml for Tf. Standard plot was represented in **Figure 18A**. Linear regression equation was found to be

$$Y=508.8*X + 20.45$$

4.5.3. Synthesis of Tf-PLGA

Generally, nanoparticles are chemically conjugated to different ligands for targeting purposes. For retaining maximum drug loading, instead of NPs, PLGA polymer was subjected for conjugation with Tf. Conjugation of PLGA with Tf was performed through very well-established EDC/NHS chemistry. **Figure 18B** outlines the synthesis procedure of Tf-PLGA. The underlying principles of the synthesis of Tf-PLGA are: activation of

www.manaraa.com

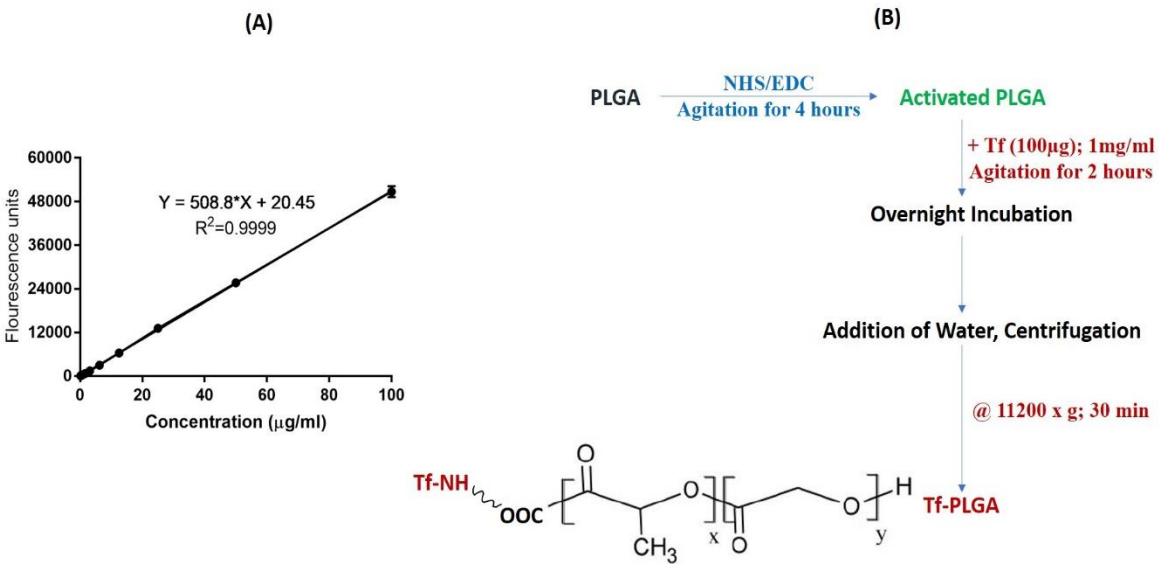

Figure. 18. A. Calibration curve for Texas-Red transferrin**. B.** Schematic representation of conjugation of PLGA polymer with Tf.

carboxylic acid groups of PLGA using NHS/EDC and conjugation of an amine group (NH_2) of transferrin with a activated PLGA. As evident from **Figure 18B**, the two-step EDC/NHS activation method enables the conjugation of Tf amino groups to the activated PLGA carboxyl groups through an amide bond formation. Tf-PLGA was collected through centrifugation after addition of water which facilitates precipitation of water insoluble Tf-PLGA.

4.5.4. FTIR

Analysis by FTIR was used to characterize conjugation of Tf with the polymer after synthesis reaction. **Figure 19** shows the FTIR spectra of Tf **(A)**, PLGA **(B)** and Tf-PLGA **(C)**. FTIR spectrum of PLGA has a peak at 1760 cm^{-1}. Spectral analysis of PLGA-Tf showed characteristic band at 1660 cm^{-1} corresponding to C=O stretch of amide bond

www.manaraa.com

formed between carboxylic groups (PLGA) and amine groups (Tf). This shift is referred to the conjugation of Tf to PLGA polymer.

4.5.5. Determination of Conjugation Efficiency

Supernatant obtained after collecting Tf conjugated PLGA following subsequent conjugation reactions was analyzed for the florescence intensity using measured at excitation/emission 590/635nm using Tecan plate reader (Tecan Spark 10M; Tecan, Männedorf, Switzerland). The amount of unconjugated Texas Red-Transferrin is calculated by comparing the measured florescence intensity value with standard curve. It was found that 10±2.3µg of Tf was unconjugated to the PLGA polymer. Conjugation efficiency of Tf was also determined through a direct approach utilizing esterase enzyme as reported earlier (147). In brief, after completion of 72 hours of incubation of Tf-AMQ NP/AMQ NP, fluorescence intensity of the supernatant was quantified to determine the presence of Tf. This presents a more reliable way to assess conjugated Tf by measuring the amount of Tf present in Tf-AMQ NPs. Esterase enzymes were used to cleave the ester linkages binding Tf to the PLGA polymer in the nanoparticles. After cleavage, Tf was separated from the formulation sample using 30 kDa MWCO filters as the supernatant and then analyzed for fluorescence intensity using Tecan plate reader (Tecan Spark 10M; Tecan, Männedorf, Switzerland). The amount of Tf conjugated was found to be 103.3 ± 9.0%, which is in correspondence with the results from supernatant analysis. No significant difference was observed between the supernatant analysis and esterase experiment results in regard to conjugation efficiency.

www.manaraa.com

4.5.6. Physicochemical characterization: Particle size, PDI and Zeta potential

Nanoparticle formulations AMQ NP and Tf-AMQ NPs were found to have average particle size and polydispersity index (PDI) of 222.3±41.7nm, 0.2±0.1; 244.1±10.5nm, 0.3±0.0 respectively, suggesting uniform particle size distribution as represented in **Fig 19D**. The zeta potential of Tf-AMQ NPs was found to be positive (8.2±1.3mV) compared to AMQ

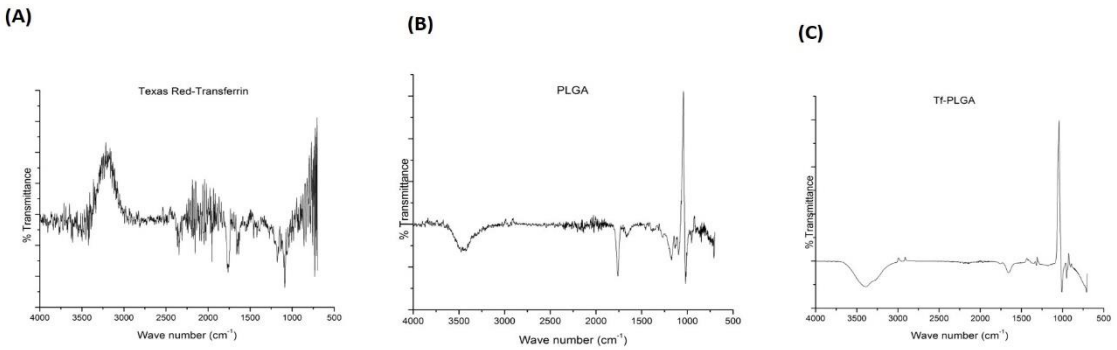

(D)

Formulation	Particle Size (nm)	PDI	Zeta Potential (mV)	%EE	% Drug Loading
AMQ NP	222.3±41.7	0.2±0.1	-11.1±5.6	31.8±1.5	1.2±0.1
Tf-AMQ NP	244.1±10.5	0.3±0.0	8.2±1.3	41.0±9.8	1.6±0.4

Figure 19. FTIR spectra of Texas Red-Transferrin **(A)**, PLGA **(B)** and Tf-PLGA **(C). D.** Characterization of non-targeted and targeted nanoparticles

NP (-11.1±5.6mV). The net surface charge of the Tf-AMQ NP may be affected due to the presence of Tf. It was assumed that presence of Tf molecules on the surface of nanoparticles is screening the surface of PLGA molecules thus reducing the exposed negative charges on the surface as reported earlier (205).

4.5.7. Drug Content

Amodiaquine was effectively encapsulated into nanoparticles, achieving % EE of 31.8±1.5% (AMQ NP), 41.0±9.8% (Tf-AMQ NP) and high % DL of 1.2±0.1% (AMQ NP), 1.6±0.4% (Tf-AMQ NP) as shown in **Figure 19D**. As Tf conjugated PLGA polymer and

www.manaraa.com

plain PLGA (1:5) were used during the preparation of nanoparticles instead of conjugating Tf onto nanoparticles, possibility for drug leaching from conjugated NPs during the conjugation and incubation process was circumvented.

4.5.8. *In-vitro* Release Studies

The drug release pattern from Tf-AQ NP in pH 5.5 buffer was represented in **Figure 20A.** The cumulative percentage of drug release after 4 hours of release study was 80.0±17.6% for Tf-AMQ NP at pH 5.5. These results demonstrate that the Tf-AMQ NPs when internalized by tumor cells will efficiently release the drug, resulting in superior cytotoxicity.

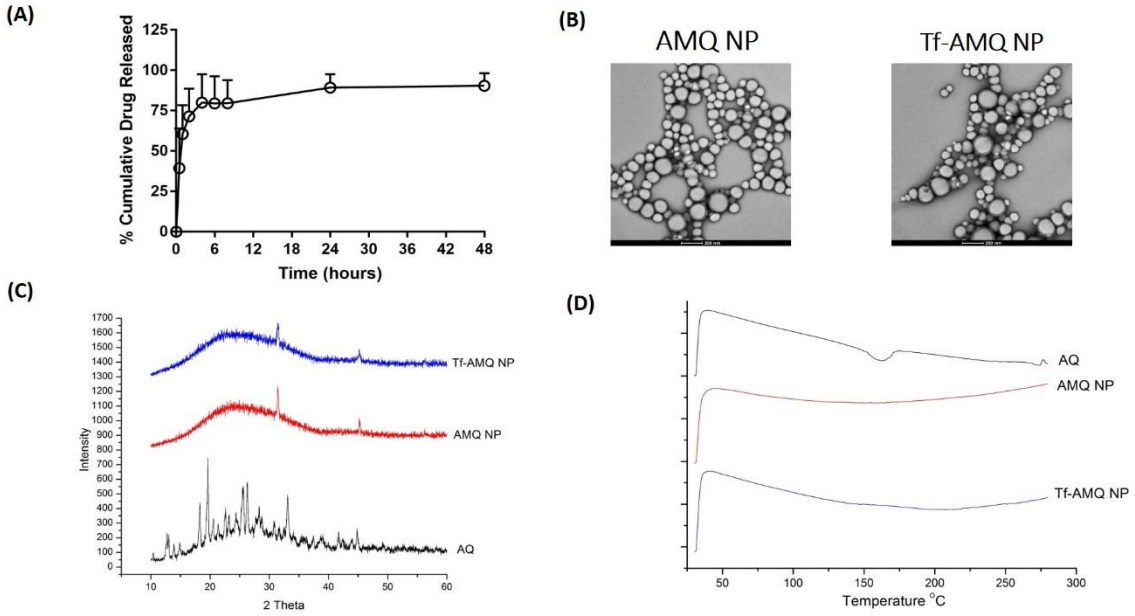

Figure 20. A. *In-vitro* release studies: % Cumulative *in vitro* drug release profile of Tf-AMQ NP. B, C. Transmission electron microscopy (TEM) images of AMQ NP and tf-AMQ NPs. Magnification 20kX**. C, D.** Solid state characterization studies: **(C)** XRD and **(D)** DSC for AQ, AMQ NP and Tf-AMQ NPs

www.manaraa.com

4.5.9. Morphological Analysis

Representative TEM images of AMQ NP and Tf-AMQ NPs were presented in **Figure 20B** revealed that the nanoparticles had spherical appearance with a smooth surface. No aggregation of nanoparticles was observed during TEM analysis which gives an indication of the uniform dispersion of nanoparticles in formulation. The results were found to be in agreement with PDI and zeta potential measurements, shown in **Figure 19D.**

4.5.10. Solid state Characterization

Powder X-ray Diffraction (PXRD): Due to its crystalline nature, AQ showed distinct peaks at 2θ values of 19.66 and 25.60 in XRD spectra whereas there were no AQ peaks present in AMQ and Tf-AMQ NP indicating encapsulation of drug inside the nanoparticles as shown in **Figure 20C**. Results were found to be consistent with our earlier studies of amodiaquine nanoparticles (198).

Differential Scanning Calorimetry (DSC): The DSC studies were performed to understand melting and crystallization behavior of AQ when present in NP formulation as compared to plain AQ. As can be seen in **Figure 20D**, thermogram of AQ showed a sharp endothermic peak at 166.8°C due to its melting transition. The absence of a sharp peak in AMQ NP and Tf-AMQ NP indicated complete drug encapsulation in the nanoparticle formulation core and suggested a consistent result with that of XRD as discussed above. Results found to be consistent with our earlier studies (198).

4.5.11. Stability Studies

Stability is a major concern while dealing with nanosized drug delivery systems due to emulsion instability and particle aggregation (53). As shown in **Figure 21**, stability

www.manaraa.com

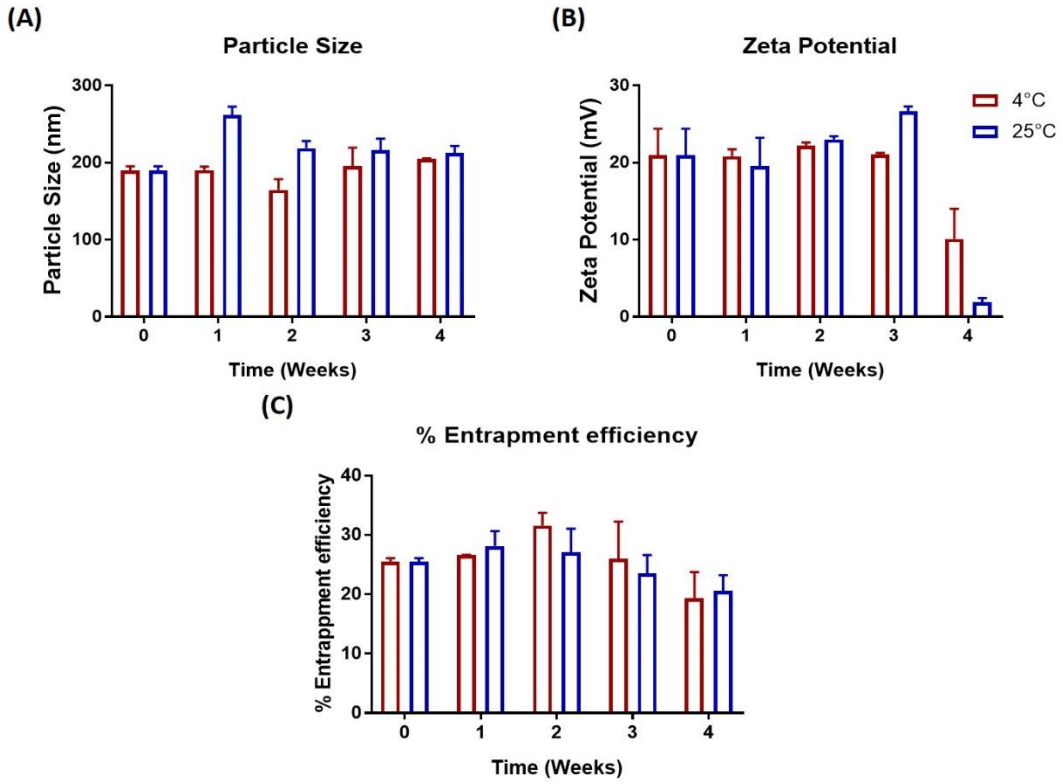

Figure 21. Influence of storage temperature and length of storage on particle size **(A)**, zeta potential **(B)** and % entrapment efficiency **(C)** of Tf-AMQ NPs. Formulations were stored at 4° and 25° over a period of 4 weeks. Data represent mean ± SD (n=3).

analysis data reveal that Tf-AMQ NP formulation was stable at 4º and 25ºC, with no significant changes in particle size, zeta potential or % entrapment efficiency **(Figure 21A-C)**. Although there observed a reduction in zeta potential after 4 weeks of storage at 25C, still the formulations were found to exhibit a positive surface charge which is very crucial in their superior cellular internalization. Here, the positive zeta potential of the Tf-AMQ NP prevents the particles from coalescing and aggregating. There was no detrimental effect of temperature and storage time on entrapment efficiency either. Altogether, the formulations were found to retain their physicochemical properties during their storage at different temperatures of 4°C and 25°C over a period of 4 weeks.

www.manaraa.com

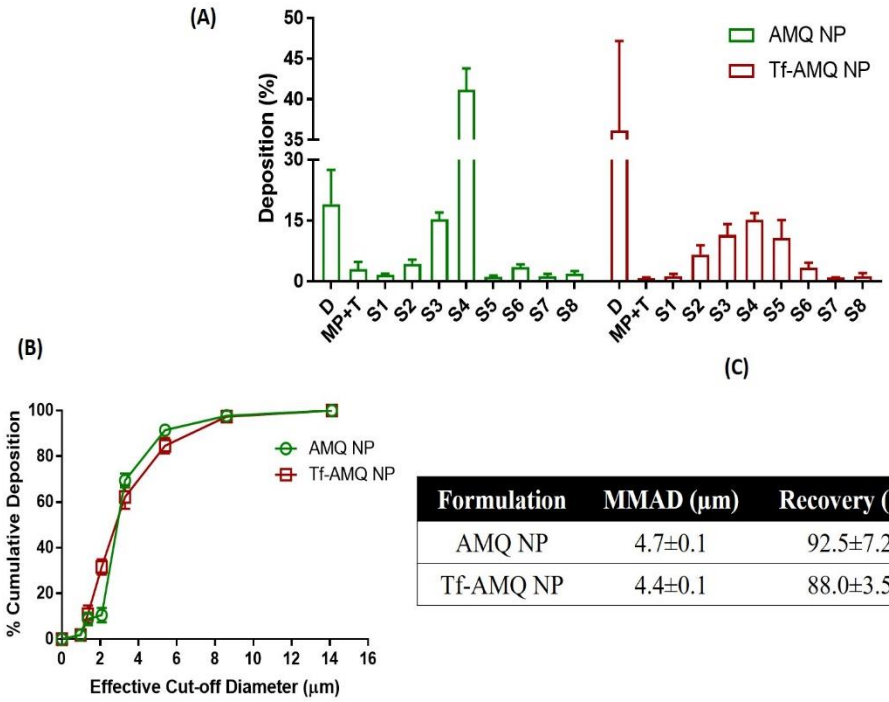

Formulation	MMAD (µm)	Recovery (%)	FPF (%)
AMQ NP	4.7±0.1	92.5±7.2	87.7±1.2
Tf-AMQ NP	4.4±0.1	88.0±3.5	83.2±3.0

Figure 22. *In-vitro* deposition profile of AMQ NP and Tf-AMQ NP. **A.** Aerosol dispersion performance as % deposited on each stage of the Next Generation Impactor™ (NGI™). **B.** Cumulative % deposition plot representing cumulative % of particles deposited at each stage. **C.** Aerosolization properties of AMQ NP and Tf-AMQ NP.

4.5.12. *In vitro* Aerosol Performance Lung Deposition test

Pulmonary route of administration facilitates local therapeutic delivery in deep lungs (206). NPs exhibiting optimal *in-vitro* aerosol lung deposition can be administered via inhalation while reducing exposure to other organs and thus reducing adverse events. Nebulizers can deliver the formulations as small droplets which will be deposited in the lung airways based on their aerodynamic properties like median aerodynamic diameter (MMAD) and FPF (207). Particle size, surface morphology and MMAD of inhaled therapeutics determine their fate and the site of deposition in deep lungs (136). MMAD within the range of 2-5 µm is essential for deep lung accumulation of particulate therapeutics, which is otherwise difficult to maintain due to inherent differences in particles' physicochemical properties (137,138).

www.manaraa.com

Aerosol deposition pattern is presented graphically in **Figure 22A** which refers to the % aerosol deposition at each stage of NGI which aids in determining the aerosol dispersion performance Relation between recovered cumulative mass and effective cut-off diameter is shown in **Figure 22B** which represents the % cumulative particles deposition plot as a function of effective cut-off diameter. To assess the respirability of Tf-AQ NPs; dose recovered from nebulizer cup and NGI stages, fine particle fraction (FPF (%)), MMAD and GSD were calculated. FPF was found to be 87.7±1.2% and 83.2±3.0% for AMQ NP and Tf-AMQ NP respectively which suggests good aerosolization performance. **Figure 22C** shows the MMAD and GSD values of 4.7±0.1 µm (AMQ NP), 4.4±0.1 µm (Tf-AMQ NP), and 1.3±0.0 (AMQ NP), 1.9±0.3 (Tf-AMQ NP) respectively, suggesting a high degree of aerosolization performance and thus NPs are capable of being delivered into targeted respirable region inside the lungs. A 92.5 ± 7.2% (AMQ NP) and 88.6 ± 3.5% (Tf-AMQ NP) recovery indicated that most of the loaded dose was recovered across all stages, demonstrating a near complete nebulization. From the results obtained, the efficacy of formulated AMQ NPs and Tf-AMQ NPs for inhalable drug delivery of AQ could be established and it can be ensured that developed nanoparticles would be able to provide a promising strategy to overcome the physiological barriers involved in respiratory delivery of anticancer therapeutics.

4.5.13. Determination of Targeting Capability

4.5.13.1. Cellular Uptake Studies

Figure 23A & 24A represents intracellular uptake of nanoparticle formulations using A549 and H1299 NSCLC cells with 3 hours **(Figure 23)** or 24 hours **(Figure 24)** of incubation. In this experiment, AQ was replaced with fluorescent coumarin to make it possible to

www.manaraa.com

visualize the uptake and accumulation. Fluorescent images taken following 3 and 24 hour incubation with Tf conjugated coumarin loaded nanoparticles clearly demonstrated significant internalization compared to plain coumarin and non-targeted coumarin nanoparticles in A549 and H1299 cancer cells even after 3 hour incubation period. It can also be observed that there was higher accumulation of the Tf-Cou NP around the nucleus (DAPI stained), the most evident location for nanoparticle disruption and drug release inside the cells (163). Presence of Tf and positive surface charge on the Tf-Cou NP enables interaction of nanoparticles with cell surfaces (negatively charged), thus further resulting in efficient cellular internalization compared to that of Cou NP and plain coumarin. With increase in incubation period from 3- to 24 hours, even Cou NP treated cells were found to demonstrate higher fluorescence as Tf-Cou NP as can be seen from **Figure 23A & 24A.**

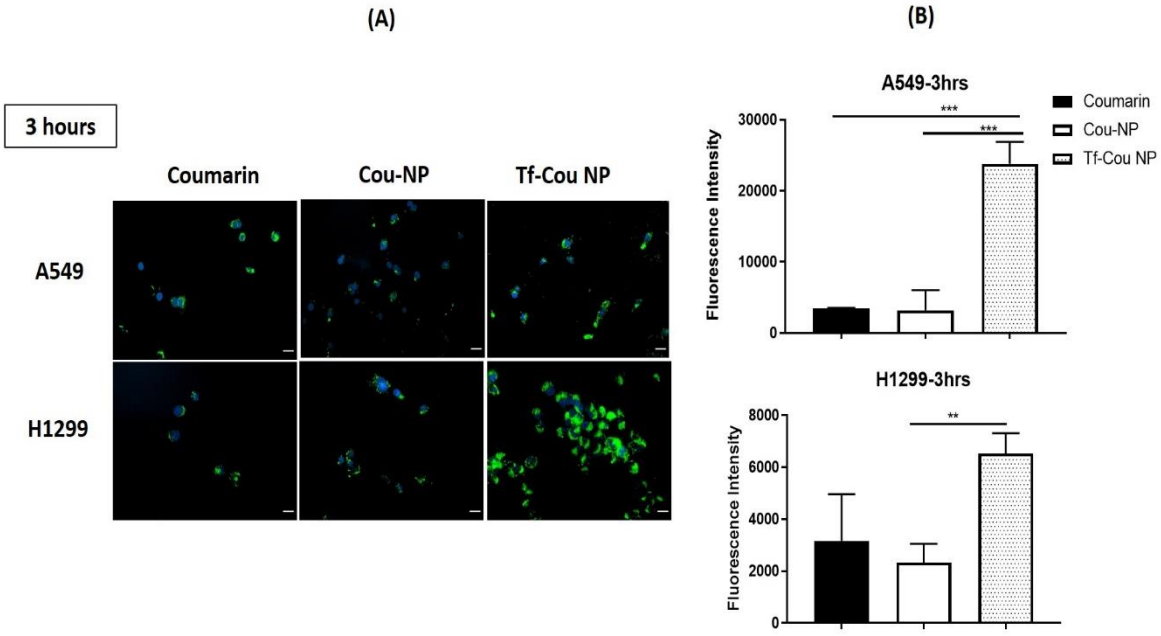

Figure 23. *In-vitro* cellular uptake of coumarin-6 loaded non-targeted and Tf-targeted nanoparticles in A549 and H1299 cells at 3 hours. Coumarin-6 plain solution is used as control. Scale b*ar* 100 µm. **A**. Fluorescence microscopy images. **B.** Quantitative representation of fluorescence intensities.

www.manaraa.com

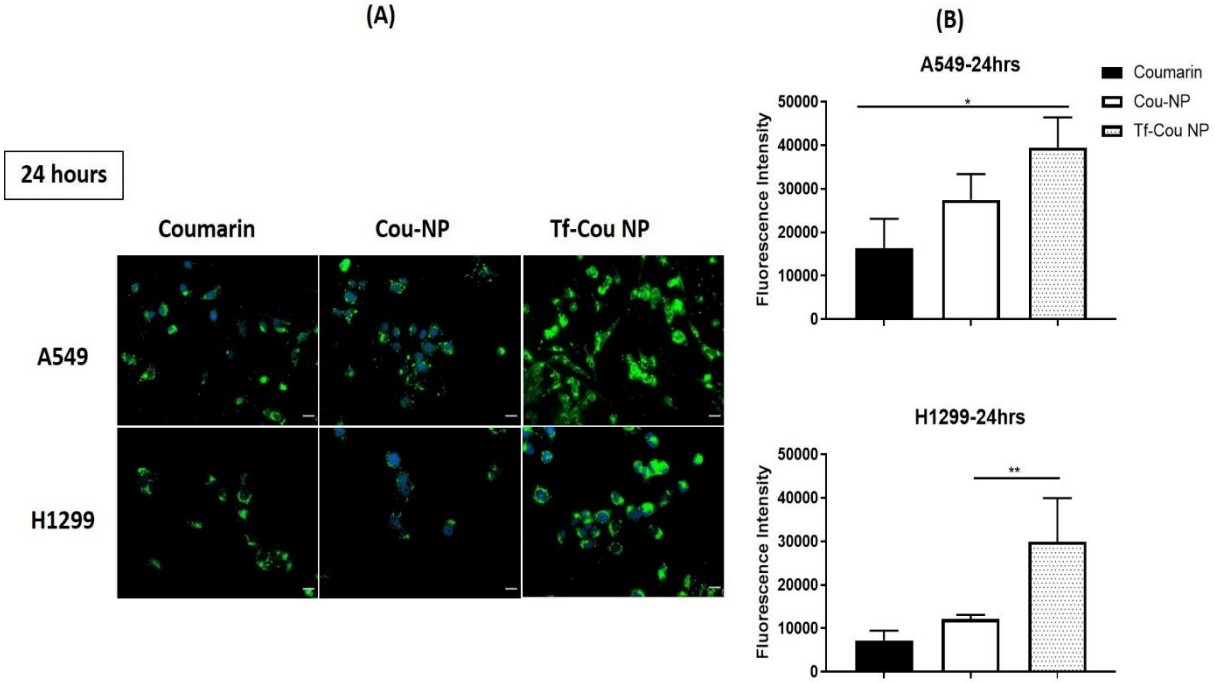

Figure 24. *In-vitro* cellular uptake of coumarin-6 loaded non-targeted and Tf-targeted nanoparticles in A549 and H1299 cells at 24 hours. Coumarin-6 plain solution is used as control. Scale b*ar* 100 µm. **A**. Fluorescence microscopy images. **B.** Quantitative representation of fluorescence intensities.

4.5.13.2. Quantification of Cellular uptake by Determining Fluorescence Intensity

The cellular uptake of Tf-Cou NP, Cou-NP and coumarin by A549 or H1299 cells was measured by fluorescence microscopy and cells were able to take up the respective treatments at various capacities as shown in **Figure 23B & 24B**. At 3hr time point, Tf-Cou NP uptake was ~6.7, 7.2: A549, ~2.8, 1.8: H1299, times higher compared with coumarin and Cou NP respectively. The fluorescence intensity of Tf-Cou NP (23928.3±3093.2: A549; 6527.6±784.3: H1299) treated cells was significantly higher when compared with Cou-NP (3291.0±2775.6: A549; 2330.0±722.0: H1299) and coumarin (3546.3±127.8: A549; 3165.6±1799.5: H1299) at 3hr time point (A549: Coumarin vs Tf-Cou NP: $p<0.001$, Cou-NP vs Tf-Cou NP: $p<0.001$; H1299: Cou-NP vs Tf-Cou NP: $p<0.01$).

www.manaraa.com

The quantitative results indicated analogous results to the fluorescence imaging shown in **Figure 23A & 24A**. Due to the presence of transferrin on the surface of nanoparticles, the uptake of the Tf-Cou NP into A549 cells is facilitated by the mutual interaction between Tf and the transferrin receptors on the cell membrane, resulting in an elevated uptake efficiency compared with Coumarin NP and plain coumarin. At 24hr time point, similar results of fluorescence intensities were obtained exhibiting highest uptake of Tf-Cou NP (39518.7±6937.2: A549; 29925.7±10056.7: H1299) compared to coumarin (16419.0±6676.1: A549; 7227.3±2237.0: H1299) and Cou-NP (27469.7±5907.3: A549; 12128.7±1025.3: H1299) at 24hr time point (A549: Coumarin vs Tf-Cou NP: $p<0.001$; H1299: Cou-NP vs Tf-Cou NP: $p<0.01$).However, the difference was not significant at 24hr time point. This might be because of saturation of all transferrin receptors.

4.5.14. Cytotoxicity Studies

Cell viability studies were performed using MTT assay to evaluate the cytotoxic potential of Tf-conjugated and non-conjugated AQ-loaded NPs versus plain drug. From this study, it was revealed that AQ cytotoxicity against NSCLC cell lines was significantly enhanced by nanoparticle encapsulation. Similar trend was found in both NSCLC cell lines: A549 and H1299. **Figures 25A & 25B** illustrate the cytotoxic effects of AQ, AMQ NP and Tf-AMQ NP in A549 and H1299 NSCLC cell lines respectively. The IC_{50} values for plain AQ, AMQ NP and Tf-AMQ NP were found to be 25.3±11.0µM, 3.0±1.7µM and 3.0±2.1µM in A549 cell line; 42.2±3.0 µM, and 37.1±11.5µM and 18.0±5.0µM in H1299 cell line respectively **(Figure 25C).** Smaller and consistent particle size and positive

www.manaraa.com

surface charge and targeting capability of Tf-AMQ NP facilitates efficient internalization of nanoparticles resulting in more accumulation of nanoparticles inside the cells, thus leading to higher cytotoxic potential at the same dose. The IC_{50} value of Tf-AMQ NP was lower than that of free AQ and AQ-loaded nanoparticle without Tf -conjugation in case of H1299 cell line which was reported to possess overexpression of transferrin receptors compared to their expression in A549 cells (107). However, to evaluate the anti-cancer efficiency of transferrin targeted nanoparticles further *in vitro* studies are performed. *In-vitro* cytotoxicity studies of Blank NP and Blank Tf-NP were performed on A549 cell line. Both Blank NP and Blank Tf-NP were found be safe from % cell viability determinations after incubating A549 or HEK cell line for 72hours which has been represented in **Figure 26A & 26B** respectively. In none of the cases was cell viability below 70% using blank nanoparticles equivalent to concentrations ranging from 0.39 to 50µM, suggesting that formulation components were not toxic by themselves. To further determine the cytotoxicity of AQ, AMQ NP and Tf-AMQ NP toward normal cells, HEK cells were incubated with respective treatments. Free AQ reduced cell viability to a greater extent (34% viable; p<) whereas AMQ NP and Tf-AMQ NP treatments resulted in ~ 70% cell viability (**Figure 26C)** when compared with untreated control cells. Hence, AMQ NP and Tf-AMQ NPs demonstrated reduced cytotoxicity when compared with plain drug. These results demonstrate that developed targeted nano drug delivery formulation markedly reduces AQ-induced toxicity to normal cells.

www.manaraa.com

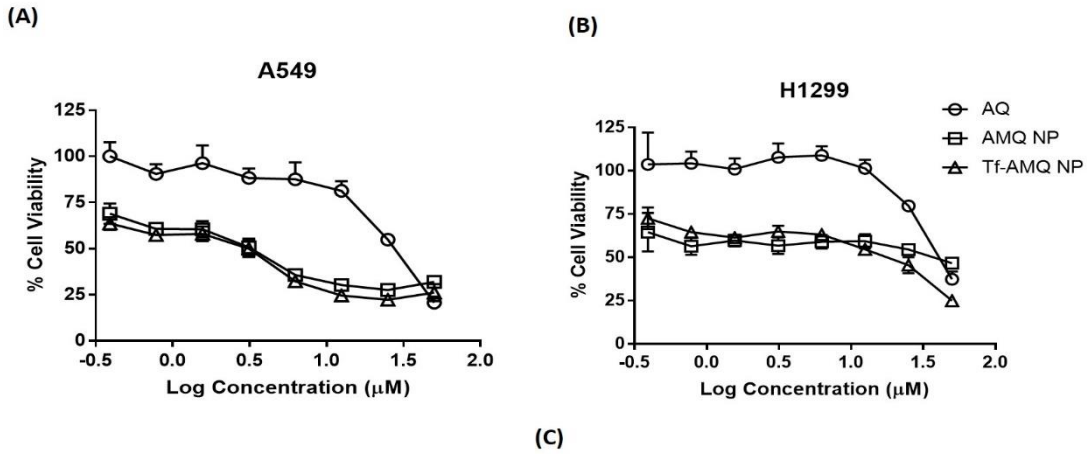

(C)

Cell Line	IC_{50} (μM)		
	AQ	AMQ NP	Tf-AMQ NP
A549	25.3±11.0	3.0±1.7	2.9±2.1
H1299	42.2±2.9	37.1±11.5	18.0±5.0[a]

[a]****, *p<0.0001*

Figure 25. Inhibitory effects on different NSCLC cell lines **A.** A549 and **B.** H1299. **C.** IC50 of AQ, AMQ NP and Tf-AMQ NP in A549 and H1299.

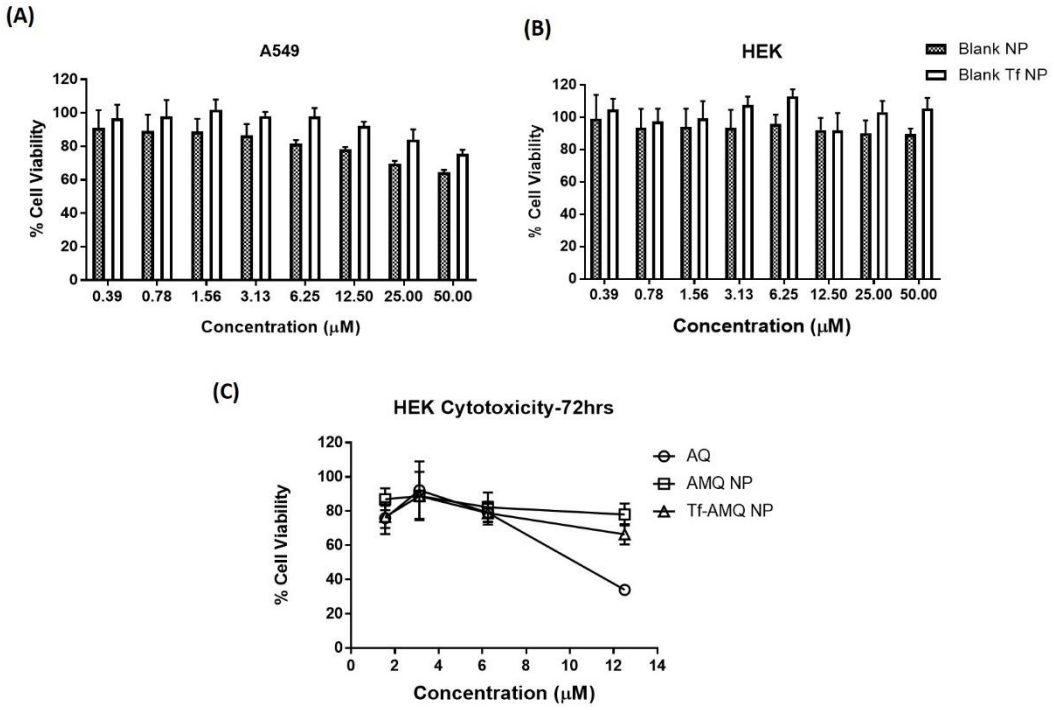

Figure 26. Safety studies: **A, B.** Cytotoxicity studies on A549 and HEK cell line after treatment with Blank NP and Blank Tf-NP. **C.** Cytotoxicity studies on A549 and HEK cell line after treatment with AQ, AMQ NP and Tf-AMQ NPs.

www.manaraa.com

4.5.15. Clonogenic Assay

Clonogenic assay is an *in-vitro* cell survival assay used to determine the colony formation capability of single cancer cells (164). AQ, AMQ NP and Tf-AMQ NP were evaluated for their long-term efficacy using clonogenic assay in A549 and H1299 cell lines. From **Figure 27A**, it can be illustrated that colony growth was significantly inhibited by Tf-AMQ NP compared to AQ and AMQ NP in A549 and H1299 cell lines. After 48 hour treatment period and 7 day incubation, % of colonies survived after treatment with 10 µM AQ, AMQ NP and Tf-AQ NP were 38.2±5.4%, 28.8±2.1% and 2.0±1.0% (**Figure 27B;** AQ vs Tf-AMQ NP: $p<0.01$, AMQ NP vs Tf-AMQ NP: $p<0.05$, Control vs Tf-AMQ NP: $p<0.0001$) considering number of colonies to be 100% in drug free treatment control wells. In case of

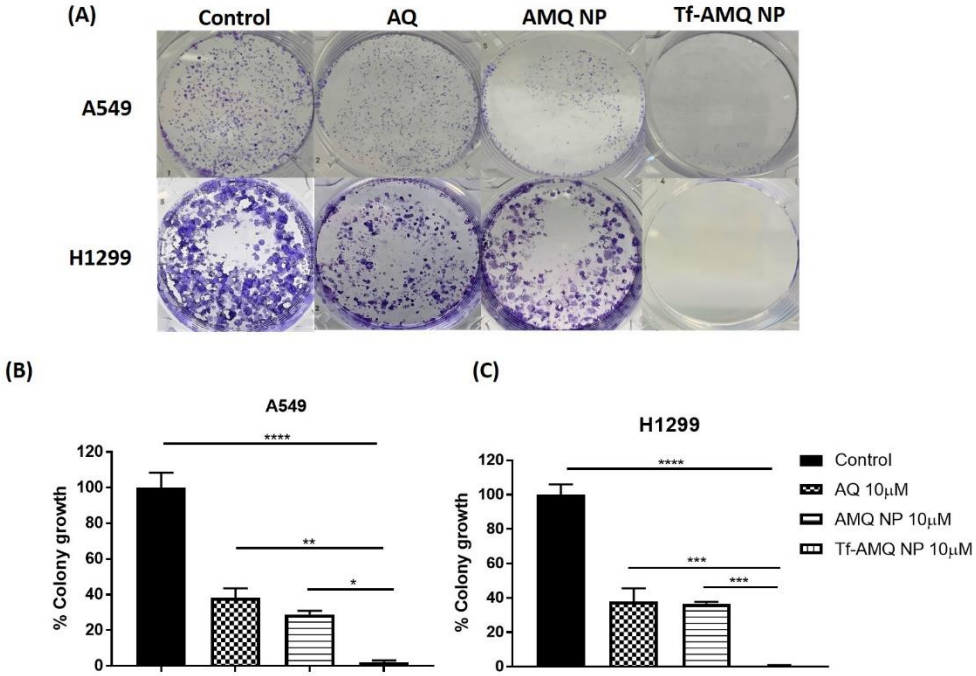

Figure 27. A. Representative images showing distinct colonies after staining in A549 and H1299 cell lines. Three different experiments were performed. **B & C.** Quantitative representation of clonogenic assay as % colony growth with AQ, AMQ NP and Tf-AMQ NPs treatment as compared to control in A549 and H1299 cell lines respectively.

www.manaraa.com

H1299 cell line, % of colony growth was found to be 38.0±7.7%, 36.7±1.1% and 0.6±0.4% AQ, AMQ NP and Tf-AMQ NP (**Figure 27C;** AQ vs Tf-AMQ NP: *p<0.001*, AMQ NP vs Tf-AMQ NP: *p<0.001,* Control vs Tf-AQ NP: *p<0.0001*). The data suggest an approximately 14.4, 19.1-fold (A549); 61.2, 63.3-fold (H1299) higher efficacy against cancer colony formation with Tf-AMQ NP as compared to AMQ NP and plain AQ respectively. This data may be considered a representative of Tf-AMQ NP's efficacy in suppressing the possibility of metastasis or new tumor growth by reproduction inhibition; and can well be linked to enhanced intracellular (and intratumoral) drug accumulation with nanoparticles formulation.

4.6. Mechanism of Action

4.6.1. Apoptotic Assay

To evaluate induced active caspase-3 enzyme, cleavage product of a fluorogenic caspase substrate, DEVD-AMC was measured. The EnzChek® Caspase-3 Assay Kit allows the detection of apoptosis by assaying for increases in μcaspase-3 and other DEVD-specific protease activities (e.g., caspase-7). As seen in **Figures 28A & 28B**, increased caspase-3 activity was observed in A549 and H1299 cells with Tf conjugated nanoparticle treatment compared to plain drug, non-targeted nanoparticle and control (fluorescence intensity measurements: A549: 1250.0±254.1 (Control), 2284.0±226.2 (AQ 25 μM), 2625.0±348.5 (AMQ NP 25 μM) and 3551.4±424.3 (Tf-AMQ NP: 25 μM); H1299: 9949.8±2395.6 (Control), 12362.4±1799.0 (AQ 25 μM), 13816.0±1591.1 (AMQ NP 25 μM) and 17227.4±1352.8 (Tf-AMQ NP 25 μM) as seen in **Figure 28A & 28B.** Treatment with Tf-AMQ NP was found to exhibit significantly higher caspase-3 levels compared to rest of the treatments (A549: Control vs Tf-AMQ NP *p<0.0001,* AMQ NP vs Tf-AMQ NP *p<0.01*

www.manaraa.com

and AQ vs Tf-AMQ NP *p<0.001;* H1299: Control vs Tf-AMQ NP *p<0.001* and AMQ NP

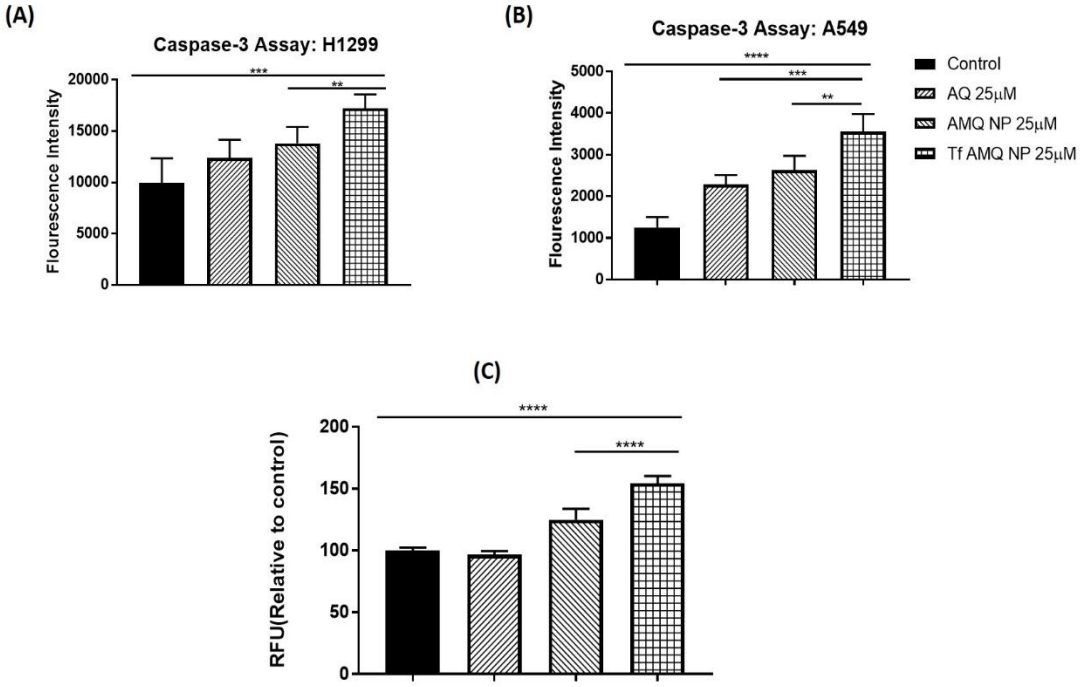

Figure 28. A, B. Detection of caspase-3 levels in H1299 and A549 cells respectively using the EnzChek® Caspase-3 Assay. **C.** Autophagy inhibition assay. Graph represents the comparison of relative fluorescence units (RFU) after incubating with respective treatments.

vs Tf-AMQ NP *p<0.01*). This experiment may signal toward presence of an alternate apoptotic pathway responsible for AQ's tumor inhibiting properties.

4.6.2. Autophagy Inhibition Assay

Nanoparticles of AQ were found to cause autophagy inhibition significantly more compared to plain drug. This was confirmed from the results of fluorescence measurements. Nanoparticle (25μM) treated cells exhibit accumulation of green fluorescent vesicles with higher intensity compared to cells treated with plain amodiaquine or starved media, as seen in **Figure 28C.** (blue fluorescence represents Hoechst 33342 nuclear stain)**.** Following normalization of data to control as 100%, relative fluorescence intensities, representing co-localization of LC3 protein and thus accumulation of

www.manaraa.com

autophagosomes, were found to be 96.5±3.0% (AQ 25 µM), 125.0±8.8% (AMQ NP 25 µM) and 154.4±5.8% (Tf-AMQ NP: 25 µM) after treating A549 cells for 18 hours (Control vs Tf-AMQ NP $p<0.0001$, AQ vs Tf-AMQ NP $p<0.0001$). Increased accumulation of autophagic vesicles is confirming autophagy inhibition which leads to tumor growth due to blockade of this crucial pathway required for the survival and proliferation of cancer cells (166).

4.7. 3D Spheroid Cell Culture Studies

As described in *Methods* section, 3D spheroid cell culture study was designed to better predict the physiological interaction of transferrin receptor targeted amodiaquine loaded NPs with tumors. In case of solid tumors, the monolayered cell cultures do not accurately mimic tumor structure, resistance to drugs and drugs' poor penetrability due to tumor microenvironment (208). To bridge the gap between *in-vitro* and *in-vivo* studies, a 3D spheroid study was carried out according to previously published studies from our group (32,147,209). These cultures (tumor spheroids) combine the ability to mimic the 3D structure of malignant tissue accurately in addition to being relevant to cancer microenvironment to which the tumor cells are exposed (210,211). A 3D *in-vitro* model was developed successfully by using specific Corning ultra-low attachment spheroid plates as reported by Elbatanony and Parvathaneni *et al* (204) so that under favorable incubation conditions, cells grow into a spheroid mass.

For this spheroid study, A549 cell line was chosen which forms spheroid masses from day 1 on culturing which were grown for 3 days. This study was performed using single dose regimen. Spheroid images were captured using inverted microscope (Laxco, Mill

www.manaraa.com

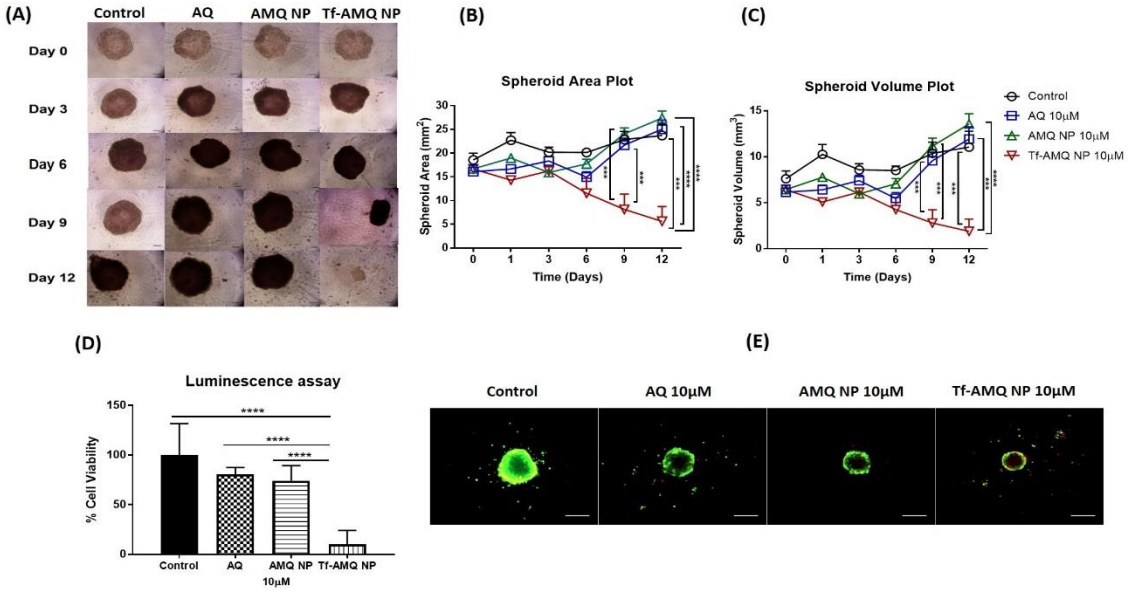

Figure 29. 3D Spheroid study: A. Spheroid images of A549 cell line. B, C. Spheroid area and volume comparison plots. Data represent mean ± SEM (n = 6). **D.** Cell viability study was performed using CellTiter-Glo® Assay on A549 Spheroids. **E.** H1299 spheroids were stained using the viability/cytotoxicity assay kit to differentiate between live and dead cell population in respective spheroids.

Creek, WA, USA) on respective days and were analyzed using the ImageJ software Version 1.44 (National Institute of Health, USA)**.** Spheroid images (**Figure 29A)**, spheroid area (**Figure 29B)** and spheroid volume (**Figure 29C)** comparisons are represented in **Figure 29**. Control group of spheroids (blank media control) found to be growing in size over a period of 12 days, whereas the growth of treated spheroids was significantly inhibited.

In this single dose study with a single treatment given on day 1, control spheroids were found to have a diameters and volumes of 2731.7±325.2 µm, 11.1 ± 1.7 mm^3 on day 12 as compared to a spheroid diameters and volumes of 2813.1±277.0 µm, 11.9 ± 1.3 mm^3 (AQ: 10µM), 2948.7±193.6 µm (AMQ NP: 10µM), 13.6 ± 1.1 mm^3 and 1101.5±830.2 µm, 1.9± 1.3 mm^3 (Tf-AMQ NP: 10µM). A significant reduction in spheroid volumes was

www.manaraa.com

observed in case of Tf-AMQ NP treated spheroids on day 9 and 12. (Day 9: 10μM: Control vs Tf-AMQ NP $p<0.001$, AQ vs Tf-AQ NP $p<0.01$, AQ NP vs Tf-AQ NP $p<0.001$; Day 12: Control vs Tf-AQ NP $p<0.001$, AQ vs Tf-AQ NP $p<0.001$, AQ NP vs Tf-AQ NP $p<0.0001$ **(Figure 29C)**. Thus, underlining a more pronounced tumor reduction potential of Tf-AMQ NP. Treatment with Tf-AQ NP resulted in a significant difference in spheroid volumes as compared to AQ, AMQ NP and control treated groups. Tumor growth suppression was continually observed until the end of the treatment.

4.7.1. CellTiter-Glo Luminescent Cell Viability Assay

While volume determination provides valuable information about external size of the tumor/spheroid, it may not accurately predict the cytotoxicity of the treatment against cells inside the core of the tumor. CellTiter-Glo luminescent cell viability assay was performed to compare counts of viable cells in treated 3D single dose spheroids on day 12 after microscopic quantification. Once again, Tf-AQ NP treated spheroids exhibited significantly reduced proportion of viable cells compared to control and their corresponding AQ, AMQ NP concentration (10μM: Control vs Tf-AMQ NP $p<0.0001$, AQ vs Tf-AMQ NP $p<0.0001$, AMQ NP vs Tf-AMQ NP $p<0.0001$). % cell viability results (111.7 ± 9.8%, 92.7 ± 27.1% and 8.1 ±9.9% for AQ, AMQ NP and Tf-AMQ NP) were graphically represented in **Figure 29D**. These results support the previous findings of 3D spheroid studies, that demonstrated enhanced anti-cancer effectiveness of Tf-AMQ NPs in comparison to AQ and AMQ NP.

www.manaraa.com

4.7.2. Live-Dead Cell Assay

In case of H1299 spheroids, live cell population (green fluorescence) for Tf-AMQ NP treated groups was found to be less compared to that of plain AQ and AMQ NP groups on day 15. **(Figure 29E)**. Reduction in live cell proportion in case of targeted nanoparticle group compared to other groups is indicating their ability of AQ NP in inhibiting tumor cell proliferation.

4.8. Discussion

Nanoparticle drug delivery systems are contributing greatly in the design and development of formulations to treat several lung disorders especially lung cancer (212). Moreover, application of targeted NPs promises immense potential owing to the recent advances in cancer therapeutics (213). Nanoparticles enable surface modifications, thus facilitate site-specific delivery through active targeting to achieve an improved therapeutic strategy and reduced toxicity (213,214). As in case of non-small cell lung cancer (NSCLC), tumor cells exhibit overexpression of certain receptors like transferrin (215). Hence, nanocarriers functionalized with transferrin as targeting ligand are able to target those cancer cells and result in enhanced drug accumulation in tumor cells further demonstrating superior anti-cancer efficacy. For instance, Upadhyay *et al* developed transferrin-decorated thymoquinone loaded nanoparticles and reported the their potential in targeting non-small cell lung cancer cells (215).

As there is a great need to discover/develop new drugs with anti-cancer efficacy due to the toxic effects caused by chemotherapeutic agents, drug repurposing provides an excellent opportunity to find novel anti-cancer uses for previously FDA approved drugs

www.manaraa.com

(2,105). Recently, nanoparticles of AQ (FDA approved anti-malarial) have been reported for their anti-cancer efficacy from our research group where cationic polymer loaded NPs were reported for their superior efficacy. Furthermore, to achieve a targeted drug delivery, a targeting ligand transferrin has been employed in the fabrication of nanoparticles in the current study. In this context, current study had explored the enhanced anti-cancer efficacy of surface functionalized amodiaquine-loaded polymeric NPs in NSCLC. Conjugation of the PLGA polymer with a targeting moiety, transferrin has been carried out successfully to address the payload to specific cancer. Schematic representation of the conjugation reactions is Further, results obtained from the conjugation efficiency determinations have assured the presence of Tf on the surface of nanoparticles. FTIR characterization have revealed the presence of an amide bond in transferrin conjugated PLGA polymer, thus confirming the formation of a covalent bond between Tf and PLGA as shown in **Figure 19**.

Physicochemical characterization of the drug loaded nanoparticles is important in the field of drug delivery, as it greatly influences the uptake and cellular interaction of the particulate system; thus, ultimately determining the fate of the entrapped drug under *in vitro* and *in vivo* conditions. Lower particle size of developed targeted NPs (244.1±10.5nm) with positive zeta potential (8.2±1.3 mV) **(Figure 19D)** enabled higher accumulation in cancer cells. Further, the nanoparticles exhibited desirable drug release kinetics under acidic pH (5.5) supporting their testing in biological systems as shown in **Figure 20A**. In addition, spherical surface with smooth morphology and narrow size distribution are evident by TEM analysis as represented in **Figure 20B**. From solid state characterization studies such as DSC and XRD, developed NPs were found to encapsulate drug inside their

www.manaraa.com

polymeric core. No characteristic XRD or endothermic peaks were observed in case of both nanoparticle formulations **(Figure 20C-D)**. Stability of the developed formulations has been evaluated in terms of physicochemical properties such as particle size, zeta potential and % entrapment efficiency. Results demonstrated that NPS possess long term stability (28 days) at both 4°C and room temperature **(Figure 21)**, thus assuring the developed conjugated NPs as effective delivery carriers with desired stability.

In achieving local delivery of therapeutics, pulmonary route of administration is of prime importance (191). As shown in **Figure 22**, developed both AQ-loaded nanoparticles have demonstrated excellent aerosolization properties confirming their superior deposition in the respirable region (bronchoalveolar) of the lungs. Hence, these nanoformulations can be administered via inhalation, facilitating local delivery to the deep lungs while reducing exposure to healthy tissues and further reducing adverse events. During *in-vitro* aerosol lung deposition test after nebulization, NPs were delivered as small droplets and deposited in the lung airways, confirming the respirability of formulated AQ nanoparticles and efficient lung deposition. Developed Tf conjugated and non-targeted amodiaquine nanoparticles are capable of providing a promising strategy to overcome the physiological barriers involved in respiratory tract, and ensuring their capability to reach the respirable regions of the lung (137).

Intracellular uptake images shown in **Figure 23A & 24A** reveal the same where Tf conjugated coumarin nanoparticles were internalized by A549 or H1299 cells efficiently within 3 hours compared to plain coumarin solution or unconjugated nanoparticles. **Figure 23B & 24B** clearly indicate that Tf-coumarin NP uptake was ~7.2 and 1.8 times higher compared with Cou NP in A549 and H1299 cells respectively after 3 hours.

www.manaraa.com

Extensive *in-vitro* cell culture studies were carried out to investigate the efficacy of AQ NP against NSCLC. Presence of transferrin on nanoparticles associates with higher cellular uptake and greater cytotoxicity in cancer cells and explains the specificity of Tf-mediated binding of conjugated NPs (170). Recently, research work conducted by Guo *et al.* has demonstrated that Tf-conjugated lipid-coated NPs were able to deliver doxorubicin to lung cancer cells both *in-vitro* and in-vivo (216). Cytotoxicity study results in the present study indicated differentiation in cell inhibition behavior between free amodiaquine and amodiaquine loaded nanoparticles either Tf conjugated or not, thus emphasizing the key role of targeted NPs internalization in enhancement of cytotoxic activity. As shown in **Figure 25B**, the cytotoxicity exhibited by transferrin conjugated amodiaquine NPs towards H1299 NSCLC cell line could be attributed to their targeting ability as respective cell line exhibits overexpression of transferrin receptors (107). To elaborate, targeted NPs exhibited a lower IC_{50} value than the plain drug and unconjugated NPs in case of AQ-loaded NPs were also evaluated for their effect of clonal expansion ability which is an important step of metastasis via clonogenic assay. Results from this study revealed that Tf-AMQ NPs have the ability to display a significant reduction in cell survival and a profound inhibition in the colony formation compared to AMQ NP or plain amodiaquine. the ability of single cells more efficiently to form colonies compared to non-targeted nanoparticles. Hence, it ensures the effectiveness of Tf-AMQ NP on long term basis while preventing tumor recurrence. Overall, Tf-AMQ NP could be further evaluated for their establishment in NSCLC treatment explicitly.

Furthermore, the potential of AQ, AMQ NP and Tf-AMQ NP was investigated and compared through apoptosis assay as apoptosis is the main mechanism of growth inhibition

www.manaraa.com

in many proliferative disorders, such as cancer. Caspases are cysteine proteases, activated in presence of death inducing stimuli (141). It was observed that Tf-AMQ NP treatment induced caspase-3 levels, demonstrating their ability to induce cell death through apoptosis as well via measurement of apoptotic marker (caspase-3). Thus, apoptotic induction could be a mechanism for its anti-cancer activity. In agreement with our earlier report on amodiaquine loaded NPs (198), amodiaquine exhibited autophagy inhibition with either targeted or non-targeted amodiaquine loaded nanoparticles demonstrating significantly higher autophagy inhibition efficiency, potentially due to higher cellular internalization of the treatment (105). This indicated the accumulation of autophagosmes which infers to the inhibition of autophagy process, essential for the further proliferation of cancer cells under stress conditions. In brief, AQ causes an increase in lysosomal pH, which inhibits lysosome function and blocks fusion of autophagosomes with the lysosomes (139), thus conserving LC-3 protein and producing a positive signal in the CYTO-ID® Autophagy detection assay as seen in **Figure 28C**.

Development of 3D *in-vitro* models is of utmost necessity today to mimic *in-vivo* solid tumor conditions which could be achieved by using specific low attachment spheroid plates as reported in our previous publications (20,32). From results seen in **Figure 29**, it can be understood that nanoparticles were able to deliver the drug to spheroids' core efficiently ensuring their clinical use. In addition, % cell viability assay results **(Figure 29D)** on day 12 of spheroid study confirmed superior anti-cancer efficacy of Tf-AMQ NP. Hence, results from this spheroid study provide a strong evidence for capability of Tf conjugated nanoparticles to deliver the drug to spheroid's core efficiently and their potential *in-vivo* efficiency, which could be extended to further preclinical studies. It can

www.manaraa.com

be understood that through the addition of a ligand (Tf) at the NP surface, NPs are directed against receptors (transferrin) exposed at the outer cell surface, simultaneously improved uptake and distribution of NPs in the tumor mass despite of complicated tumor microenvironment (217).

Taken together, we present the first report of transferrin conjugated nanoparticles for delivery of amodiaquine for the treatment of NSCLC. Different *in-vitro* cell culture studies as well as 3D spheroid models illustrated the pronounced efficiency of amodiaquine-loaded transferrin functionalized nanoparticles in NSCLC treatment.

4.9. Conclusion

From the present study, it can be concluded that inhalable transferrin conjugated nanoparticles of amodiaquine could be successfully formulated by a scalable high-pressure homogenization (HPH) approach. Formulated NPs were characterized for their physicochemical properties, found to have favorable particle size and surface charge facilitating efficient cellular internalization. Developed targeted AQ loaded NPs were compared with their counterpart (non-targeted AQ loaded nanoparticles) in their anti-cancer efficacy against NSCLC. Several *in-vitro* cell culture studies including cytotoxicity studies and 3D spheroid studies, assays exhibiting the autophagy inhibition and colony formation where superior efficacy of transferrin conjugated NPs has been confirmed. Altogether along with apoptosis inhibition capability of Tf-AMQ NPs, results are promising them as a potential treatment strategy for NSCLC. Going forward, it would be a great idea to evaluate the therapeutic activity of transferrin decorated AQ-loaded NPs in *in-vivo* models.

www.manaraa.com

CHAPTER 5

5. Development and Characterization of Folic acid Conjugated Amodiaquine Loaded Nanoparticles-Efficacy in Cancer Treatment

Non-small cell lung cancer (NSCLC) is a malignant tumor type with overexpression of certain receptors such as transferrin (Tf), folate etc. (FRα) etc. Hence targeting these receptors through specific ligands is of considerable interest. Especially, FRα regulates cellular uptake of folate molecules (FRα) (218). By targeting these receptors on cancer cells through specific targeting ligands is advocated to achieve superior anti-cancer efficacy. Hence, conjugation of receptor-specific ligand FA can specifically target multiple cancer cells facilitating targeted drug delivery of therapeutics. NSCLC cell lines such as A549, cervical cancer cell line (HeLa) and breast cancer cell line (MDAMV-231) were employed in the current study. We aim to develop scalable folic acid conjugated AQ-loaded nanoparticles (FA-AQ NPs) for targeted and efficient cancer treatment regimen.

5.1. Introduction

Cancer is the leading cause of deaths worldwide although there are several treatment regimens available for the treatment. Moreover, main limitations of the current therapies include resistance against chemotherapeutic agents and the adverse events/toxicity effects with majority of the current regimens. Thus, it raised attention of many researchers to explore new drugs or new therapies for an effective cancer therapy (219). While discovery or development of new drugs takes longer time periods, drug repurposing has become an

www.manaraa.com

attractive strategy to discover new uses of old FDA approved drugs (2). Hence, utilization of old drugs against new indication is very crucial.

All of the cancer types share majority of the features such as uncontrolled cell growth and probability for metastasis. When it comes to pathophysiology of cancer cells, majority of the cancer cells exhibit overexpression of certain receptors such as transferrin (Tf), folate (FRα) etc. which play a crucial role in iron homeostasis, cellular proliferation (Tf) and regulating cellular uptake of folate molecules (FRα). By targeting these receptors on cancer cells through specific targeting ligands is advocated to achieve superior anti-cancer efficacy. Cancer cells necessitate more iron for their uncontrolled growth and proliferation, resulting in overexpression of folic acid-receptors (FA) in several malignant tumors including breast, cervical cancers including NSCLC. A glycosylphosphatidylinositol-anchored cell surface receptor (FRα) for folic acid has been known to be overexpressed in several human tumors such as non-small cell lung cancer, cervical, ovarian and breast cancers (220). Targeting FRα receptors through folic acid offers many potential advantages pertaining to its small size and promising pharmacokinetic properties of the folic acid conjugates. Moreover, this targeting ligand could reduce probability of immunogenicity, allowing for repeated administration; offers simple and well-defined conjugation chemistry enabling easier conjugation reactions (221). As the expression of folate receptors is highly restricted in normal tissues and presence of high receptor affinity of folic acid results in its high tumor tissue specificity. Further internalization of FA receptor–ligand complex takes place via endocytosis (221). While nanoparticles enable the delivery of therapeutics effectively, conjugation of targeting moieties would be of great importance in achieving a safer drug delivery. Several

www.manaraa.com

nanocarrier systems such as liposomes and polymeric nanoparticles have been developed for the purpose of selective targeting against tumors. Utilizing targeted NPs in drug delivery establishes a platform for an efficient, tumor-specific interactions by interacting with receptors on the surface of cancer cells (190). Several other studies have investigated the targeting potential of drug-folic acid conjugates against different cancers as summarized by Lutz *et al* (222).

Based on the previous investigations from our research group (198), amodiaquine (FDA approved anti-malarial drug) has been chosen for evaluating its superior efficacy through a combination of nanoparticle encapsulation and targeting. PLGA-based folic acid-conjugated NPs of amodiaquine, 4-[(7-chloroquinolin-4-yl) amino]-2-[(diethylamino) methyl] phenol (AQ) were formulated using a scalable, reproducible high-pressure homogenization (HPH) approach and evaluated for their anti-cancer efficacy. Recently, superior anti-cancer efficacy of AQ-loaded nanoparticles against NSCLC has been reported in a research study published from our group. In the current project, we aim to achieve a further tumor targeting efficacy through folic acid decorated nanoparticles.

In the present study, the anticancer activity of folic acid conjugated amodiaquine loaded nanoparticles (FA-AQ NP) against FA-receptors expressing cancer cells has been evaluated. Process of functionalization/conjugation refers to the chemical addition of targeting ligand folic acid to enhance the target nanoparticles to the lung tumor tissue. AQ-loaded NPs with folic acid ligand conjugated were prepared and were then characterized by various analytical techniques such as for their physicochemical properties and also targeting capability. Thereafter several 2D and 3D cell culture studies were carried out to assess the specificity of the folate receptors and to determine whether nanoparticles are

www.manaraa.com

exhibiting more anti-cancer efficacy than the plain drug. Targeted nanoparticles were evaluated to verify the hypothesis that folic acid decorated NPs are capable of demonstrating superior efficacy in treating multiple cancers.

5.2.Materials and Methods

5.2.1. Materials

Poly (lactic-*co*-glycolic) (PLGA 50:50, 7-17 kDa, acid terminated), poly vinyl alcohol (PVA) and amodiaquine (AQ) were purchased from Sigma-Aldrich (St. Louis, MO, USA). Folic acid was obtained from Fisher Scientific (Hampton, NH, USA). A549 (NSCLC) cell line was obtained from ATCC (Manassas, VA, USA) and maintained in RPMI-1640 medium (Corning) supplemented with 10% FBS (Atlanta Biologicals, R&D Systems, Minneapolis, MN, USA), sodium pyruvate and penicillin-streptomycin (Corning, NY, USA) at 5% CO_2/37°C. Human embryonic kidney (HEK-293), HeLa and MDAMB-231 cell lines were obtained from ATCC and maintained in DMEM medium (Corning) supplemented with 10% FBS and penicillin- streptomycin at 5% CO_2/37°C. 3-(4,5-dimethylthiazol-2-yl)-2,5-diphenyltetrazolium bromide (MTT), dichloromethane (DCM), dimethyl sulfoxide (DMSO), coumarin-6, crystal violet dye, 16% paraformaldehyde (PFA) solution, Triton X100, diethyl ether, HPLC grade methanol, acetonitrile (ACN) and water were purchased from Fisher Scientific (Hampton, NH, USA). Molecular biology kits, supplies, and antibodies were purchased from other commercial vendors which are listed at appropriate places throughout the manuscript. All other solvents including UPLC grade chemicals and solvents, unless it is otherwise specified, were purchased from Fisher Scientific (Hampton, NH, USA).

www.manaraa.com

5.2.2. Development of UPLC method for Determination of Amodiaquine (AQ)

A reverse-phase liquid chromatography method was developed for quantifying AQ using Waters series Acquity UPLC (Waters, USA). Detailed description of method was reported in our recent publication (198).

5.2.3. Calibration Curve for Folic acid

Standard solutions (15.6, 31.3, 125 and 250 μg/ml) of folic acid were prepared by diluting with DMSO. Absorbance was measured at 256nm using SPARK Tecan plate reader (Tecan Spark 10M; Tecan, Männedorf, Switzerland). The calibration curve was constructed between concentration of FA and absorbance values.

5.2.4. Synthesis of PLGA–PEG–FA Conjugate

Target-specific drug delivery through utilization of FA ligand has been carried out by employing a surface-activation method as reported earlier with slight modifications (223). A brief synthetic scheme for the PLGA–PEG–FOL conjugate preparation was prepared is represented in **Figure 30B**. Briefly, PLGA solution (1g/8mL DCM) was activated by 80 mg EDCI and 57.5 mg NHS at room temperature for 24 hours under gentle stirring. Obtained solution was filtered and precipitated by dropping into ice-cold diethyl ether (50mL) and the resulting product of activated PLGA was completely dried under vacuum. Then organic solution of activated PLGA (0.5g/4mL DCM) was added slowly to PEG–bis-amine solution (50 mg/1mL DCM) in a dropwise manner. This reaction was carried out for 6 hours under room temperature, then the resultant solution was precipitated by the addition of ice-cold diethyl ether (25mL). The precipitated product, amine-terminated di-block copolymer, PLGA–PEG–NH2 was filtered and dried. FOL-conjugated di-block copolymer

www.manaraa.com

was synthesized by coupling the PLGA–PEG–NH2 di-block copolymer with an activated folic acid. Briefly, 250 mg di-block copolymer dissolved in 2.5ml dimethyl sulfoxide (DMSO) was mixed with 6.5mg folic acid and 6.5 mg EDCI. The reaction was performed at room temperature for 7 hours and then mixed with 50 ml cold methanol and filtered through the paper filter. The precipitate on the filter was dried under vacuum, and then dissolved in 25mL DCM; in this way, free FOL was precipitated in DCM but conjugated FOL was dissolved, after centrifugation at 21,000 x g; the supernatant was dried under vacuum. Collected conjugated PLGA after centrifugation was analyzed for the conjugation efficiency and utilized in the formulation of nanoparticles.

5.2.5. Determination of Conjugation Efficiency

The conjugation percentage was calculated by determining the amount of folic acid conjugated in PLGA–PEG–FOL. A known amount (0.59-0.81mg) of dried PLGA–PEG–FOL was dissolved in DMSO and an UV absorbance value at 256nm was measured to determine the concentration of conjugated folic acid.

5.2.6. Formulation of FA Conjugated AQ NPs (FA-AQ NPs)

Non-targeted and folic acid conjugated amodiaquine nanoparticles were formulated through HPH process. Nanoparticles were formulated through using an established high pressure homogenization technique which was recently published by our research group with slight modifications (198). Briefly, AQ-loaded nanoparticles were prepared by using organic solution of polymer PLGA 502H (20mg/1ml of DCM, aqueous solution of AQ (5mg/0.5ml), a stabilizer (20ml of 1% w/v polyvinyl alcohol solution in PBS). FA-conjugated NPs were formulated using both PLGA and FA-conjugated PLGA i.e. PLGA-

www.manaraa.com

PEG-FA at 5:1 ratio while other formulation components are the same as for non-targeted AQ-loaded NPs. A stable pre-emulsion was formed through probe homogenization at 25,000 RPM for 10 minutes. Obtained pre-emulsion was processed through high-pressure homogenizer (Nano DeBee®) at homogenization pressure of 30,000 psi and seven number of cycles to recirculate the formulation with reverse flow pattern. These process parameters have been chosen based on our previous investigations as reported in our recent publication (198). Later, formulations were subjected for rotary vacuum evaporation using rotary evaporator (Wilmad-LabGlass, Vineland, NJ, USA) for 10 min under reduced pressure of 200 bar at room temperature for organic solvent removal followed by washing of nanoparticles for removal of excess PVA. Then, NPS were washed for removal of excess PVA and were re-dispersed in milliQ water.

5.2.7. Physicochemical characterization: Particle size, PDI and Zeta potential

Physicochemical properties such as size, polydispersity, and surface charge of AQ NP Rota and FA-AQ NPs were measured using Malvern® zeta-sizer. Drug loading efficiency was measured using Waters UPLC by quantifying AQ.

5.2.8. Drug Content

Encapsulated drug amount in nanoparticle formulation was determined using a direct vesicle lysis approach. To 20µL of formulation, 1,980µL of ACN:water:DCM – 98:1.5:0.5 was added followed by centrifugation for 45 min at 4°C at 21,000 x g to lyse nanoparticles and to acquire loaded drug into the analyzing solution. Obtained supernatant was analyzed for the drug content using UPLC and % EE/%DL was calculated.

$$\%\ Entrapment\ efficiency\ (\%EE) = \left[\frac{Drug\ entrapped\ in\ nanoparticles}{Total\ drug\ added\ initially}\right] \times 100 \qquad \textbf{(Eq. 1)}$$

www.manaraa.com

$$\%\ Drug\ loading\ (\%DL) = \left[\frac{Drug\ entrapped\ in\ nanoparticles}{Total\ polymer+drug\ added}\right] \times 100 \quad \textbf{(Eq. 2)}$$

5.2.9. Morphological Analysis

Imaging of unconjugated and conjugated amodiaquine nanoparticles was performed using transmission electron microscopy (TEM) for assessing nanoparticles' morphology. The Formvar® carbon-coated copper grids 400-mesh (Electron Microscopy Sciences, PA, USA) were made hydrophilic using glow discharge plasma treatment for 60s. About 5 µL of diluted nanoparticles sample was added to the grid and allowed to adhere for 1 minute. The samples were negatively stained by adding 5 µL of uranyl acetate (1%) and excess was removed by using Whatman filter paper after 30s. This process was repeated twice and the sample was finally allowed to air dry. The grids were then imaged using Tecnai Spirit TWIN TEM operated at 120 kV voltage.

5.2.10. Solid-state Characterization Studies

Powder X-ray Diffraction (PXRD) Studies: The samples were first lyophilized into dry powders using Labconco FreeZone® freeze dryer system. X-ray diffraction spectroscopy was carried out using XRD-6000 (Shimadzu, Kyoto, Japan). The diffractometry was performed by using a graphite monochromator consisting of copper-Kα1 radiation of wavelength 1.5418 Å operating at 40 kV, 30 mA. The samples were spread uniformly on a glass micro sample holder and were analyzed in the range of 5 to 60° at the scanning speed of 2° (2θ)/minute.

Differential Scanning Calorimetry (DSC) Studies: The thermograms for AQ, AQ NP Rota and FA-AQ NP were generated by closed pan technique using a DSC 6000 (PerkinElmer, Inc; CT, USA) equipped with an intra-cooler accessory. An accurately

www.manaraa.com

weighed sample (2mg) was sealed in an aluminum pan and analyzed against a sealed empty aluminum pan maintained as reference. Study was performed over a temperature range of 30°- 300°C The heating rate was maintained at 10°C/min.

5.2.11. Stability Studies

Stability of FA-AQ NPs was evaluated while storing the triplicate samples at temperatures of 4ºC and 25ºC for 4-week period as reported previously (53). Aliquot of each sample was withdrawn at the end of week 1, 2, 3 and 4; diluted with water (100-fold) and analyzed for physicochemical characteristics such as particle size, PDI and zeta potential using Malvern Zeta Sizer as described earlier. Entrapment efficiency was determined by lysing the samples using UPLC.

5.2.12. Determination of Targeting Capability

5.2.12.1. Cellular Uptake Studies using Fluorescence Microscopy

Cellular uptake studies were performed in order to determine the effect of NP loading and folic acid targeting on intracellular uptake of the drug encapsulated using a protocol reported earlier (201). NPs for cellular uptake were formulated by replacing AQ with coumarin-6 (1mg), a fluorescent dye since it offers simple and sensitive detection for easier tracking while it has been frequently used in cellular uptake studies of PLGA nanoparticles. In brief, A549 cells were plated in 8 chambered tissue culture (TC) treated cell imaging cover glass (Eppendorf, Hauppauge, NY, USA) at a seeding density of 10,000 cells/chamber followed by overnight incubation. Next day, cells were incubated with coumarin-6, coumarin-6 loaded unconjugated and FA conjugated nanoparticles at 1 µg/mL concentration in fresh culture medium for 3 hours. After 3 hours, cells were washed with

www.manaraa.com

ice cold PBS twice and fixed with 4% paraformaldehyde (PFA) for 10 min. Fixed cells were washed again with ice cold PBS twice. Then, the chamber was removed and 20µL of vectashield hardset mount with DAPI nuclear stain (H1500, Vector laboratories, Burlingame, CA, UAS) was placed on a glass slide dropwise followed by placing a cover glass. After hardening of mounting medium overnight at 4°C, slides were imaged using EVOS-FL microscope at 20X magnification (Thermo Scientific, Waltham, MA, USA).

5.2.12.2. Quantification of Cellular Uptake by Determining Fluorescence Intensity

A549, HeLa and MDAMB-231 cells were seeded into 24-well assay plates at 1 x 10^5 cells/well. Next day, cells were incubated them with 1ml at 1µg/ml concentration of coumarin, coumarin-loaded NPs and folic acid conjugated coumarin nanoparticles at 5% CO_2/37°C for 3 hours. After 3 hours, media was removed from the wells and washed three times with ice-cold PBS. Cells were harvested using trypsin and to the obtained cell pellets, 100 µl of 0.5% Triton X-100 was added for cell lysis. These samples were kept for sonication for one hour at 4°C. The fluorescence intensity of supernatants from each sample was measured for coumarin quantification at Ex/Em of 420/465nm (Tecan Spark 10M; Tecan, Männedorf, Switzerland).

5.2.13. Cytotoxicity Studies

AQ NP Rota, FA-AQ NPs along with plain AQ were evaluated for their cytotoxicity in multiple cancer cell lines: A549 (non-small cell lung cancer, NSCLC); HeLa (cervical cancer) and MDAMB-231 (breast cancer) as reported earlier with slight modifications (146,147). HeLa and MDAMB-231 cell lines were chosen because of their characteristic to exhibit overexpression of folic acid receptors (220). In brief, A549 cells were grown in

www.manaraa.com

FBS supplemented RPMI-1640 media and HeLa, MDAMB-231 cells were grown in FBS supplemented DMEM media as described in *Materials* section, and were seeded in TC treated 96-well plates (Eppendorf, Hauppauge, NY, USA) at a seeding density of 2,500 cells/well (7,500 cells/cm^2), incubated overnight for adherence at 37°C/5% CO_2, and treatments were added next day at different AQ concentrations ranging from 0.39-50 µM. Corresponding volumes of AQ NP Rota and FA-AQ NPs were calculated based on the drug entrapment efficiency. Blank culture media was added as control. After 72 hours of incubation, % cell viability was determined by performing MTT assay as described earlier (20), by reading the absorbance of dissolved formazan crystals at 570 nm (Tecan Spark 10M; Tecan, Männedorf, Switzerland). Further cytotoxicity studies were performed following same protocol to evaluate the safety of drug-free nanoparticles (HEK) using equivalent amounts of Blank NP at concentrations of 0.39, 0.78, 1.56, 3.13, 6.25, 12.5, 25 and 50µM with 72 hours of incubation period.

5.2.14. Clonogenic Assay

Clonogenic assay is an *in-vitro* cell survival assay which is based on the single cell's capability to grow into a colony. A colony forming assay was performed to evaluate long-term cytotoxicity of AQ, AQ NP Rota and FA-AQ NP toward colony inhibition was determined. The protocol reported previously (149,201) was briefly modified and followed in this study. HeLa or MDAMB-231 cells were seeded in 6-well cell culture plates at seeding density of 500 cells/well for each cell line. After overnight incubation and adherence of cells, cells were subjected to AQ, AQ NP Rota and FA-AQ NP (10µM), or control treatments for 48 hours after which media was replaced with fresh culture medium on alternative days for 7 days. On 7th day, formed colonies were washed with ice-cold PBS

www.manaraa.com

and stained with 0.01% (w/v) crystal violet followed by washing with distilled water as reported earlier. Colonies were photographed using digital camera and the mean number of colonies from three independent experiments were counted by colony counter software Open CFU (150).

5.2.15. 3D Spheroid Cell Culture Studies

An effective cancer therapy is not only determined by enhanced cellular uptake or cytotoxic potential, but also improved penetrability of nanoparticles into solid tumors. 3D spheroid cell culture studies are capable of mimicking the *in-vivo* features of tumors as reported in our previous studies (147). Briefly, 2,000 cells per well were seeded in Corning® ultralow attachment spheroid 96-well plate (Corning, NY, USA) and were incubated overnight at 37°C/5% CO_2. For later 3 days, spheroids were allowed to grow into solid tumor mass due to the shape of these ultra-low attachment cell culture plates. On day 3, all the wells were observed for spheroid formation with a rigid margin. Images were captured using inverted microscope (Laxco, Mill Creek, WA, USA). Next day, media was replaced with either fresh media (control) or respective treatments of AQ, AQ NP Rota or FA-AQ NP. Briefly, spheroids were treated with 20µM concentration of AQ, AQ NP Rota and FA-AQ NP (to maintain original concentrations of 10µM employed in the beginning), and images were captured. 100µL of media was replaced with fresh media on further days of imaging. Images were captured on day 1, 3, 6 and 9, 12 and 15 days following treatment. in a gentle manner to avoid the bubble formation and the aspiration of spheroid itself. NIH ImageJ software (Version 1.44) was used to measure diameter of all the spheroids and spheroid volumes were calculated.

www.manaraa.com

5.2.16. Live-Dead cell assay

Live-dead cell assay was performed on spheroids on day 15 of single dosing in therapeutic model according to manufacturer's protocol. Briefly, 100µL of 2µM calcein AM/4µM Ethidium homodimer III (EthD-III) staining solution was added to spheroids after complete removal of media from the respective wells. The plate was incubated for 45 min at room temperature. This provides green/red fluorescent staining of viable and dead cells, respectively. Images were captured using (EVOS-FL, Thermo Fisher Scientific) and mean red fluorescence intensity/mm^2 of spheroid was quantified using ImageJ software which signifies the presence of live cells in spheroid mass.

Data Analysis and Statistical Evaluation

All data were addressed as mean ± SD or SEM, with n=3 unless otherwise mentions. Three trials of cytotoxicity studies were performed for each control or treatment with n=6 for each trial data. Unpaired student's t-test was used to compare two groups and one-way ANOVA followed by *Tukey's* multiple comparisons test was used to compare more than two groups using GraphPad Prism software (Version 7.04 for Windows, GraphPad Software, San Diego, California USA). A p value of<0.05 was considered statistically significant and was presented in data figures as a single asterisk (*). However, some studies have demonstrated a smaller p-value of 0.01 or less, which is included at respective places.

5.3.Results

5.3.1. Development of UPLC method for Determination of Amodiaquine (AQ)

A rapid, UPLC method was developed for determination of AQ. Retention time was found to be 0.731 min with run time of 1.5 min. Peak was eluted with good resolution. The

www.manaraa.com

method provided excellent linearity between 0.05 to 6 µg/mL. Further details of this developed method have been reported in a recent publication from our group (198).

5.3.2. Calibration curve for Folic acid

Calibration curve for folic acid has been plotted between absorbance and concentration of FA. The linear regression data for the calibration curve showed good linear relationship over the concentration range 15.6-250 µg/ml for FA. Standard plot was represented in **Figure 30A**. Linear regression equation was found to be

$$Y=0.001039*X + 0.04648$$

5.3.3. Synthesis of PLGA-PEG-FA

Synthesized conjugate of PLGA-PEG-FA has been carried out via a set of reactions to activate PLGA first followed by subsequent conjugation reactions. presents more reactive γ-COOH group of folic acid which facilitates binding of folic acid with the folate receptor as reported earlier by Valencia *et al* (224). The chemistry presented here for the synthesis

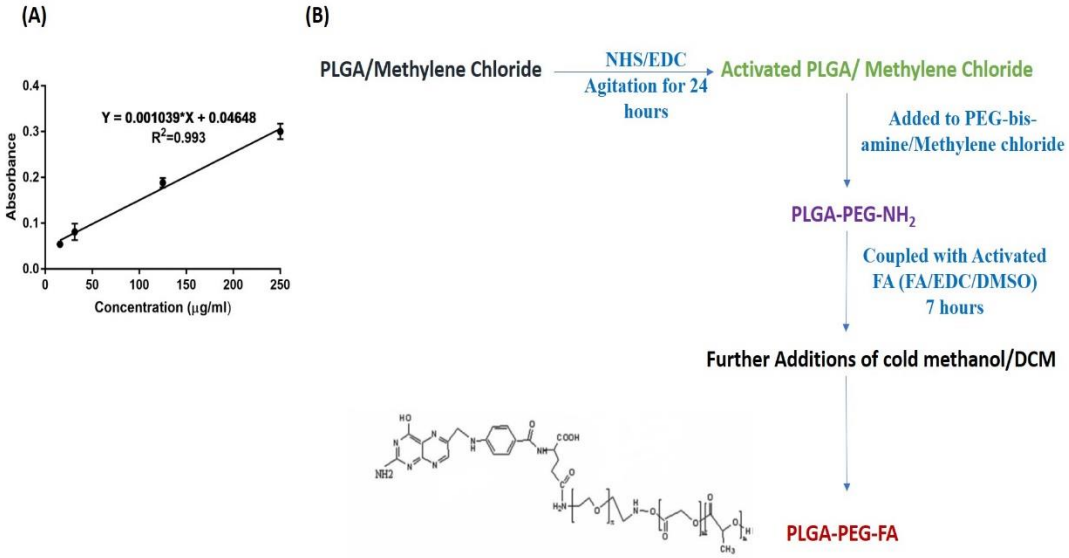

Figure 30. A. Calibration curve for Folic acid. **B**. Schematic representation of conjugation of PLGA polymer with Folic acid.

www.manaraa.com

of PLGA-PEG-FA allowed for the conjugation of targeting ligand, folic acid. In brief, activated PLGA was conjugated with PEG moiety which is further conjugated with carboxyl group of FA via its amine group. **Figure 30B** outlines the synthesis procedure of PLGA-PEG-FA.

5.3.4. Determination of Conjugation Efficiency

Conjugate, PLGA-PEG-FA was analyzed for the amount of folic acid. Known amount of PLGA-PEG-FA was dissolved in DMSO and the resultant solution was analyzed for the absorbance at 256nm using Tecan plate reader (Tecan Spark 10M; Tecan, Männedorf, Switzerland). The amount of conjugated FA is calculated by comparing the measured absorbance value with standard curve. Amount of folic acid conjugated per 1 mg of PLGA-PEG-FA was found to be 27.8±2.1µg.

5.3.5. Physicochemical characterization: Particle size, PDI and Zeta potential

Nanoparticle formulations AQ NP Rota and FA-AQ NPs were found to have average particle size and polydispersity index (PDI) of 197.5±1.7nm, 0.1±0.0; 203.4±8.8nm, 0.2±0.1 respectively, suggesting uniform particle size distribution as represented in **Fig 31A**. Negative zeta potential of both NPs was found to ~ -23mV. The high absolute value of zeta potential indicates a high electric charge on the surface of the drug-loaded NPs, which can cause strong repellent forces among particles to prevent aggregation of the NPs.

5.3.6. Drug Content

Amodiaquine was effectively encapsulated into nanoparticles, achieving % EE of 20.8±1.6% (AQ NP Rota), 24.9.0±5.4% (FA-AQ NP) and high % DL of 1.6±0.1% (AQ NP Rota), 1.9±0.4% (FA-AQ NP) as shown in **Figure 31A**. As FA conjugated PLGA

www.manaraa.com

polymer and plain PLGA (1:5) were used during the preparation of nanoparticles instead of conjugating FA onto nanoparticles, possibility for drug leaching from conjugated NPs during the conjugation and incubation process was circumvented.

5.3.7. Morphological Studies

Representative TEM images of AQ NP Rota and FA-AQ NPs were presented in **Figures 31B & 31C** revealed that the nanoparticles had a spherical shape with a smooth surface.

(A)

Formulation	Particle Size (nm)	PDI	Zeta Potential (mV)	%EE	% Drug Loading
AQ NP Rota	197.5±1.7	0.1±0.0	-23.9±2.0	20.8±1.6	1.6±0.1
FA-AQ NP	203.4±8.8	0.2±0.1	-24.1±7.2	24.9±5.4	1.9±0.4

(B) AQ NP Rota

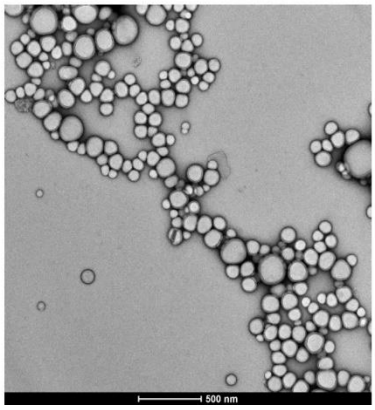

(C) FA-AQ NP

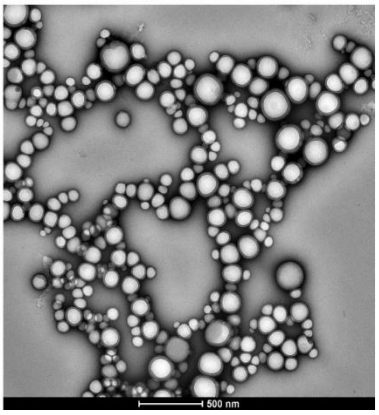

Figure 31. A. Characterization of non-targeted and targeted nanoparticles. B, C. Transmission electron microscopy (TEM) images of AQ NP Rota and FA-AQ NPs. Magnification 20kX**.**

No aggregation of nanoparticles was observed during TEM analysis which gives an indication of the relatively monodispersed size distribution of nanoparticles in formulation. The results were found to be in agreement with PDI and zeta potential measurements, shown in **Figure 31A.**

www.manaraa.com

5.3.8. Solid state Characterization

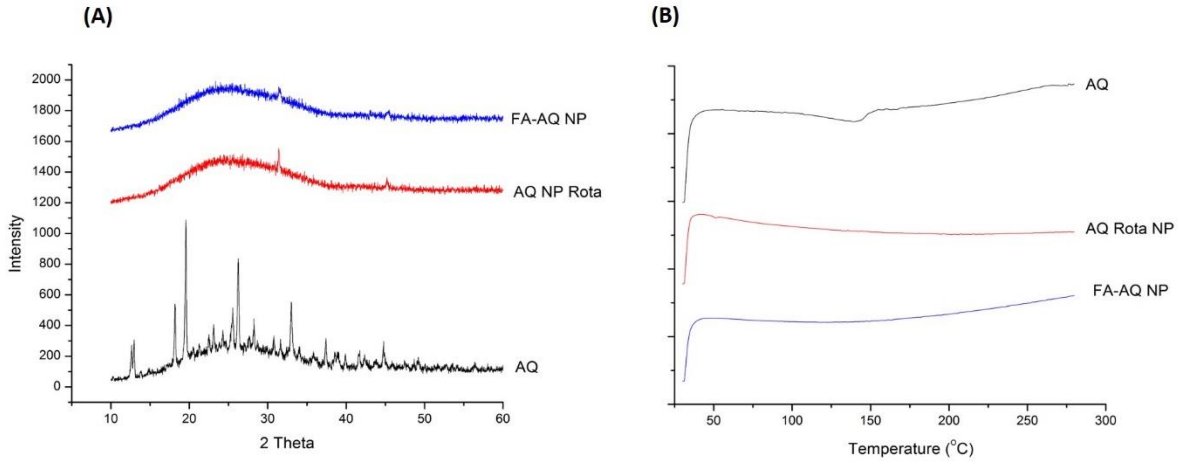

Figure 32. A, B. Solid state characterization studies: **(A)** XRD and **(B)** DSC for AQ, AQ NP Rota and FA-AQ NPs

Powder X-ray Diffraction (PXRD): Due to its crystalline nature, AQ showed distinct peaks at 2θ values of 19.92 and 25.88 in XRD spectra whereas there were no AQ peaks present in AQ and FA-AQ NP indicating encapsulation of drug inside the nanoparticles as shown in **Figure 32A**. Results were found to be consistent with our earlier studies of amodiaquine nanoparticles (198).

Differential Scanning Calorimetry (DSC): The DSC studies were performed to understand melting and crystallization behavior of AQ when present in NP formulation as compared to plain AQ. As can be seen in **Figure 32B**, thermogram of AQ showed a sharp endothermic peak at 166.8°C due to its melting transition. The absence of a sharp peak in AQ NP Rota and FA-AQ NP indicated complete drug encapsulation in the nanoparticle formulation core and suggested a consistent result with that of XRD as discussed above. Results found to be consistent with our earlier studies (198).

www.manaraa.com

5.3.9. Stability Studies

Stability is a major concern while dealing with nanosized drug delivery systems due to emulsion instability and particle aggregation (53). As shown in **Figure 33**, stability analysis data reveal that FA-AQ NP formulation was stable at 4º and 25ºC, with no significant changes in particle size, zeta potential or % entrapment efficiency **(Figure 33A-C)**. Although there observed a reduction in zeta potential after 4 weeks of storage at 25C, still the formulations were found to exhibit a positive surface charge which is very crucial in their superior cellular internalization. Here, the positive zeta potential of the FA-AQ NP prevents the particles from coalescing and aggregating. There was no detrimental effect of temperature and storage time on entrapment efficiency either. Altogether, the formulations

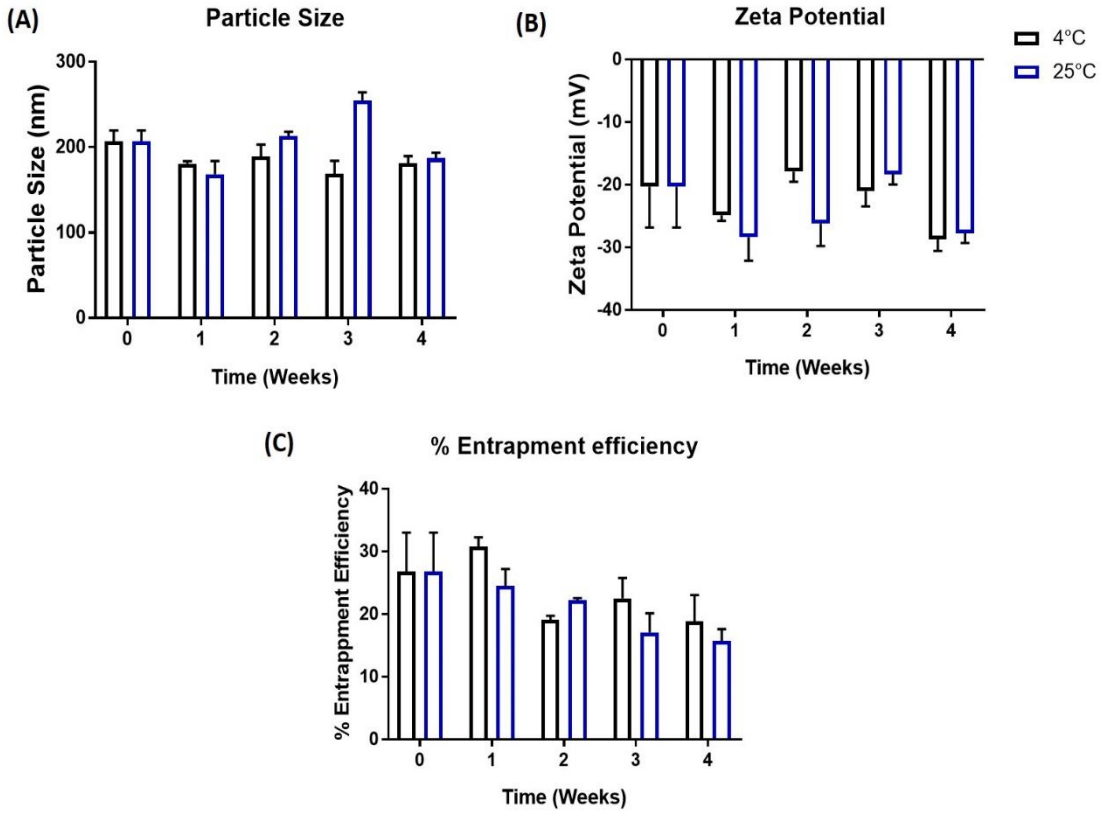

Figure 33. Influence of storage temperature and length of storage on particle size **(A)**, zeta potential **(B)** and % entrapment efficiency **(C)** of FA-AQ NPs. Formulations were stored at 4° and 25° C over a period of 4 weeks. Data represent mean ± SD (n=3).

www.manaraa.com

were found to retain their physicochemical properties during their storage at different temperatures of 4°C and 25°C over a period of 4 weeks.

5.3.10. Determination of Targeting Capability

5.3.10.1. Cellular Uptake Studies using Fluorescence Microscopy

Figure 34A represents intracellular uptake of nanoparticle formulations using A549 cells with 3 hours of incubation. In this experiment, AQ was replaced with fluorescent coumarin to make it possible to visualize the uptake and accumulation. Fluorescent images taken following 3-hour incubation with FA conjugated coumarin loaded nanoparticles clearly demonstrated significant internalization compared to plain coumarin and non-targeted coumarin nanoparticles in A549 cells. It can also be observed that there was higher accumulation of the FA-C NP around the nucleus (DAPI stained), the most evident location for nanoparticle disruption and drug release inside the cells (163). Presence of FA on the FA-C NP enables interaction of nanoparticles with cell thus further resulting in efficient cellular internalization compared to that of C NP and plain coumarin.

5.3.10.2. Quantification of Cellular uptake by Determining Fluorescence Intensity:

The cellular uptake of FA-C NP, C NP and coumarin by A549, HeLa and MDAMB-231 cells was measured by fluorescence microscopy and cells were able to take up the respective treatments at various capacities as shown in **Figure 34B-D**. At 3hr time point, FA-C NP uptake was ~7.6, 2.6: (A549), ~2.3, 1.6 (HeLa) and ~5.7, 1.8 (MDAMB-231) times higher compared to coumarin and C NP respectively. The fluorescence intensity of FA-C NP (23230.7±8927.8: A549; 37276.0±8773.1: HeLa; 42113.3±6115.8: MDAMB-231) treated cells was significantly higher when compared with C NP (9042.6±5819.8:

www.manaraa.com

A549; 23151.0±7241.0: HeLa; 23830.0±4587.6: MDAMB-231) and coumarin (2991.3±127.8: A549; 16300.0±3576.3: HeLa; 7434.0±4431.6: MDAMB-231) at 3hr time point (A549: Coumarin vs FA-C NP: $p<0.05$; HeLa: Coumarin vs FA-C NP: $p<0.05$; MDAMB-231: Coumarin vs FA-C NP: $p<0.05$). The quantitative results indicated analogous results to the fluorescence imaging shown in **Fig 34A**. Due to the presence of folic acid on the surface of nanoparticles, the uptake of the FA-C NP into cells is facilitated by the mutual interaction between FA and the folic acid receptors on the cell membrane, resulting in an elevated uptake efficiency compared with Coumarin NP and plain coumarin (A549) or plain coumarin (Hela, MDAMB-231).

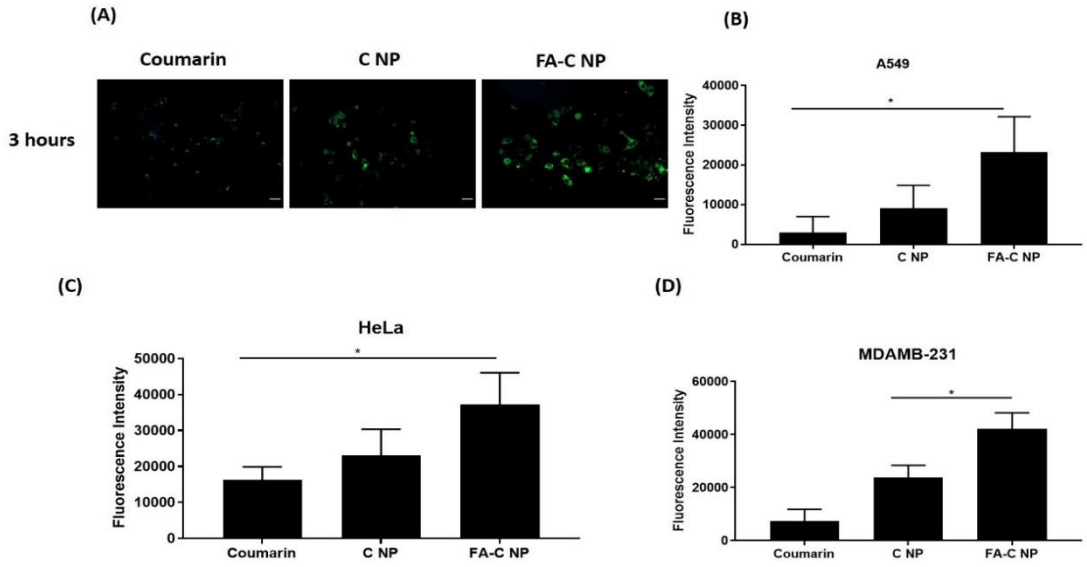

Figure 34. *In-vitro* cellular uptake of coumarin-6 loaded non-targeted and FA-targeted nanoparticles. **A**. Fluorescence microscopy images in A549 at 3 hours**. B, C** and **D.** Quantitative representation of cellular uptake through fluorescence measurements in A549 **(B)**, HeLa **(C)** and MDAMB-231 **(D)** cell lines. Coumarin-6 plain solution is used

5.3.11. Cytotoxicity Studies

www.manaraa.com

Cell viability studies were performed using MTT assay to evaluate the cytotoxic potential of FA-conjugated and non-conjugated AQ-loaded NPs versus plain drug. From this study, it was revealed that AQ cytotoxicity against A459, HeLa and MDAMB-231 cell lines was significantly enhanced by nanoparticle encapsulation. **Figure 35A-C** illustrate the cytotoxic effects of AQ, AQ NP Rota and FA-AQ NP in A549, HeLa and MDAMB-231 cell lines respectively. The IC_{50} values for plain AQ, AQ NP Rota and FA-AQ NP were found to be 18.3±4.5µM, 11.5±11.8µM and 12.7±9.8µM in HeLa cell line; 17.5±6.6 µM, and 30.0±17.5µM and 11.5±8.3µM in MDAMB-231 cell line respectively **(Figure 35E).** The IC_{50} value of FA-AQ NP was lower than that of free AQ and AQ-loaded nanoparticle without FA-conjugation in case of MDAMB-231 cell line (AQ NP Rota vs FA-C NP: *p<0.0001*which was reported to possess overexpression of folic acid receptors compared to their expression in A549 cells (220). However, to evaluate the anti-cancer efficiency of

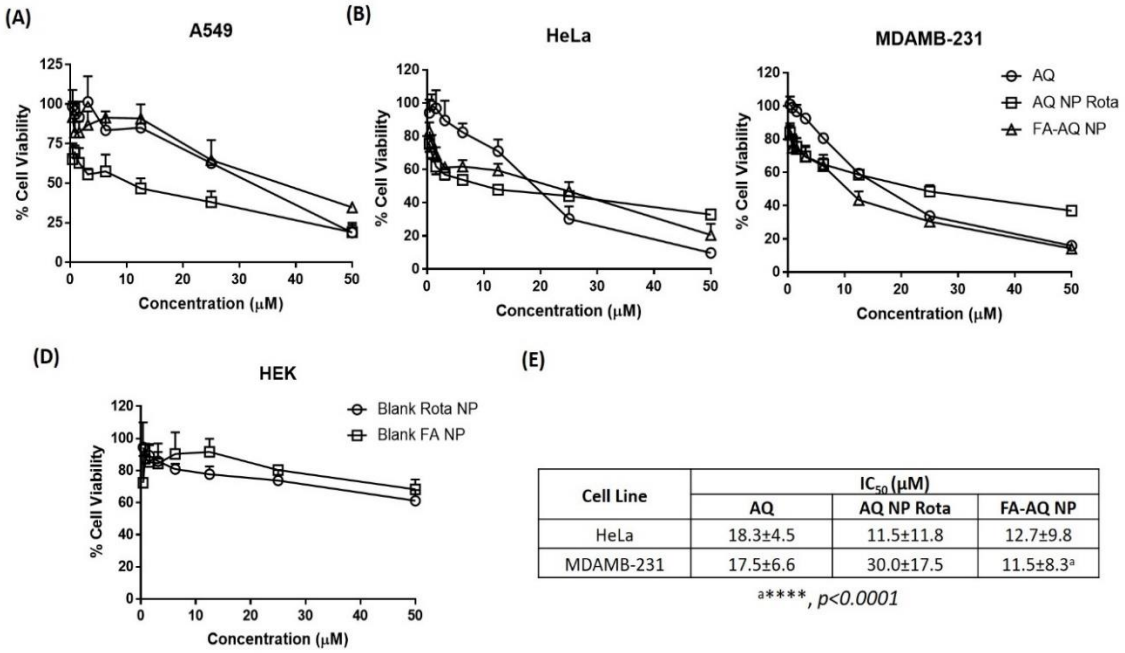

Cell Line	IC_{50} (µM)		
	AQ	AQ NP Rota	FA-AQ NP
HeLa	18.3±4.5	11.5±11.8	12.7±9.8
MDAMB-231	17.5±6.6	30.0±17.5	11.5±8.3[a]

[a]****, *p<0.0001*

Figure 35. Inhibitory effects on different cell lines **A.** A549, **B.** HeLa, C. MDAMB-231 and D. HEK; after treatments with AQ, AQ NP Rota and FA-AQ NP. **C.** IC_{50} of AQ, AQ NP Rota and FA-AQ NP in HeLa and MDAMB-231.

folic acid targeted nanoparticles further *in vitro* studies are performed. *In-vitro* cytotoxicity

www.manaraa.com

studies of Blank NP and Blank FA-NP were performed on A549 cell line. Both Blank NP and Blank FA-NP were found be safe from % cell viability determinations after incubating HEK cell line for 72hours which has been represented in **Figure 35D.** In none of the cases was cell viability below 70% using blank nanoparticles equivalent to concentrations ranging from 0.39 to 50µM, suggesting that formulation components were not toxic by themselves.

5.3.12. Clonogenic Assay

Clonogenic assay is an *in-vitro* cell survival assay used to determine the colony formation

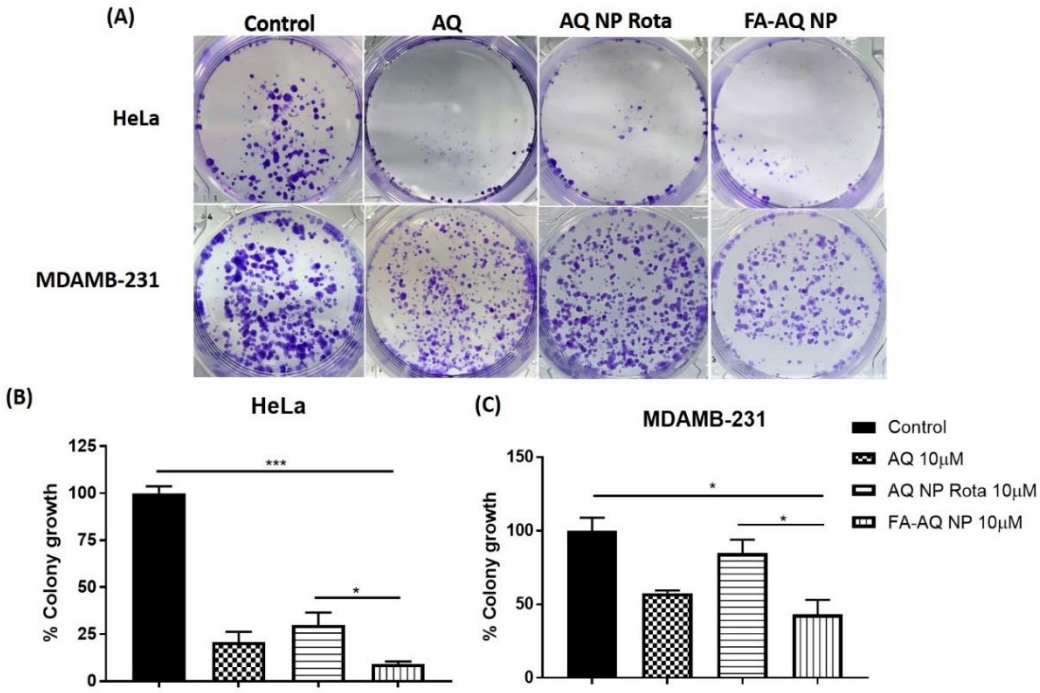

Figure 36. A. Representative images showing distinct colonies after staining in HeLa and MDAMB-231 cell lines. Three different experiments were performed. **B & C.** Quantitative representation of clonogenic assay as % colony growth with AQ, AQ NP Rota and FA-AQ NPs treatment as compared to control in HeLa and MDAMB-231 cell lines respectively.

capability of single cancer cells (164). AQ, AQ NP Rota and FA-AQ NP were evaluated

www.manaraa.com

for their long-term efficacy using clonogenic assay in HeLa and MDAMB-231 cell lines. From **Figure 36A**, it can be illustrated that colony growth was significantly inhibited by FA-AQ NP compared to AQ and AQ NP Rota in HeLa and MDAMB-231 cell lines. After 48 hour treatment period and 7 day incubation, % of colonies survived after treatment with 10 μM AQ, AQ NP Rota and FA-AQ NP were 20.9±5.3%, 29.9±6.6% and 9.2±1.1% (HeLa, **Figure 36B,** AQ NP Rota vs FA-AQ NP: $p<0.05$, Control vs FA-AQ NP: $p<0.05$) considering number of colonies to be 100% in drug free treatment control wells. In case of MDAMB-231 cell line, % of colony growth was found to be 57.6±1.8%, 84.8±9.2% and 43.2±9.9% with AQ, AQ NP Rota and FA-AQ NP (**Figure 36C;** AQ NP Rota vs FA-AQ NP: $p<0.05$, Control vs FA-AQ NP: $p<0.05$) The data suggest an approximately 2.3, 3.2-fold (HeLa); 2-fold (MDAMB-231) stronger decrease in colony-forming ability with FA-AQ NP as compared to AQ NP Rota, plain AQ; AQ NP Rota respectively. This data may be considered a representative of FA-AQ NP's efficacy in suppressing the possibility of metastasis or new tumor growth by reproduction inhibition; and can well be linked to enhanced intracellular (and intratumoral) drug accumulation with nanoparticles formulation.

5.3.13. 3D Spheroid Cell Culture Studies

As described in *Methods* section, 3D spheroid cell culture study was designed to better predict the physiological interaction of folic acid receptor targeted amodiaquine loaded NPs with tumors. In case of solid tumors, the monolayered cell cultures do not accurately mimic tumor structure, resistance to drugs and drugs' poor penetrability due to tumor microenvironment (208). To bridge the gap between *in-vitro* and *in-vivo* studies, a 3D spheroid study was carried out according to previously published studies from our group.

www.manaraa.com

These cultures (tumor spheroids) combine the ability to mimic the 3D structure of malignant tissue accurately in addition to being relevant to cancer microenvironment to which the tumor cells are exposed (210,211). A 3D *in-vitro* model was developed successfully by using specific Corning ultra-low attachment spheroid plates as reported by Vaidya *et al* (225) so that under favorable incubation conditions, cells grow into a spheroid mass.

For this spheroid study, A549 cell line was chosen which forms spheroid masses from day 1 on culturing which were grown for 3 days. This study was performed using single dose regimen. Spheroid images were captured using inverted microscope (Laxco, Mill Creek, WA, USA) on respective days and were analyzed using the ImageJ software Version 1.44 (National Institute of Health, USA)**.** Spheroid images (HeLa: **Figure 37A**, MDAMB-231: **Figure 37B)**, and spheroid volume (**Figures 38A & 38B)** comparisons are represented. Control group of spheroids (blank media control) found to be growing in size over a period of 15 days, whereas the growth of treated spheroids was significantly inhibited.

In this single dose study with a single treatment given on day 1, control spheroids of HeLa cell line were found to have volumes of 64.1 ± 2.7 mm^3 on day 15 as compared to spheroid volumes of 51.8 ± 3.8 mm^3 (AQ: 10µM); 53.3±7.0 mm^3 (AQ NP Rota: 10µM) and 39.3 ± 2.3 mm^3 (FA-AQ NP: 10µM). A significant reduction in spheroid volumes was observed in case of FA-AQ NP treated spheroids on day 15. (Control vs FA-AQ NP

www.manaraa.com

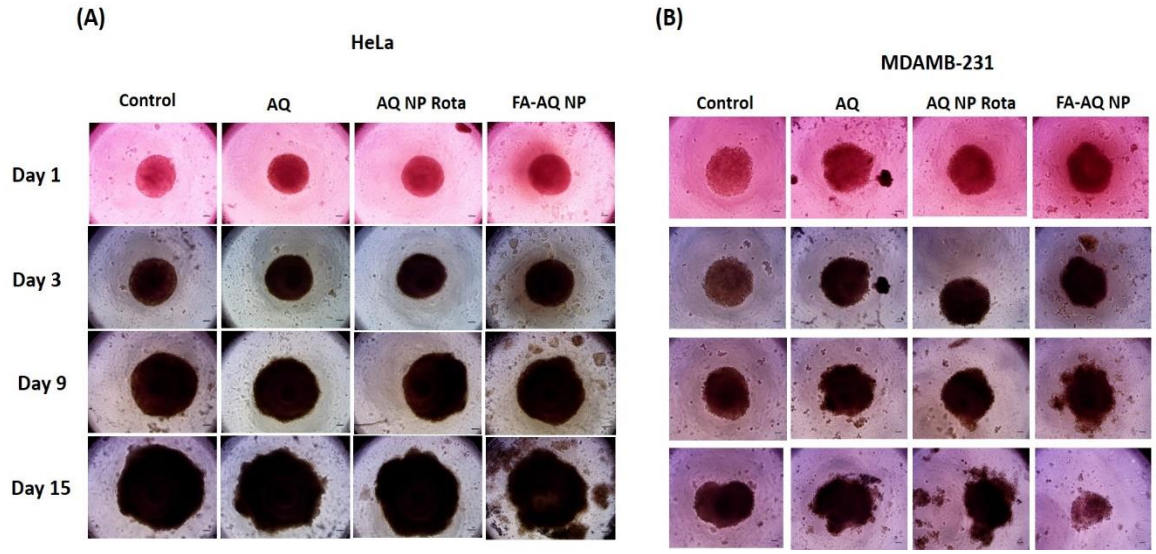

Figure 37. 3D Spheroid study: A, B. Spheroid images of HeLa **(A)** and MDAMB-231 **(B)** cell lines after treating with control, AQ, AQ NP Rota and FA-AQ NP. Images represent n=8 for each treatment. Scale bar is 400µM.

p<0.0001, AQ vs FA-AQ NP *p<0.05)* **(Figure 38A)**. While MDAMB-231 control spheroids of HeLa cell line were found to have volumes of 11.4 ± 0.7 mm^3 on day 15 as compared to spheroid volumes of 14.2 ± 1.6 mm^3 (AQ: 10µM); 13.0±1.3 mm^3 (AQ NP Rota: 10µM) and 8.8 ± 1.6 mm^3 (FA-AQ NP: 10µM). A significant reduction in spheroid volumes was observed in case of FA-AQ NP treated spheroids on day 15. (AQ vs FA-AQ NP, *p<0.05)* **(Figure 38B)**. Thus, underlining a more pronounced tumor reduction potential of FA-AQ NP. Treatment with FA-AQ NP resulted in a significant difference in spheroid volumes as compared to AQ and control treated groups. Tumor growth suppression was continually observed until the end of the treatment.

5.3.14. Live-Dead Cell Assay

Determining viable and dead cells within a solid spheroid mass can be carried out by live-dead cell assay. Developed drug-loaded nanocarriers facilitate drug's entry into the inner core of the tumor while 2D tumor volume measurements may not reveal a

www.manaraa.com

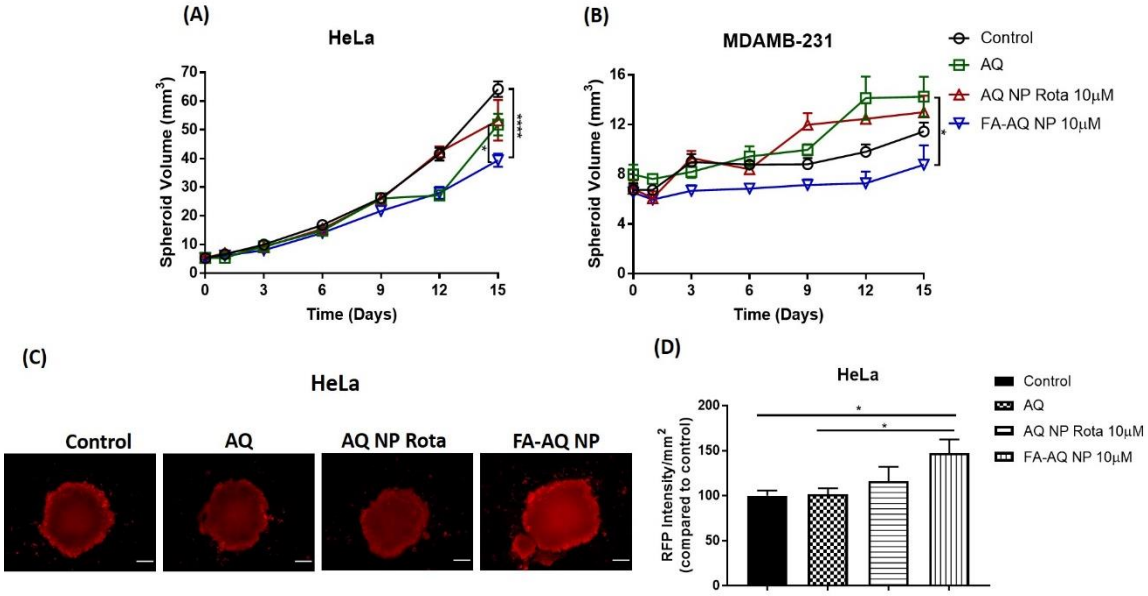

Figure 38. 3D Spheroid study: Spheroid volume comparison plots for HeLa (A) and MDAMB-231 (B) spheroids. Data represent mean ± SEM (n = 8). **C.** Live-Dead Cell assay: Red fluorescence Intensity demonstrated by HeLa Spheroids. **D.** Cell viability study was performed using CellTiter-Glo® Assay on HeLa Spheroids.

nanoformulation's efficacy in penetrating tumor core, as the spheroid masses consist of dead cell core surrounded by a well-established structural periphery of live cells. 3D spheroids are also grown over an extended period, with intratumoral core regions being exposed to environmental conditions like lack of O_2, and nutrients, resulting in presence of necrotic and quiescent cells in the core regions (165). Therefore, it is necessary to quantify actual dead cell portions out of a spheroid mass. **Figures 38C & 38D** are representing terminal spheroid images on day 15th after treatment and respective quantification plot of red fluorescence intensity respectively. While AQ NP Rota and FA-AQ NP treatments demonstrated reduction in tumor volume, higher red fluorescence (dead cells) was seen with FA-AQ NP treatment in case of HeLa spheroids as seen in **Figure 38D.** Red fluorescence intensity comparison on day 15th day of single dose (FA-AQ NP) post treatment period revealed presence of dead cells, 1.5, 1.3, 1.5 folds lower as compared to

www.manaraa.com

control, AQ NP Rota, FA-AQ NP (Control vs FA-AQ NP: $p<0.05$, AQ vs FA-AQ NP: $p<0.05$).

5.4.Discussion

The main aim of this study was to develop a strategy for increased delivery of amodiaquine to tumor cells while avoiding off-target effects through folic acid targeting. To accomplish this goal, folic acid decorated nanoparticles have been developed and evaluated for their anti-cancer efficacy in multiple cancer cell lines such as NSCLC, cervical and breast cancer types. As targeting specific tumor cells is relevant in the treatment of cancer therapies, it has become a very well-studied approach in delivering anticancer drugs which exert serious side effects due to their non-specific activity on non-cancerous cells. Folate receptors are generally overexpressed on the surface of several human cancer cells, including cervical, ovarian and breast cancer types. Thus, utilization of targeted drug delivery system imparts drug delivery systems the distinguishing feature between healthy and cancer cells. Folic acid presents an attractive targeting ligand for selective delivery, and thus is used for the surface conjugation to NPs. In the current study, highly monodisperse polymeric nanoparticles with high amodiaquine loading and folate decorated on the NP surface for site-specific targeting. The advantage of targeting folic acid receptors was exploited by the group of Rosenholm *et al.* (synthesized folate-conjugated porous hybrid silica nanoparticles for targeting to cancer cells) (226) and Liu *et al* (synthesis of folic acid conjugated nanoparticles of mixed lipid monolayer shell and biodegradable polymer core for targeted delivery of docetaxel) (227). Recently, Cheung *et al* have highlighted the importance of folic acid receptor targeting by summarizing the role of folic acid receptors with a special focus on treatment approaches (228).

www.manaraa.com

Conjugation of the PLGA polymer with a targeting moiety have been carried out successfully to address the payload to specific cancer. Further, results obtained from the conjugation efficiency determinations have assured the presence of FA on the surface of nanoparticles. Physicochemical characterization of the drug loaded nanoparticles is of important in the field of drug delivery, as it greatly influences the uptake and cellular interaction of the particulate system; thus, ultimately determining the fate of the entrapped drug under *in vitro* and *in vivo* conditions. Lower particle size of developed targeted NPs (203.4±8.8nm) with high absolute zeta potential (~-20 mV) enabled higher accumulation in cancer cells. In addition, spherical surface with smooth morphology and narrow size distribution are evident by TEM analysis as represented in **Figures 31B & 31C**. Solid state characterization studies such as XRD and DSC revealed the encapsulation of AQ inside the nanoparticle formulations. Stability study results confirmed the capability of developed targeted NPs to retain their physicochemical properties even after a period of 4 weeks when stores under both refrigerated and room temperatures as shown in **Figure 33**.

Intracellular uptake images shown in **Figure 34** reveal that FA conjugated coumarin nanoparticles were internalized by A549 cells efficiently within 3 hours compared to plain coumarin solution or unconjugated nanoparticles. **Figures 34B-D** clearly indicates that FA-coumarin NP uptake was higher compared with coumarin in A549, HeLa and MDAMB-231 cells.

Extensive *in-vitro* cell culture studies were carried out to investigate the efficacy of AQ NP against NSCLC. Presence of folic acid on nanoparticles associates with higher cellular uptake and greater cytotoxicity in cancer cells and explains the specificity of FA-mediated binding of conjugated NPs (170). Recently, research work conducted by

www.manaraa.com

Angelopoulou *et al.* has demonstrated that FA-conjugated pegylated magnetic NPs to deliver doxorubicin to cancer cells of solid tumors. (229). Cytotoxicity study results in the present study indicated differentiation in cell inhibition behavior between free amodiaquine and amodiaquine loaded nanoparticles either FA conjugated or not, thus emphasizing the key role of NPs internalization in enhancement of cytotoxic activity. As shown in **Figure 35**, the cytotoxicity exhibited by folic acid conjugated amodiaquine NPs towards various cancer cell lines could be attributed to their targeting ability. Interestingly, targeted NPs exhibited a lower IC_{50} value than the plain drug and unconjugated NPs in case of MDAMB-231 cell line which was reported to exhibit overexpression of folic acid receptors compared to A549 cells (220). Clonogenic assay study revealed that FA-AQ NPs can inhibit the ability of single cells more efficiently to form colonies compared to non-targeted nanoparticles. Hence, it ensures the effectiveness of FA-AQ NP on long term basis while preventing tumor recurrence. Overall, FA-AQ NP could be further evaluated for their establishment in cancer treatment explicitly.

Development of 3D *in-vitro* models is of utmost necessity today to mimic *in-vivo* solid tumor conditions which could be achieved by using specific low attachment spheroid plates as reported in our previous publications (20,32). From results seen in **Figures 38A & 9B**, it can be understood that nanoparticles were able to deliver the drug to spheroids' core efficiently ensuring their clinical use. Results from this spheroid study provide a strong evidence for capability of FA conjugated nanoparticles to deliver the drug to spheroid's core efficiently and their potential *in-vivo* efficiency, which could be extended to further preclinical studies. It can be understood that through the addition of a ligand (FA) at the NP surface, NPs are directed against receptors (folic acid) exposed at the outer cell

www.manaraa.com

surface, simultaneously improved uptake and distribution of NPs in the tumor mass despite of complicated tumor microenvironment (217). Furthermore, the potential of AQ NP Rota and FA-AQ NP was investigated and compared through different studies such as clonogenic assay and ex-vivo spheroid studies. In addition, increased red fluorescence intensities observed inside FA-AQ NP treated spheroid cores indicated the capability of targeted NPs in reaching the solid core of tumors in 3D environment as seen in **Figure 38C & 38D.**

Taken together, results from the current study including *in-vitro* cell culture studies as well as 3D spheroid models illustrating the pronounced efficiency of amodiaquine-loaded folic acid functionalized nanoparticles in NSCLC treatment.

5.5.Conclusion

In the present study, it can be concluded that folic acid conjugated nanoparticles of amodiaquine were successfully formulated by a scalable high-pressure homogenization (HPH) approach. Formulated NPs were characterized for their physicochemical properties, found to have favorable particle size and surface charge facilitating efficient cellular internalization. Developed targeted AQ loaded NPs were compared with their counterpart (non-targeted AQ loaded nanoparticles) in their anti-cancer efficacy against NSCLC. Several *in-vitro* cell culture studies including cytotoxicity studies and 3D spheroid studies, assays exhibiting colony formation inhibitory behavior where superior efficacy of folic acid conjugated NPs has been confirmed. Altogether along with apoptosis inhibition capability of FA-AQ NPs, results are promising them as a potential treatment strategy for multiple cancer types.

www.manaraa.com

6. CONCLUSION

In summary, nanotechnology-based drug repurposing of amodiaquine along with the feasibility towards a inhalable and targeted therapy presents a promising strategy in NSCLC treatment. Transferrin conjugated amodiaquine nanoparticles can be a potential inhalable treatment strategy for targeting NSCLC thus reducing the dose, side effects. While the *in-vitro* and *ex-vivo* results are promising, *in-vivo* studies are required to encompass the full spectrum of this approach's feasibility. Moreover, folic-acid decorated amodiaquine-loaded nanoparticles have also demonstrated excellent anti-cancer efficacy in multiple cancer types suggesting further exploration of the developed systems in future studies.

Future Directions:

Repurposed, targeted nanomedicine presents a promising strategy for the treatment of non-small cell lung cancer. Even though, the current study has demonstrated the efficacy of transferrin targeted nanoparticles, further exploration of anti-cancer mechanisms involved in their efficacy is highly encouraged. Especially, amodiaquine properties such as its ability to accumulate in the acidic environments and to disrupt lysosomal pH are further withdrawing attention of researchers by the scope available to study amodiaquine's anti-cancer properties. Understanding in-depth knowledge of the biological pathways involved in the anti-cancer efficacy of developed nanoparticles is recommended. Combination of drug repurposing and nanotechnology with targeting platform exhibits considerable therapeutic potential in treating lung cancer tumors. Altogether, we propose that our nanoparticles are capable for NSCLC treatment with a great potential for clinical translation after performing further *in-vivo* studies.

www.manaraa.com

7. REFERENCES

1. Tomar V, Mazumder M, Chandra R, Yang J, Sakharkar MK. Small Molecule Drug Design. In: Ranganathan S, Gribskov M, Nakai K, Schönbach C, editors. Encyclopedia of Bioinformatics and Computational Biology. Oxford: Academic Press; 2019. p. 741–60.

2. Parvathaneni V, Kulkarni NS, Muth A, Gupta V. Drug repurposing: a promising tool to accelerate the drug discovery process. Drug Discov Today. 2019 Jun 22;

3. Yang W, Veroniaina H, Qi X, Chen P, Li F, Ke PC. Soft and Condensed Nanoparticles and Nanoformulations for Cancer Drug Delivery and Repurpose. Adv Ther. 2020;3(1):1900102.

4. Gns HS, Gr S, Murahari M, Krishnamurthy M. An update on Drug Repurposing: Re-written saga of the drug's fate. Biomed Pharmacother. 2019 Feb 1;110:700–16.

5. Pillaiyar T, Meenakshisundaram S, Manickam M, Sankaranarayanan M. A medicinal chemistry perspective of drug repositioning: Recent advances and challenges in drug discovery. Eur J Med Chem. 2020 Apr 2;112275.

6. Repurposing Drugs [Internet]. National Center for Advancing Translational Sciences. 2017 [cited 2020 Apr 7]. Available from: https://ncats.nih.gov/preclinical/repurpose

7. Talevi A, Bellera CL. Challenges and opportunities with drug repurposing: finding strategies to find alternative uses of therapeutics. Expert Opin Drug Discov. 2020 Apr 2;15(4):397–401.

8. Lage OM, Ramos MC, Calisto R, Almeida E, Vasconcelos V, Vicente F. Current Screening Methodologies in Drug Discovery for Selected Human Diseases. Mar Drugs. 2018 Aug;16(8):279.

9. Patra JK, Das G, Fraceto LF, Campos EVR, Rodriguez-Torres M del P, Acosta-Torres LS, et al. Nano based drug delivery systems: recent developments and future prospects. J Nanobiotechnology. 2018 Sep 19;16.

10. Czech T, Lalani R, Oyewumi MO. Delivery Systems as Vital Tools in Drug Repurposing. AAPS PharmSciTech. 2019 Feb 15;20(3):116.

11. Pushpakom S, Iorio F, Eyers PA, Escott KJ, Hopper S, Wells A, et al. Drug repurposing: progress, challenges and recommendations. Nat Rev Drug Discov. 2018 Oct 12;

12. Using Old Drugs in New Ways - Cancer Today.

13. Padhy BM, Gupta YK. Drug repositioning: Re-investigating existing drugs for new therapeutic indications. J Postgrad Med. 2011 Apr 1;57(2):153.

14. Amol Khanapure, Pem Chuki, Avinash De Sousa. Drug Repositioning: old drugs for new indications. Indian J Appl Res. 2014 Aug;4(8):462–6.

المنارة للاستشارات
www.manaraa.com

15. Murteira S, Ghezaiel Z, Karray S, Lamure M. Drug reformulations and repositioning in pharmaceutical industry and its impact on market access: reassessment of nomenclature. J Mark Access Health Policy. 2013 Jan;1(1):21131.

16. Croset SCJ. Drug repositioning and indication discovery using description logics. :228.

17. Xue H, Li J, Xie H, Wang Y. Review of Drug Repositioning Approaches and Resources. Int J Biol Sci. 2018 Jul 13;14(10):1232–44.

18. Park K. A review of computational drug repurposing. Transl Clin Pharmacol. 2019 Jun;27(2):59–63.

19. Vleet TRV, Liguori MJ, James J. Lynch III, Rao M, Warder S. Screening Strategies and Methods for Better Off-Target Liability Prediction and Identification of Small-Molecule Pharmaceuticals: SLAS Discov Adv Life Sci RD. 2018 Sep 10;

20. Parvathaneni V, Kulkarni NS, Shukla SK, Farrales PT, Kunda NK, Muth A, et al. Systematic Development and Optimization of Inhalable Pirfenidone Liposomes for Non-Small Cell Lung Cancer Treatment. Pharmaceutics. 2020 Feb 28;12(3).

21. Jin G, Wong STC. Toward better drug repositioning: prioritizing and integrating existing methods into efficient pipelines. Drug Discov Today. 2014 May;19(5):637–44.

22. Wu H, Huang J, Zhong Y, Huang Q. DrugSig: A resource for computational drug repositioning utilizing gene expression signatures. PLOS ONE. 2017 May 31;12(5):e0177743.

23. Sun W, Zheng W, Simeonov A. Drug discovery and development for rare genetic disorders. Am J Med Genet A. 2017 Sep;173(9):2307–22.

24. Talevi A. Drug repositioning: current approaches and their implications in the precision medicine era. Expert Rev Precis Med Drug Dev. 2018 Jan 2;3(1):49–61.

25. Parvathaneni V, Gupta V. Utilizing drug repurposing against COVID-19 – Efficacy, limitations, and challenges. Life Sci. 2020 Oct 15;259:118275.

26. Lyapustina S. Regulatory pitfalls and opportunities when repurposing for inhalation therapy. Adv Drug Deliv Rev. 2018 Aug 1;133:57–65.

27. Ferrari R, Lüscher TF. Reincarnated medicines: using out-dated drugs for novel indications. Eur Heart J. 2016 Sep 1;37(33):2571–6.

28. 9 old drugs that learned new tricks: The head of the National Institutes of Health shares medicines that turned out to have multiple uses [Internet]. TED Blog. 2013 [cited 2020 Oct 10]. Available from: https://blog.ted.com/9-old-drugs-that-learned-new-tricks-the-head-of-the-national-institutes-of-health-shares-medicines-that-turned-out-to-have-multiple-uses/

29. Oprea TI, Bauman JE, Bologa CG, Buranda T, Chigaev A, Edwards BS, et al. Drug Repurposing from an Academic Perspective. Drug Discov Today Ther Strateg. 2011;8(3–4):61–9.

www.manaraa.com

30. Pelaz B, Alexiou C, Alvarez-Puebla RA, Alves F, Andrews AM, Ashraf S, et al. Diverse Applications of Nanomedicine. ACS Nano. 2017 28;11(3):2313–81.

31. Rana V, Sharma R. Chapter 5 - Recent Advances in Development of Nano Drug Delivery. In: Mohapatra SS, Ranjan S, Dasgupta N, Mishra RK, Thomas S, editors. Applications of Targeted Nano Drugs and Delivery Systems. Elsevier; 2019. p. 93–131. (Micro and Nano Technologies).

32. Vaidya B, Kulkarni NS, Shukla SK, Parvathaneni V, Chauhan G, Damon JK, et al. Development of inhalable quinacrine loaded bovine serum albumin modified cationic nanoparticles: Repurposing quinacrine for lung cancer therapeutics. Int J Pharm. 2020 Mar 15;577:118995.

33. Shukla SK, Kulkarni NS, Chan A, Parvathaneni V, Farrales P, Muth A, et al. Metformin-Encapsulated Liposome Delivery System: An Effective Treatment Approach against Breast Cancer. Pharmaceutics. 2019 Nov;11(11):559.

34. Jaromin A, Zarnowski R, Piętka-Ottlik M, Andes DR, Gubernator J. Topical delivery of ebselen encapsulated in biopolymeric nanocapsules: drug repurposing enhanced antifungal activity. Nanomed. 2018 May 1;13(10):1139–55.

35. Shukla SK, Kulkarni NS, Farrales P, Kanabar DD, Parvathaneni V, Kunda NK, et al. Sorafenib Loaded Inhalable Polymeric Nanocarriers against Non-Small Cell Lung Cancer. Pharm Res. 2020 Mar 12;37(3):67.

36. Gupta V, Gupta N, Shaik IH, Mehvar R, McMurtry IF, Oka M, et al. Liposomal fasudil, a rho-kinase inhibitor, for prolonged pulmonary preferential vasodilation in pulmonary arterial hypertension. J Control Release. 2013 Apr 28;167(2):189–99.

37. Martins JP, das Neves J, de la Fuente M, Celia C, Florindo H, Günday-Türeli N, et al. The solid progress of nanomedicine. Drug Deliv Transl Res. 2020 Mar 5;

38. Suk KH, Gopinath SCB. Drug Encapsulated Nanoparticles for Treating Targeted Cells. Curr Med Chem. 2017;24(30):3310–21.

39. Vaidya B, Kulkarni NS, Shukla SK, Parvathaneni V, Chauhan G, Damon JK, et al. Development of inhalable quinacrine loaded bovine serum albumin modified cationic nanoparticles: Repurposing quinacrine for lung cancer therapeutics. Int J Pharm. 2020 Mar 15;577:118995.

40. Anderson JM, Shive MS. Biodegradation and biocompatibility of PLA and PLGA microspheres. Adv Drug Deliv Rev. 2012 Dec 1;64:72–82.

41. Chandolu V, Dass CR. Treatment of lung cancer using nanoparticle drug delivery systems. Curr Drug Discov Technol. 2013 Jun;10(2):170–6.

42. Parvathaneni V, Goyal M, Kulkarni NS, Shukla SK, Gupta V. Nanotechnology Based Repositioning of an Anti-Viral Drug for Non-Small Cell Lung Cancer (NSCLC). Pharm Res. 2020 Jun 8;37(7):123.

www.manaraa.com

43. Obeid MA, Al Qaraghuli MM, Alsaadi M, Alzahrani AR, Niwasabutra K, Ferro VA. Delivering natural products and biotherapeutics to improve drug efficacy. Ther Deliv. 2017 Oct 24;8(11):947–56.

44. Barbosa EJ, Löbenberg R, de Araujo GLB, Bou-Chacra NA. Niclosamide repositioning for treating cancer: Challenges and nano-based drug delivery opportunities. Eur J Pharm Biopharm. 2019 Aug 1;141:58–69.

45. Meng H, Xu Y. Pirfenidone-loaded liposomes for lung targeting: preparation and in vitro/in vivo evaluation. Drug Des Devel Ther. 2015;9:3369–76.

46. Sercombe L, Veerati T, Moheimani F, Wu SY, Sood AK, Hua S. Advances and Challenges of Liposome Assisted Drug Delivery. Front Pharmacol. 2015;6:286.

47. Olusanya TOB, Haj Ahmad RR, Ibegbu DM, Smith JR, Elkordy AA. Liposomal Drug Delivery Systems and Anticancer Drugs. Mol Basel Switz. 2018 Apr 14;23(4).

48. Matbou Riahi M, Sahebkar A, Sadri K, Nikoofal-Sahlabadi S, Jaafari MR. Stable and sustained release liposomal formulations of celecoxib: In vitro and in vivo anti-tumor evaluation. Int J Pharm. 2018 Apr 5;540(1):89–97.

49. Yallapu MM, Jaggi M, Chauhan SC. Curcumin nanoformulations: a future nanomedicine for cancer. Drug Discov Today. 2012 Jan;17(1–2):71–80.

50. Tulbah AS, Pisano E, Scalia S, Young PM, Traini D, Ong HX. Inhaled simvastatin nanoparticles for inflammatory lung disease. Nanomed. 2017 Sep 20;12(20):2471–85.

51. Costabile G, d'Angelo I, Rampioni G, Bondì R, Pompili B, Ascenzioni F, et al. Toward Repositioning Niclosamide for Antivirulence Therapy of Pseudomonas aeruginosa Lung Infections: Development of Inhalable Formulations through Nanosuspension Technology. Mol Pharm. 2015 Aug 3;12(8):2604–17.

52. Wang Z-Y, Zhang H-Y. Rational drug repositioning by medical genetics. Nat Biotechnol. 2013 Dec;31(12):1080–2.

53. Gupta V, Gupta N, Shaik IH, Mehvar R, McMurtry IF, Oka M, et al. Liposomal fasudil, a rho-kinase inhibitor, for prolonged pulmonary preferential vasodilation in pulmonary arterial hypertension. J Controlled Release. 2013 Apr 28;167(2):189–99.

54. Maranhão RC, Guido MC, de Lima AD, Tavares ER, Marques AF, Tavares de Melo MD, et al. Methotrexate carried in lipid core nanoparticles reduces myocardial infarction size and improves cardiac function in rats. Int J Nanomedicine. 2017 May 17;12:3767–84.

55. Barbieri LR, Lourenço-Filho DD, Tavares ER, Carvalho PO, Gutierrez PS, Maranhão RC, et al. Influence of Drugs Carried in Lipid Nanoparticles in Coronary Disease of Rabbit Transplanted Heart. Ann Thorac Surg. 2017 Aug 1;104(2):577–83.

56. Novac N. Challenges and opportunities of drug repositioning. Trends Pharmacol Sci. 2013 May;34(5):267–72.

المنارة للاستشارات
www.manaraa.com

57. Mangoni AA, Tommasi S, Zinellu A, Sotgia S, Carru C, Piga M, et al. Repurposing existing drugs for cardiovascular risk management: a focus on methotrexate. Drugs Context. 2018 Nov 14;7.

58. Kanai O, Fujita K, Nakatani K, Mio T. Repetitive responses to nanoparticle albumin-bound paclitaxel and carboplatin in malignant pleural mesothelioma. Respirol Case Rep. 2016 Jan 14;4(1):28–31.

59. Shukla SK, Chan A, Parvathaneni V, Gupta V. Metformin-loaded chitosomes for treatment of malignant pleural mesothelioma – A rare thoracic cancer. Int J Biol Macromol. 2020 Oct 1;160:128–41.

60. Kulkarni NS, Vaidya B, Parvathaneni V, Bhanja D, Gupta V. Repurposing Quinacrine for Treatment of Malignant Mesothelioma: In-Vitro Therapeutic and Mechanistic Evaluation. Int J Mol Sci. 2020 Jan;21(17):6306.

61. Jojo GM, Kuppusamy G, De A, Karri VVSNR. Formulation and optimization of intranasal nanolipid carriers of pioglitazone for the repurposing in Alzheimer's disease using Box-Behnken design. Drug Dev Ind Pharm. 2019 Jul;45(7):1061–72.

62. Bruinsmann FA, Richter Vaz G, de Cristo Soares Alves A, Aguirre T, Raffin Pohlmann A, Stanisçuaski Guterres S, et al. Nasal Drug Delivery of Anticancer Drugs for the Treatment of Glioblastoma: Preclinical and Clinical Trials. Mol Basel Switz. 2019 Nov 26;24(23).

63. Roney C, Kulkarni P, Arora V, Antich P, Bonte F, Wu A, et al. Targeted nanoparticles for drug delivery through the blood-brain barrier for Alzheimer's disease. J Control Release Off J Control Release Soc. 2005 Nov 28;108(2–3):193–214.

64. Kim D, Chen Z, Zhou L-F, Huang S-X. Air pollutants and early origins of respiratory diseases. Chronic Dis Transl Med. 2018 Jun 7;4(2):75–94.

65. A Patient's Guide to Respiratory Disease [Internet]. US News & World Report. [cited 2020 Apr 27]. Available from: https://health.usnews.com/conditions/respiratory-disease

66. Prins Kurt W., Thenappan Thenappan, Weir E. Kenneth, Kalra Rajat, Pritzker Marc, Archer Stephen L. Repurposing Medications for Treatment of Pulmonary Arterial Hypertension: What's Old Is New Again. J Am Heart Assoc. 2019 Jan 8;8(1):e011343.

67. New "Old" Therapies in Pulmonary Arterial Hypertension: A Clinical Roundtable [Internet]. Pulmonology Advisor. 2019 [cited 2020 Oct 10]. Available from: https://www.pulmonologyadvisor.com/home/topics/pulmonary-hypertension/new-old-therapies-in-pulmonary-arterial-hypertension-a-clinical-roundtable/

68. Rashid J, Alobaida A, Al-Hilal TA, Hammouda S, McMurtry IF, Nozik-Grayck E, et al. Repurposing rosiglitazone, a PPAR-γ agonist and oral antidiabetic, as an inhaled formulation, for the treatment of PAH. J Control Release Off J Control Release Soc. 2018 Jun 28;280:113–23.

www.manaraa.com

69. Boyapally R, Pulivendala G, Bale S, Godugu C. Niclosamide alleviates pulmonary fibrosis in vitro and in vivo by attenuation of epithelial-to-mesenchymal transition, matrix proteins & Wnt/β-catenin signaling: A drug repurposing study. Life Sci. 2019 Mar 1;220:8–20.

70. Pena A. Livantra, Repurposed for Treating PAH, Gets FDA Orphan Drug Status [Internet]. [cited 2020 Oct 10]. Available from: https://pulmonaryhypertensionnews.com/2018/08/16/livantra-fda-orphan-drug-status-repurposed-for-pah-treatment/

71. Rashid J, Patel B, Nozik-Grayck E, McMurtry IF, Stenmark KR, Ahsan F. Inhaled sildenafil as an alternative to oral sildenafil in the treatment of pulmonary arterial hypertension (PAH). J Control Release Off J Control Release Soc. 2017 Mar 28;250:96–106.

72. Teymouri Rad R, Dadashzadeh S, Vatanara A, Alavi S, Ghasemian E, Mortazavi SA. Tadalafil nanocomposites as a dry powder formulation for inhalation, a new strategy for pulmonary arterial hypertension treatment. Eur J Pharm Sci. 2019 May 15;133:275–86.

73. Kruse RL, Vanijcharoenkarn K. Drug repurposing to treat asthma and allergic disorders: Progress and prospects. Allergy. 2018;73(2):313–22.

74. Lammers T, Sofias AM, van der Meel R, Schiffelers R, Storm G, Tacke F, et al. Dexamethasone nanomedicines for COVID-19. Nat Nanotechnol. 2020 Aug;15(8):622–4.

75. Roth Gregory A., Huffman Mark D., Moran Andrew E., Feigin Valery, Mensah George A., Naghavi Mohsen, et al. Global and Regional Patterns in Cardiovascular Mortality From 1990 to 2013. Circulation. 2015 Oct 27;132(17):1667–78.

76. MacRae CA, Roden DM, Loscalzo J. The Future of Cardiovascular Therapeutics. Circulation. 2016 Jun 21;133(25):2610–7.

77. Thind GS, Agrawal PR, Hirsh B, Saravolatz L, Chen-Scarabelli C, Narula J, et al. Mechanisms of myocardial ischemia-reperfusion injury and the cytoprotective role of minocycline: scope and limitations. Future Cardiol. 2015;11(1):61–76.

78. Nidorf SM, Eikelboom JW, Budgeon CA, Thompson PL. Low-dose colchicine for secondary prevention of cardiovascular disease. J Am Coll Cardiol. 2013 Jan 29;61(4):404–10.

79. Sharma TS, Wasko MCM, Tang X, Vedamurthy D, Yan X, Cote J, et al. Hydroxychloroquine Use Is Associated With Decreased Incident Cardiovascular Events in Rheumatoid Arthritis Patients. J Am Heart Assoc. 2016 Jan 4;5(1).

80. Shapiro M, Levy Y. The association between hydroxychloroquine treatment and cardiovascular morbidity among rheumatoid arthritis patients. Oncotarget. 2018 Jan 19;9(5):6615–22.

81. Floris A, Piga M, Mangoni AA, Bortoluzzi A, Erre GL, Cauli A. Protective Effects of Hydroxychloroquine against Accelerated Atherosclerosis in Systemic Lupus Erythematosus. Mediators Inflamm. 2018 Feb 18;2018.

www.manaraa.com

82. Martín Giménez VM, Kassuha DE, Manucha W. Nanomedicine applied to cardiovascular diseases: latest developments. Ther Adv Cardiovasc Dis. 2017 Apr;11(4):133–42.

83. Matoba T, Koga J, Nakano K, Egashira K, Tsutsui H. Nanoparticle-mediated drug delivery system for atherosclerotic cardiovascular disease. J Cardiol. 2017 Sep 1;70(3):206–11.

84. Carbone M, Ly BH, Dodson RF, Pagano I, Morris PT, Dogan UA, et al. Malignant Mesothelioma: Facts, Myths and Hypotheses. J Cell Physiol. 2012 Jan;227(1):44–58.

85. Szymiczek A, Pastorino S, Larson D, Tanji M, Pellegrini L, Xue J, et al. FTY720 inhibits mesothelioma growth in vitro and in a syngeneic mouse model. J Transl Med. 2017 Mar 15;15.

86. Barbarino M, Cesari D, Intruglio R, Indovina P, Namagerdi A, Bertolino FM, et al. Possible repurposing of pyrvinium pamoate for the treatment of mesothelioma: A pre-clinical assessment. J Cell Physiol. 2018 Sep 1;233(9):7391–401.

87. Shimazu K, Tada Y, Morinaga T, Shingyoji M, Sekine I, Shimada H, et al. Metformin produces growth inhibitory effects in combination with nutlin-3a on malignant mesothelioma through a cross-talk between mTOR and p53 pathways. BMC Cancer [Internet]. 2017 May 2 [cited 2020 Oct 11];17. Available from: https://www.ncbi.nlm.nih.gov/pmc/articles/PMC5414226/

88. Hwang S-H, Kim M-C, Ji S, Yang Y, Jeong Y, Kim Y. Glucose starvation induces resistance to metformin through the elevation of mitochondrial multidrug resistance protein 1. Cancer Sci. 2019 Apr;110(4):1256–67.

89. Types of Brain Disorders - SNMMI [Internet]. [cited 2020 Apr 29]. Available from: http://www.snmmi.org/AboutSNMMI/Content.aspx?ItemNumber=1781

90. Ontaneda D, Thompson AJ, Fox RJ, Cohen JA. Progressive multiple sclerosis: prospects for disease therapy, repair, and restoration of function. The Lancet. 2017 Apr;389(10076):1357–66.

91. Twohig D, Nielsen HM. α-synuclein in the pathophysiology of Alzheimer's disease. Mol Neurodegener. 2019 Jun 11;14(1):23.

92. Poewe W, Seppi K, Tanner CM, Halliday GM, Brundin P, Volkmann J, et al. Parkinson disease. Nat Rev Dis Primer. 2017 Mar 23;3:17013.

93. Davie CA. A review of Parkinson's disease. Br Med Bull. 2008 Feb 18;86(1):109–27.

94. van Ettekoven CN, van de Beek D, Brouwer MC. Update on community-acquired bacterial meningitis: guidance and challenges. Clin Microbiol Infect. 2017 Sep;23(9):601–6.

95. Brain Diseases [Internet]. WebMD. [cited 2019 Mar 22]. Available from: https://www.webmd.com/brain/brain-diseases

96. Ajiboye N, Chalouhi N, Starke RM, Zanaty M, Bell R. Unruptured Cerebral Aneurysms: Evaluation and Management. Sci World J. 2015;2015:1–10.

www.manaraa.com

97. Zhang Y, Zhai M, Chen Z, Han X, Yu F, Li Z, et al. Dual-modified liposome codelivery of doxorubicin and vincristine improve targeting and therapeutic efficacy of glioma. Drug Deliv. 2017 Jan;24(1):1045–55.

98. Saraiva C, Praça C, Ferreira R, Santos T, Ferreira L, Bernardino L. Nanoparticle-mediated brain drug delivery: Overcoming blood–brain barrier to treat neurodegenerative diseases. J Controlled Release. 2016 Aug;235:34–47.

99. Rasper M, Schäfer A, Piontek G, Teufel J, Brockhoff G, Ringel F, et al. Aldehyde dehydrogenase 1 positive glioblastoma cells show brain tumor stem cell capacity. Neuro-Oncol. 2010 Oct 1;12(10):1024–33.

100. da Silveira EF, Chassot JM, Teixeira FC, Azambuja JH, Debom G, Beira FT, et al. Ketoprofen-loaded polymeric nanocapsules selectively inhibit cancer cell growth in vitro and in preclinical model of glioblastoma multiforme. Invest New Drugs. 2013 Dec;31(6):1424–35.

101. Zhou J, Patel TR, Sirianni RW, Strohbehn G, Zheng M-Q, Duong N, et al. Highly penetrative, drug-loaded nanocarriers improve treatment of glioblastoma. Proc Natl Acad Sci U S A. 2013 Jul 16;110(29):11751–6.

102. Agarwal NB, Jain S, Nagpal D, Agarwal NK, Mediratta PK, Sharma KK. Liposomal formulation of curcumin attenuates seizures in different experimental models of epilepsy in mice. Fundam Clin Pharmacol. 2013 Apr;27(2):169–72.

103. El-Moslemany RM, Eissa MM, Ramadan AA, El-Khordagui LK, El-Azzouni MZ. Miltefosine lipid nanocapsules: Intersection of drug repurposing and nanotechnology for single dose oral treatment of pre-patent schistosomiasis mansoni. Acta Trop. 2016 Jul;159:142–8.

104. Alhakamy NA, Md S. Repurposing Itraconazole Loaded PLGA Nanoparticles for Improved Antitumor Efficacy in Non-Small Cell Lung Cancers. Pharmaceutics. 2019 Dec 16;11(12).

105. Salentin S, Adasme MF, Heinrich JC, Haupt VJ, Daminelli S, Zhang Y, et al. From malaria to cancer: Computational drug repositioning of amodiaquine using PLIP interaction patterns. Sci Rep. 2017 12;7(1):11401.

106. Katsaros N, Anagnostopoulou A. Rhodium and its compounds as potential agents in cancer treatment. Crit Rev Oncol Hematol. 2002 Jun;42(3):297–308.

107. Wu Y, Xu J, Chen J, Zou M, Rusidanmu A, Yang R. Blocking transferrin receptor inhibits the growth of lung adenocarcinoma cells in vitro. Thorac Cancer. 2018 Feb;9(2):253–61.

108. Shen Y, Li X, Dong D, Zhang B, Xue Y, Shang P. Transferrin receptor 1 in cancer: a new sight for cancer therapy. :16.

109. Li X, Valdes SA, Alzhrani RF, Hufnagel S, Hursting SD, Cui Z. Zoledronic Acid-containing Nanoparticles With Minimum Premature Release Show Enhanced Activity Against Extraskeletal Tumor. ACS Appl Mater Interfaces. 2019 Feb 20;11(7):7311–9.

www.manaraa.com

110. Willenbacher E, Khan SZ, Mujica SCA, Trapani D, Hussain S, Wolf D, et al. Curcumin: New Insights into an Ancient Ingredient against Cancer. Int J Mol Sci. 2019 Apr 12;20(8).

111. Pal K, Laha D, Parida PK, Roy S, Bardhan S, Dutta A, et al. An In Vivo Study for Targeted Delivery of Curcumin in Human Triple Negative Breast Carcinoma Cells Using Biocompatible PLGA Microspheres Conjugated with Folic Acid. J Nanosci Nanotechnol. 2019 Jul 1;19(7):3720–33.

112. Venkatesan P, Puvvada N, Dash R, Prashanth Kumar BN, Sarkar D, Azab B, et al. The potential of celecoxib-loaded hydroxyapatite-chitosan nanocomposite for the treatment of colon cancer. Biomaterials. 2011 May 1;32(15):3794–806.

113. Zappa C, Mousa SA. Non-small cell lung cancer: current treatment and future advances. Transl Lung Cancer Res. 2016 Jun;5(3):288–300.

114. Parvathaneni V, Kulkarni NS, Muth A, Gupta V. Drug repurposing: a promising tool to accelerate the drug discovery process. Drug Discov Today. 2019 Oct;24(10):2076–85.

115. Paliwal R, Babu RJ, Palakurthi S. Nanomedicine Scale-up Technologies: Feasibilities and Challenges. AAPS PharmSciTech. 2014 Jul 22;15(6):1527–34.

116. Bobo D, Robinson KJ, Islam J, Thurecht KJ, Corrie SR. Nanoparticle-Based Medicines: A Review of FDA-Approved Materials and Clinical Trials to Date. Pharm Res. 2016 Oct 1;33(10):2373–87.

117. Jenning V, Lippacher A, Gohla SH. Medium scale production of solid lipid nanoparticles (SLN) by high pressure homogenization. J Microencapsul. 2002 Jan 1;19(1):1–10.

118. Gupta S, Kesarla R, Chotai N, Misra A, Omri A. Systematic Approach for the Formulation and Optimization of Solid Lipid Nanoparticles of Efavirenz by High Pressure Homogenization Using Design of Experiments for Brain Targeting and Enhanced Bioavailability. BioMed Res Int. 2017;

119. Muthu MS, Wilson B. Challenges posed by the scale-up of nanomedicines. Nanomed. 2012 Mar 1;7(3):307–9.

120. Hoyer H, Schlocker W, Greindl M, Ostermann T, Bernkop-Schnürch A. Preparation and evaluation of thiomer nanoparticles via high pressure homogenization. J Microencapsul. 2010 Sep 1;27(6):487–95.

121. Grumezescu AM. Nanoscale Fabrication, Optimization, Scale-up and Biological Aspects of Pharmaceutical Nanotechnology. William Andrew; 2017. 704 p.

122. Patrignani F, Lanciotti R. Applications of High and Ultra High Pressure Homogenization for Food Safety. Front Microbiol. 2016;7:1132.

123. Shi A, Li D, Wang L, Li B, Adhikari B. Preparation of starch-based nanoparticles through high-pressure homogenization and miniemulsion cross-linking: Influence of various process parameters on particle size and stability. Carbohydr Polym. 2011 Feb 1;83(4):1604–10.

المنارة للاستشارات
www.manaraa.com

124. Ding Y, Kan J. Optimization and characterization of high pressure homogenization produced chemically modified starch nanoparticles. J Food Sci Technol. 2017 Dec;54(13):4501–9.

125. Petersen K, Steckel H. A DOE Approach to Investigate the Influence of Process-Parameters and Composition on the Stability of Emulsions Stabilized by Marine Polysaccharides Prepared by High-Pressure Homogenization. J Dispers Sci Technol. 2014 Jun 3;35(6):789–98.

126. Patel B, Gupta V, Ahsan F. PEG-PLGA based large porous particles for pulmonary delivery of a highly soluble drug, low molecular weight heparin. J Control Release Off J Control Release Soc. 2012 Sep 10;162(2):310–20.

127. Abdelaziz HM, Gaber M, Abd-Elwakil MM, Mabrouk MT, Elgohary MM, Kamel NM, et al. Inhalable particulate drug delivery systems for lung cancer therapy: Nanoparticles, microparticles, nanocomposites and nanoaggregates. J Controlled Release. 2018 Jan 10;269:374–92.

128. Lee W-H, Loo C-Y, Traini D, Young PM. Inhalation of nanoparticle-based drug for lung cancer treatment: Advantages and challenges. Asian J Pharm Sci. 2015 Dec 1;10(6):481–9.

129. Vaidya B, Kulkarni NS, Shukla SK, Parvathaneni V, Chauhan G, Damon JK, et al. Development of Inhalable Quinacrine Loaded Bovine Serum Albumin Modified Cationic Nanoparticles: Repurposing Quinacrine for Lung Cancer Therapeutics. Int J Pharm. 2020 Jan 11;118995.

130. Youngren-Ortiz SR, Hill DB, Hoffmann PR, Morris KR, Barrett EG, Forest MG, et al. Development of Optimized, Inhalable, Gemcitabine-Loaded Gelatin Nanocarriers for Lung Cancer. J Aerosol Med Pulm Drug Deliv. 2017 Oct;30(5):299–321.

131. Guzmán EAT, Sun Q, Meenach SA. Development and Evaluation of Paclitaxel-Loaded Aerosol Nanocomposite Microparticles and Their Efficacy Against Air-Grown Lung Cancer Tumor Spheroids. ACS Biomater Sci Eng. 2019 Dec 9;5(12):6570–80.

132. Abdelaziz HM, Elzoghby AO, Helmy MW, Abdelfattah E-ZA, Fang J-Y, Samaha MW, et al. Inhalable Lactoferrin/Chondroitin-Functionalized Monoolein Nanocomposites for Localized Lung Cancer Targeting. ACS Biomater Sci Eng. 2020 Feb 10;6(2):1030–42.

133. Mangal S, Gao W, Li T, Zhou Q (Tony). Pulmonary delivery of nanoparticle chemotherapy for the treatment of lung cancers: challenges and opportunities. Acta Pharmacol Sin. 2017 Jun;38(6):782–97.

134. Ahmad J, Akhter S, Rizwanullah M, Amin S, Rahman M, Ahmad MZ, et al. Nanotechnology-based inhalation treatments for lung cancer: state of the art. Nanotechnol Sci Appl. 2015 Nov 19;8:55–66.

135. Anderson CF, Grimmett ME, Domalewski CJ, Cui H. Inhalable nanotherapeutics to improve treatment efficacy for common lung diseases. Wiley Interdiscip Rev Nanomed Nanobiotechnol. 2020 Jan;12(1):e1586.

المنارة للاستشارات
www.manaraa.com

136. Carvalho TC, Peters JI, Williams RO. Influence of particle size on regional lung deposition--what evidence is there? Int J Pharm. 2011 Mar 15;406(1–2):1–10.

137. Dabbagh A, Abu Kasim NH, Yeong CH, Wong TW, Abdul Rahman N. Critical Parameters for Particle-Based Pulmonary Delivery of Chemotherapeutics. J Aerosol Med Pulm Drug Deliv. 2017 Oct 12;31(3):139–54.

138. Johal B, Howald M, Fischer M, Marshall J, Venthoye G. Fine Particle Profile of Fluticasone Propionate/Formoterol Fumarate Versus Other Combination Products: the DIFFUSE Study. Comb Prod Ther. 2013 Dec 1;3(1):39–51.

139. Qiao S, Tao S, Rojo de la Vega M, Park SL, Vonderfecht AA, Jacobs SL, et al. The antimalarial amodiaquine causes autophagic-lysosomal and proliferative blockade sensitizing human melanoma cells to starvation- and chemotherapy-induced cell death. Autophagy. 2013 Dec;9(12):2087–102.

140. Espinoza JA, Zisi A, Kanellis DC, Carreras-Puigvert J, Henriksson M, Hühn D, et al. The antimalarial drug amodiaquine stabilizes p53 through ribosome biogenesis stress, independently of its autophagy-inhibitory activity. Cell Death Differ. 2019 Jul 8;

141. Liu G, Pei F, Yang F, Li L, Amin AD, Liu S, et al. Role of Autophagy and Apoptosis in Non-Small-Cell Lung Cancer. Int J Mol Sci. 2017 Feb 10;18(2).

142. Nano DeBEE High Pressure Homogenizer | Homogenizers.net [Internet]. [cited 2020 May 7]. Available from: https://homogenizers.net/products/nano-debee-high-pressure-homogenizer

143. Dong Y, Feng S-S. Poly(d,l-lactide-co-glycolide) (PLGA) nanoparticles prepared by high pressure homogenization for paclitaxel chemotherapy. Int J Pharm. 2007 Sep 5;342(1):208–14.

144. Stocke NA, Meenach SA, Arnold SM, Mansour HM, Hilt JZ. Formulation and characterization of inhalable magnetic nanocomposite microparticles (MnMs) for targeted pulmonary delivery via spray drying. Int J Pharm. 2015 Feb 20;479(2):320–8.

145. Price DN, Stromberg LR, Kunda NK, Muttil P. In Vivo Pulmonary Delivery and Magnetic-Targeting of Dry Powder Nano-in-Microparticles. Mol Pharm. 2017 Dec 4;14(12):4741–50.

146. Vaidya B, Parvathaneni V, Kulkarni NS, Shukla SK, Damon JK, Sarode A, et al. Cyclodextrin modified erlotinib loaded PLGA nanoparticles for improved therapeutic efficacy against non-small cell lung cancer. Int J Biol Macromol. 2019 Feb 1;122:338–47.

147. Kulkarni NS, Parvathaneni V, Shukla SK, Barasa L, Perron JC, Yoganathan S, et al. Tyrosine kinase inhibitor conjugated quantum dots for non-small cell lung cancer (NSCLC) treatment. Eur J Pharm Sci Off J Eur Fed Pharm Sci. 2019 May 15;133:145–59.

148. Liang C-C, Park AY, Guan J-L. In vitro scratch assay: a convenient and inexpensive method for analysis of cell migration in vitro. Nat Protoc. 2007;2(2):329–33.

www.manaraa.com

149. Franken NAP, Rodermond HM, Stap J, Haveman J, van Bree C. Clonogenic assay of cells in vitro. Nat Protoc. 2006;1(5):2315–9.

150. Geissmann Q. OpenCFU, a New Free and Open-Source Software to Count Cell Colonies and Other Circular Objects. PLOS ONE. 2013 Feb 15;8(2):e54072.

151. White E. The role for autophagy in cancer. J Clin Invest. 2015 Jan 2;125(1):42–6.

152. Kauntz H, Bousserouel S, Gossé F, Raul F. Silibinin triggers apoptotic signaling pathways and autophagic survival response in human colon adenocarcinoma cells and their derived metastatic cells. Apoptosis Int J Program Cell Death. 2011 Oct;16(10):1042–53.

153. Lossi L, Castagna C, Merighi A. Caspase-3 Mediated Cell Death in the Normal Development of the Mammalian Cerebellum. Int J Mol Sci [Internet]. 2018 Dec 12 [cited 2019 Aug 27];19(12). Available from: https://www.ncbi.nlm.nih.gov/pmc/articles/PMC6321612/

154. Gross K, Karagiannides I, Thomou T, Koon HW, Bowe C, Kim H, et al. Substance P promotes expansion of human mesenteric preadipocytes through proliferative and antiapoptotic pathways. Am J Physiol - Gastrointest Liver Physiol. 2009 May;296(5):G1012–9.

155. Hall RD, Le TM, Haggstrom DE, Gentzler RD. Angiogenesis inhibition as a therapeutic strategy in non-small cell lung cancer (NSCLC). Transl Lung Cancer Res. 2015 Oct;4(5):515–23.

156. Miller JE, Monsanto SP, Ahn SH, Khalaj K, Fazleabas AT, Young SL, et al. Interleukin-33 modulates inflammation in endometriosis. Sci Rep. 2017 Dec 20;7(1):17903.

157. Arora S, Swaminathan SK, Kirtane A, Srivastava SK, Bhardwaj A, Singh S, et al. Synthesis, characterization, and evaluation of poly (D,L-lactide-co-glycolide)-based nanoformulation of miRNA-150: potential implications for pancreatic cancer therapy. Int J Nanomedicine. 2014 Jun 18;9:2933–42.

158. Ray S, Mishra A, Mandal T, Sa B, Chakraborty J. Optimization of the process parameters for fabrication of polymer coated layered double hydroxide-methotrexate nanohybrid for possible treatment of osteosarcoma. RSC Adv. 2015 Nov 27;5.

159. Ogbonna JDN, Attama AA, Ofokansi KC, Patil SB, Basarkar GD. Optimization of formulation processes using Design Expert® Software for preparation of polymeric blends-artesunate-amodiaquine HCl microparticles. J Drug Deliv Sci Technol. 2017 Jun 1;39:36–49.

160. Timbul Partogi H, Soewandhi S, Jessie Sofia P, Wikarsa S. Identification of physical interaction between anti malarial drugs combination artesunate-amodiaquine hydrochloride. Int J Pharm Pharm Sci. 2013 Jan 1;5:206–10.

161. Patlolla RR, Chougule M, Patel AR, Jackson T, Tata PN, Singh M. Formulation, Characterization and Pulmonary Deposition of Nebulized Celecoxib Encapsulated

www.manaraa.com

Nanostructured Lipid Carriers. J Control Release Off J Control Release Soc. 2010 Jun 1;144(2):233–41.

162. Clénet D. Accurate prediction of vaccine stability under real storage conditions and during temperature excursions. Eur J Pharm Biopharm. 2018 Apr 1;125:76–84.

163. Gratton SEA, Ropp PA, Pohlhaus PD, Luft JC, Madden VJ, Napier ME, et al. The effect of particle design on cellular internalization pathways. Proc Natl Acad Sci. 2008 Aug 19;105(33):11613–8.

164. Rajendran V, Jain MV. In Vitro Tumorigenic Assay: Colony Forming Assay for Cancer Stem Cells. Methods Mol Biol Clifton NJ. 2018;1692:89–95.

165. Verifying Cell-Based Assays for Use with 3D Models [Internet]. [cited 2020 May 8]. Available from: https://www.promega.com/resources/pubhub/2019/verifying-cell-based-assays-for-use-with-3d-models/

166. Yuan L, Zhang F, Qi X, Yang Y, Yan C, Jiang J, et al. Chiral polymer modified nanoparticles selectively induce autophagy of cancer cells for tumor ablation. J Nanobiotechnology. 2018 Jul 11;16(1):55.

167. Tseng C-L, Wang T-W, Dong G-C, Yueh-Hsiu Wu S, Young T-H, Shieh M-J, et al. Development of gelatin nanoparticles with biotinylated EGF conjugation for lung cancer targeting. Biomaterials. 2007 Sep 1;28(27):3996–4005.

168. Sharma N, Madan P, Lin S. Effect of process and formulation variables on the preparation of parenteral paclitaxel-loaded biodegradable polymeric nanoparticles: A co-surfactant study. Asian J Pharm Sci. 2016 Jun 1;11(3):404–16.

169. Dong Y, Feng S-SS-S. Methoxy poly(ethylene glycol)-poly(lactide) (MPEG-PLA) nanoparticles for controlled delivery of anticancer drugs. Biomaterials. 2004 Jun;25(14):2843–9.

170. Fröhlich E. The role of surface charge in cellular uptake and cytotoxicity of medical nanoparticles. Int J Nanomedicine. 2012;7:5577–91.

171. Iyer R, Hsia CCW, Nguyen KT. Nano-Therapeutics for the Lung: State-of-the-Art and Future Perspectives. Curr Pharm Des. 2015;21(36):5233–44.

172. Ravikumar P, Menon JU, Punnakitikashem P, Gyawali D, Togao O, Takahashi M, et al. Nanoparticle facilitated inhalational delivery of erythropoietin receptor cDNA protects against hyperoxic lung injury. Nanomedicine Nanotechnol Biol Med. 2016 Apr;12(3):811–21.

173. Hulkower KI, Herber RL. Cell Migration and Invasion Assays as Tools for Drug Discovery. Pharmaceutics. 2011 Mar 11;3(1):107–24.

174. Tchoryk A, Taresco V, Argent RH, Ashford M, Gellert PR, Stolnik S, et al. Penetration and Uptake of Nanoparticles in 3D Tumor Spheroids. Bioconjug Chem. 2019 May 15;30(5):1371–84.

www.manaraa.com

175. Zhang Y-R, Lin R, Li H-J, He W, Du J-Z, Wang J. Strategies to improve tumor penetration of nanomedicines through nanoparticle design. WIREs Nanomedicine Nanobiotechnology. 2019;11(1):e1519.

176. DeCicco-Skinner KL, Henry GH, Cataisson C, Tabib T, Gwilliam JC, Watson NJ, et al. Endothelial Cell Tube Formation Assay for the In Vitro Study of Angiogenesis. J Vis Exp JoVE. 2014 Sep 1;(91).

177. Le Q-V, Choi J, Oh Y-K. Nano delivery systems and cancer immunotherapy. J Pharm Investig. 2018 Sep 1;48(5):527–39.

178. Farjadian F, Ghasemi A, Gohari O, Roointan A, Karimi M, Hamblin MR. Nanopharmaceuticals and nanomedicines currently on the market: challenges and opportunities. Nanomed. 2019 Jan;14(1):93–126.

179. Martins JP, das Neves J, de la Fuente M, Celia C, Florindo H, Günday-Türeli N, et al. The solid progress of nanomedicine. Drug Deliv Transl Res [Internet]. 2020 Mar 5 [cited 2020 Mar 18]; Available from: https://doi.org/10.1007/s13346-020-00743-2

180. Din F ud, Aman W, Ullah I, Qureshi OS, Mustapha O, Shafique S, et al. Effective use of nanocarriers as drug delivery systems for the treatment of selected tumors. Int J Nanomedicine. 2017 Oct 5;12:7291–309.

181. Yhee JY, Im J, Nho RS. Advanced Therapeutic Strategies for Chronic Lung Disease Using Nanoparticle-Based Drug Delivery. J Clin Med [Internet]. 2016 Sep 20 [cited 2020 Mar 19];5(9). Available from: https://www.ncbi.nlm.nih.gov/pmc/articles/PMC5039485/

182. Lee H-Y, Mohammed KA, Nasreen N. Nanoparticle-based targeted gene therapy for lung cancer. Am J Cancer Res. 2016 May 1;6(5):1118–34.

183. Ridge CA, McErlean AM, Ginsberg MS. Epidemiology of lung cancer. Semin Interv Radiol. 2013 Jun;30(2):93–8.

184. Herbst RS, Morgensztern D, Boshoff C. The biology and management of non-small cell lung cancer. Nature. 2018 Jan;553(7689):446–54.

185. Tran S, DeGiovanni P-J, Piel B, Rai P. Cancer nanomedicine: a review of recent success in drug delivery. Clin Transl Med [Internet]. 2017 Dec 11 [cited 2020 Mar 19];6. Available from: https://www.ncbi.nlm.nih.gov/pmc/articles/PMC5725398/

186. Bahrami B, Hojjat-Farsangi M, Mohammadi H, Anvari E, Ghalamfarsa G, Yousefi M, et al. Nanoparticles and targeted drug delivery in cancer therapy. Immunol Lett. 2017 Oct 1;190:64–83.

187. Pooja D, Kulhari H, Tunki L, Chinde S, Kuncha M, Grover P, et al. Nanomedicines for targeted delivery of etoposide to non-small cell lung cancer using transferrin functionalized nanoparticles. RSC Adv. 2015 Jun 2;5(61):49122–31.

www.manaraa.com

188. Bhushan B, Khanadeev V, Khlebtsov B, Khlebtsov N, Gopinath P. Impact of albumin based approaches in nanomedicine: Imaging, targeting and drug delivery. Adv Colloid Interface Sci. 2017 Aug 1;246:13–39.

189. Daniels TR, Bernabeu E, Rodríguez JA, Patel S, Kozman M, Chiappetta DA, et al. Transferrin receptors and the targeted delivery of therapeutic agents against cancer. Biochim Biophys Acta. 2012 Mar;1820(3):291–317.

190. Ramasamy T, Ruttala HB, Gupta B, Poudel BK, Choi H-G, Yong CS, et al. Smart chemistry-based nanosized drug delivery systems for systemic applications: A comprehensive review. J Controlled Release. 2017 Jul 28;258:226–53.

191. Rosière R, Berghmans T, De Vuyst P, Amighi K, Wauthoz N. The Position of Inhaled Chemotherapy in the Care of Patients with Lung Tumors: Clinical Feasibility and Indications According to Recent Pharmaceutical Progresses. Cancers. 2019 Mar 7;11(3).

192. Singh AP, Biswas A, Shukla A, Maiti P. Targeted therapy in chronic diseases using nanomaterial-based drug delivery vehicles. Signal Transduct Target Ther. 2019 Aug 30;4(1):1–21.

193. Ahmad J, Akhter S, Rizwanullah M, Amin S, Rahman M, Ahmad MZ, et al. Nanotechnology-based inhalation treatments for lung cancer: state of the art. Nanotechnol Sci Appl. 2015 Nov 19;8:55–66.

194. Kuzmov A, Minko T. Nanotechnology approaches for inhalation treatment of lung diseases. J Controlled Release. 2015 Dec 10;219:500–18.

195. Velino C, Carella F, Adamiano A, Sanguinetti M, Vitali A, Catalucci D, et al. Nanomedicine Approaches for the Pulmonary Treatment of Cystic Fibrosis. Front Bioeng Biotechnol. 2019;7:406.

196. Rijt SH van, Bein T, Meiners S. Medical nanoparticles for next generation drug delivery to the lungs. Eur Respir J. 2014 Sep 1;44(3):765–74.

197. Whitney JF, Clark JM, Griffin TW, Gautam S, Leslie KO. Transferrin receptor expression in nonsmall cell lung cancer. Histopathologic and clinical correlates. Cancer. 1995;76(1):20–5.

198. Parvathaneni V, Kulkarni NS, Chauhan G, Shukla SK, Elbatanony R, Patel B, et al. Development of pharmaceutically scalable inhaled anti-cancer nanotherapy – Repurposing amodiaquine for non-small cell lung cancer (NSCLC). Mater Sci Eng C. 2020 May 31;111139.

199. Das M, Dilnawaz F, Sahoo SK. Targeted nutlin-3a loaded nanoparticles inhibiting p53-MDM2 interaction: novel strategy for breast cancer therapy. Nanomed. 2011 Apr;6(3):489–507.

200. Abdou EM, Kandil SM, Morsi A, Sleem MW. In-vitro and in-vivo respiratory deposition of a developed metered dose inhaler formulation of an anti-migraine drug. Drug Deliv. 2019 Jul 5;26(1):689–99.

www.manaraa.com

201. Vaidya B, Parvathaneni V, Kulkarni NS, Shukla SK, Damon JK, Sarode A, et al. Cyclodextrin modified erlotinib loaded PLGA nanoparticles for improved therapeutic efficacy against non-small cell lung cancer. Int J Biol Macromol. 2019 Feb 1;122:338–47.

202. Wang X, Parvathaneni V, Shukla SK, Kanabar DD, Muth A, Gupta V. Cyclodextrin Complexation for Enhanced Stability and Non-invasive Pulmonary Delivery of Resveratrol—Applications in Non-small Cell Lung Cancer Treatment. AAPS PharmSciTech. 2020 Jul 6;21(5):183.

203. Shukla SK, Kulkarni NS, Farrales P, Kanabar DD, Parvathaneni V, Kunda NK, et al. Sorafenib Loaded Inhalable Polymeric Nanocarriers against Non-Small Cell Lung Cancer. Pharm Res. 2020 Mar 12;37(3):67.

204. Elbatanony RS, Parvathaneni V, Kulkarni NS, Shukla SK, Chauhan G, Kunda NK, et al. Afatinib-loaded inhalable PLGA nanoparticles for localized therapy of non-small cell lung cancer (NSCLC)—development and in-vitro efficacy. Drug Deliv Transl Res [Internet]. 2020 Jun 16 [cited 2020 Nov 1]; Available from: https://doi.org/10.1007/s13346-020-00802-8

205. Frasco MF, Almeida GM, Santos-Silva F, Pereira M do C, Coelho MAN. Transferrin surface-modified PLGA nanoparticles-mediated delivery of a proteasome inhibitor to human pancreatic cancer cells. J Biomed Mater Res A. 2015 Apr;103(4):1476–84.

206. Borghardt JM, Kloft C, Sharma A. Inhaled Therapy in Respiratory Disease: The Complex Interplay of Pulmonary Kinetic Processes. Can Respir J [Internet]. 2018 [cited 2020 Mar 27]; Available from: https://www.hindawi.com/journals/crj/2018/2732017/

207. Labiris NR, Dolovich MB. Pulmonary drug delivery. Part I: physiological factors affecting therapeutic effectiveness of aerosolized medications. Br J Clin Pharmacol. 2003 Dec;56(6):588–99.

208. Jo Y, Choi N, Kim K, Koo H-J, Choi J, Kim HN. Chemoresistance of Cancer Cells: Requirements of Tumor Microenvironment-mimicking In Vitro Models in Anti-Cancer Drug Development. Theranostics. 2018 Oct 22;8(19):5259–75.

209. Wang X, Parvathaneni V, Shukla SK, Kulkarni NS, Muth A, Kunda NK, et al. Inhalable resveratrol-cyclodextrin complex loaded biodegradable nanoparticles for enhanced efficacy against non-small cell lung cancer. Int J Biol Macromol. 2020 Dec 1;164:638–50.

210. Breslin S, O'Driscoll L. Three-dimensional cell culture: the missing link in drug discovery. Drug Discov Today. 2013 Mar;18(5–6):240–9.

211. Fennema E, Rivron N, Rouwkema J, van Blitterswijk C, de Boer J. Spheroid culture as a tool for creating 3D complex tissues. Trends Biotechnol. 2013 Feb;31(2):108–15.

212. Sharma P, Mehta M, Dhanjal DS, Kaur S, Gupta G, Singh H, et al. Emerging trends in the novel drug delivery approaches for the treatment of lung cancer. Chem Biol Interact. 2019 Aug 25;309:108720.

المنارة للاستشارات
www.manaraa.com

213. Jahan ST, Sadat SMA, Walliser M, Haddadi A. Targeted Therapeutic Nanoparticles: An Immense Promise to Fight against Cancer. J Drug Deliv. 2017;2017:e9090325.

214. Soe ZC, Kwon JB, Thapa RK, Ou W, Nguyen HT, Gautam M, et al. Transferrin-Conjugated Polymeric Nanoparticle for Receptor-Mediated Delivery of Doxorubicin in Doxorubicin-Resistant Breast Cancer Cells. Pharmaceutics. 2019 Feb;11(2):63.

215. Upadhyay P, Sarker S, Ghosh A, Gupta P, Das S, Ahir M, et al. Transferrin-decorated thymoquinone-loaded PEG-PLGA nanoparticles exhibit anticarcinogenic effect in non-small cell lung carcinoma via the modulation of miR-34a and miR-16. Biomater Sci. 2019 Oct 1;7(10):4325–44.

216. Guo Y, Wang L, Lv P, Zhang P. Transferrin-conjugated doxorubicin-loaded lipid-coated nanoparticles for the targeting and therapy of lung cancer. Oncol Lett. 2015 Mar 1;9(3):1065–72.

217. Millard M, Yakavets I, Zorin V, Kulmukhamedova A, Marchal S, Bezdetnaya L. Drug delivery to solid tumors: the predictive value of the multicellular tumor spheroid model for nanomedicine screening. Int J Nanomedicine. 2017 Oct 31;12:7993–8007.

218. Frigerio B, Bizzoni C, Jansen G, Leamon CP, Peters GJ, Low PS, et al. Folate receptors and transporters: biological role and diagnostic/therapeutic targets in cancer and other diseases. J Exp Clin Cancer Res. 2019 Mar 12;38(1):125.

219. Zhang Z, Zhou L, Xie N, Nice EC, Zhang T, Cui Y, et al. Overcoming cancer therapeutic bottleneck by drug repurposing. Signal Transduct Target Ther. 2020 Jul 2;5(1):1–25.

220. Yu Y, Wang J, Kaul SC, Wadhwa R, Miyako E. Folic Acid Receptor-Mediated Targeting Enhances the Cytotoxicity, Efficacy, and Selectivity of Withania somnifera Leaf Extract: In vitro and in vivo Evidence. Front Oncol [Internet]. 2019 Jul 4 [cited 2020 Nov 1];9. Available from: https://www.ncbi.nlm.nih.gov/pmc/articles/PMC6621239/

221. Fernández M, Javaid F, Chudasama V. Advances in targeting the folate receptor in the treatment/imaging of cancers. Chem Sci. 2017 Dec 18;9(4):790–810.

222. Lutz RJ. Targeting the folate receptor for the treatment of ovarian cancer. Transl Cancer Res. 2015 Apr 2;4(1):118-126–126.

223. Esmaeili F, Ghahremani MH, Ostad SN, Atyabi F, Seyedabadi M, Malekshahi MR, et al. Folate-receptor-targeted delivery of docetaxel nanoparticles prepared by PLGA–PEG–folate conjugate. J Drug Target. 2008 Jan 1;16(5):415–23.

224. Valencia PM, Hanewich-Hollatz MH, Gao W, Karim F, Langer R, Karnik R, et al. Effects of ligands with different water solubilities on self-assembly and properties of targeted nanoparticles. Biomaterials. 2011 Sep;32(26):6226–33.

225. Vaidya B, Parvathaneni V, Kulkarni NS, Shukla SK, Damon JK, Sarode A, et al. Cyclodextrin modified erlotinib loaded PLGA nanoparticles for improved therapeutic efficacy against non-small cell lung cancer. Int J Biol Macromol. 2019 Feb 1;122:338–47.

www.manaraa.com

226. Rosenholm JM, Meinander A, Peuhu E, Niemi R, Eriksson JE, Sahlgren C, et al. Targeting of Porous Hybrid Silica Nanoparticles to Cancer Cells. ACS Nano. 2009 Jan 27;3(1):197–206.

227. Liu Y, Li K, Pan J, Liu B, Feng S-S. Folic acid conjugated nanoparticles of mixed lipid monolayer shell and biodegradable polymer core for targeted delivery of Docetaxel. Biomaterials. 2010 Jan;31(2):330–8.

228. Cheung A, Bax HJ, Josephs DH, Ilieva KM, Pellizzari G, Opzoomer J, et al. Targeting folate receptor alpha for cancer treatment. Oncotarget. 2016 May 27;7(32):52553–74.

229. Angelopoulou A, Kolokithas-Ntoukas A, Fytas C, Avgoustakis K. Folic Acid-Functionalized, Condensed Magnetic Nanoparticles for Targeted Delivery of Doxorubicin to Tumor Cancer Cells Overexpressing the Folate Receptor. ACS Omega. 2019 Dec 24;4(26):22214–27.

المنارة للاستشارات
www.manaraa.com

Vita

Name	*Vineela Parvathaneni*
Baccalaureate Degree	*Bachelor of Science*, *Sri Padmavathi Mahila Viswavidyalayam, Tirupati* *Major: Pharmacy*
Date Graduated	*August, 2010*
Other Degrees and Certificates	*Master of Science, Chalapathi institute of Pharmaceutical Sciences, Guntur, Major: Pharmaceutical Sciences*
Date Graduated	*November, 2012*

www.manaraa.com